UKOOA phase II Task 3: Aerobic and anaerobic degradation of drill cuttings – results from small scale laboratory experiments

Appendixes

Report RF – 2001/217

Appendix 1

Aerobic degradation trial data

Trial 1 - aerobic

Oxygen

No	Content	day 1 ppm	Day 14 ppm	Day 28 ppm	Day 56 ppm	Day 229 ppm
1	**reference sediment**	8,43	5,11	6,76	4,62	5,00
2	**Beryl A 20%**		2,22	5,76	4,12	5,27
3	**Beryl A**			4,10		
4	**Beryl A**	6,21		4,37		
5	**Beryl A**			3,95		
6	**Ekofisk 2/4 A 20%**		0,43	4,27	5,12	3,10
7	**Ekofisk 2/4 A**		1,82			
8	**Frøy 20%**		1,16	5,03	3,20	3,51
9	**Frøy**					
10	**Lille-Frigg 20%**		2,77	4,09	4,92	3,28
11	**Lille-Frigg**		2,64	3,46	3,49	3,70
12	**Ekofisk 2/4 C 20%**		1,61	4,52	4,01	3,09
13	**Ekofisk 2/4 C**					
15	**Beryl A, 20ºC**		1,90	0,63		
16	**Beryl A, 20ºC**					
17	**Beryl A, +N+P, 20ºC**		1,07			
18	**Beryl A, +N+P, 20ºC**					
19	**Beryl A, 5ºC**		1,83	0,88	3,43	
20	**Beryl A, 5ºC**					
0	**Beryl A, +HgCl2**			2,7	2,30	

pH

No	Content	day 1 pH	Day 14 pH	Day 28 pH	Day 56 pH	Day 229 pH
1	**reference sediment**	7,65	7,33	7,19	7,33	7,24
2	**Beryl A 20%**	8,86	8,20	7,78	7,65	7,37
3	**Beryl A**	9,07		8,34		
4	**Beryl A**	8,92		8,47		
5	**Beryl A**	8,94		8,53		
6	**Ekofisk 2/4 A 20%**	9,01	8,30	8,12	8,04	7,67
7	**Ekofisk 2/4 A**		8,75			
8	**Frøy 20%**	7,80	7,21	7,06	7,07	7,05
9	**Frøy**					
10	**Lille-Frigg 20%**	8,51	8,22	7,81	7,59	7,62
11	**Lille-Frigg**		8,65	8,47	8,46	8,47
12	**Ekofisk 2/4 C 20%**	8,12	7,38	7,23	7,05	7,10
13	**Ekofisk 2/4 C**					
15	**Beryl A, 20ºC**		8,60			
16	**Beryl A, 20ºC**					
17	**Beryl A, +N+P, 20ºC**	8,77	8,60	8,47		
18	**Beryl A, +N+P, 20ºC**					
19	**Beryl A, 5ºC**		8,70	8,78	8,58	
20	**Beryl A, 5ºC**					
0	**Beryl A, +HgCl2**				8,33	

Microbial activity (FDA)

No	Content	day 1 A490/g	Day 14 A490/g	Day 28 A490/g	Day 56 A490/g	Day 229 A490/g
1	**reference sediment**	0,152	0,294	0,165	0,133	0,083
2	**Beryl A 20%**	0,074	0,148	0,104	0,130	0,063
3	**Beryl A**	0,013	0,018	0,014	0,015	0,017
4	**Beryl A**	0,011	0,016	0,015	0,011	0,016
5	**Beryl A**	0,015	0,015	0,018	0,009	0,020
6	**Ekofisk 2/4 A 20%**	0,056	0,060	0,085	0,000	0,061
7	**Ekofisk 2/4 A**	0,112	0,096	0,094	0,082	0,106
8	**Frøy 20%**	0,112	0,135	0,098	0,026	0,026
9	**Frøy**	0,238	0,308	0,027	0,061	0,000
10	**Lille-Frigg 20%**	0,064	0,080	0,087	0,073	0,055
11	**Lille-Frigg**	0,010	0,018	0,019	0,016	0,023
12	**Ekofisk 2/4 C 20%**	0,045	0,106	0,121	0,067	0,009
13	**Ekofisk 2/4 C**	0,036	0,046	0,044	0,041	0,008
15	**Beryl A, 20ºC**		0,011	0,016	0,010	0,017
16	**Beryl A, 20ºC**		0,010	0,013		
17	**Beryl A, +N+P, 20ºC**		0,013	0,015	0,010	0,043
18	**Beryl A, +N+P, 20ºC**					
19	**Beryl A, 5ºC**		0,016	0,018	0,012	0,069
20	**Beryl A, 5ºC**					
0	**Beryl A, +HgCl2**			0,009	0,010	

Appendix 2

Anaerobic degradation trial data

Trial 2 - anaerobic

Sulfide

No	Content	day 1 ppm	Day 28 ppm	Day 56 ppm	100 ppm
1	**reference sediment**	<0,2	<0,2	<0,2	<0,2
2	**Beryl A 20%**	<0,2	<0,2	<0,2	<0,2
3	**Beryl A**	<0,2	<0,2	<0,2	<0,2
4	**Beryl A**	<0,2	<0,2	<0,2	<0,2
5	**Beryl A**	<0,2	<0,2	<0,2	
6	**Ekofisk 2/4 A 20%**	0,4	<0,2	<0,2	1,6
7	**Ekofisk 2/4 A**	0,8	<0,2	2,3	6,2
8	**Frøy 20%**	0,5	<0,2	1,9	119,0
9	**Frøy**	0,9	<0,2	9,3	345,2
10	**Lille-Frigg 20%**	0,7	<0,2	0,7	<0,2
11	**Lille-Frigg**	0,6	<0,2	0,7	<0,2
12	**Ekofisk 2/4 C 20%**	0,6	<0,2	<0,2	<0,2
13	**Ekofisk 2/4 C**	1,1	<0,2	<0,2	0,1
15	**Beryl A, 20ºC**		<0,2	<0,2	<0,2
16	**Beryl A, 20ºC**				
17	**Beryl A, +N+P, 20ºC**		<0,2	<0,2	<0,2
18	**Beryl A, +N+P, 20ºC**				
19	**Beryl A, 5ºC**		<0,2	<0,2	<0,2
20	**Beryl A, 5ºC**				

Oxygen

No	Content	day 1 ppm	Day 28 ppm	Day 56 ppm	100 ppm
1	**reference sediment**	3,06	2,33	3,07	1,49
2	**Beryl A 20%**	3,21	2,10	0,80	0,40
3	**Beryl A**	3,04	2,13	1,22	0,64
4	**Beryl A**	3,10	3,01	1,25	0,48
5	**Beryl A**	2,96	2,47	1,88	
6	**Ekofisk 2/4 A 20%**	2,76	1,35	1,03	0,30
7	**Ekofisk 2/4 A**	2,25	0,88	0,32	0,16
8	**Frøy 20%**	2,95	2,13	0,19	0,07
9	**Frøy**	2,79	2,61	0,03	0,00
10	**Lille-Frigg 20%**	3,30	2,67	1,98	1,72
11	**Lille-Frigg**	3,30	2,76	2,54	2,38
12	**Ekofisk 2/4 C 20%**	3,02	1,67	1,42	0,60
13	**Ekofisk 2/4 C**	2,80	1,55	0,74	0,54
15	**Beryl A, 20ºC**	2,42	1,25	1,27	0,78
16	**Beryl A, 20ºC**				
17	**Beryl A, +N+P, 20ºC**	2,24	2,92	1,42	0,71
18	**Beryl A, +N+P, 20ºC**				
19	**Beryl A, 5ºC**	3,09	4,12	2,50	2,18
20	**Beryl A, 5ºC**				

pH

No	Content	day 1 pH	Day 28 pH	Day 56 pH	Day 100 pH
1	**reference sediment**	7,64	7,25	7,40	6,84
2	**Beryl A 20%**	8,37	8,12	7,67	7,79
3	**Beryl A**	8,96	8,48	8,21	8,20
4	**Beryl A**	8,87	8,64	8,05	7,99
5	**Beryl A**	8,94	8,54	8,30	
6	**Ekofisk 2/4 A 20%**	8,52	8,13	7,98	8,25
7	**Ekofisk 2/4 A**	9,16	8,76	8,19	8,38
8	**Frøy 20%**	7,89	7,39	6,96	7,05
9	**Frøy**	7,76	7,06	6,89	7,07
10	**Lille-Frigg 20%**	8,37	8,38	8,01	7,95
11	**Lille-Frigg**	8,80	8,71	8,40	8,35
12	**Ekofisk 2/4 C 20%**	7,92	7,25	7,32	7,38
13	**Ekofisk 2/4 C**	8,34	7,23	7,38	7,37
15	**Beryl A, 20ºC**	8,93	7,77	7,78	7,88
16	**Beryl A, 20ºC**				
17	**Beryl A, +N+P, 20ºC**	8,89	8,44	8,00	8,13
18	**Beryl A, +N+P, 20ºC**				
19	**Beryl A, 5ºC**	8,95	8,87	8,81	8,75
20	**Beryl A, 5ºC**				

Microbial activity (FDA)

No	Content	day 1 A490/g	Day 28 A490/g	Day 56 A490/g	Day 100 A490/g
1	**reference sediment**	0,152	0,123	0,169	0,162
2	**Beryl A 20%**	0,074	0,129	0,238	0,279
3	**Beryl A**	0,013	0,074	0,114	0,129
4	**Beryl A**	0,011	0,049	0,126	0,141
5	**Beryl A**	0,015	0,006	0,106	
6	**Ekofisk 2/4 A 20%**	0,056	0,217	0,305	0,371
7	**Ekofisk 2/4 A**	0,112	0,336	0,555	0,471
8	**Frøy 20%**	0,112	0,295	0,654	0,721
9	**Frøy**	0,238	0,754	1,050	1,445
10	**Lille-Frigg 20%**	0,064	0,071	0,123	0,112
11	**Lille-Frigg**	0,010	0,000	0,035	0,041
12	**Ekofisk 2/4 C 20%**	0,045	0,079	0,143	0,164
13	**Ekofisk 2/4 C**	0,036	0,058	0,084	0,097
15	**Beryl A, 20ºC**		0,079	0,109	0,108
16	**Beryl A, 20ºC**				
17	**Beryl A, +N+P, 20ºC**		0,031	0,130	0,161
18	**Beryl A, +N+P, 20ºC**				
19	**Beryl A, 5ºC**		0,017	0,073	0,060
20	**Beryl A, 5ºC**				

Appendix 3

Master thesis of Inger Smedberg

Fluorescence as a screening method for THC in sediment samples

Hovedoppgave (MsC)

University College Stavanger

Spring 2001

Acknowledgement

I would like to give my best thanks to Grete Jonsson, who was my supervisor at Rogalandsforskning in Mekjarvik. I would also like to thank Grethe Kjeilen for involving me in the UKOOA project, and thanks to Sigfryd Torgrimsen and Kjell Birger Øysæd for guidance at the laboratory in Mekjarvik.

Also thanks to Peter Ruoff at Stavanger University College, who showed enthusiasm and encouragement for my work.

Inger Smedberg

Abstract

The aim of the project that this thesis is part of is to decide what is the best environmental option for dealing with cuttings piles.

One of the parameters used for predicting the natural degradation of oil in cuttings piles was total hydrocarbon (THC) concentration. THC was decided by use of gas chromatography, a time consuming and thus expensive method. The main objective of this work was to investigate if there exists a correlation between total hydrocarbon concentration and aromatic content in sediment samples from cuttings piles. Aromatic content is decided from fluorescence analysis. If a correlation was observed and fluorescence analysis could be used for prediction of THC, that would give a time and cost benefit.

This work started by making fluorescence measurements on previously extracted sediment samples. THC measurements had also been made. From this work it occurred that many factors were affecting the fluorescence response of a sample. Some of these effects, inner filter effect, resonance energy transfer and self-absorption were then investigated. These investigations led to the awareness that the relationship between concentration and fluorescence response is not necessarily linear, and that the combinations and concentrations of species present in the solution measured can affect the observed fluorescence.

After these investigations had been made, samples assigned the work on the thesis were extracted and prepared for gas chromatographic and fluorescence measurements. THC was decided and fluorescence measurements were made. It appeared that the experimental set-up was not ideal, and due to this no conclusion about the correlation could be drawn.

Abbreviations

UKOOA	UK offshore Operators Association
OBM	oil-based drilling muds
WBM	water-based drilling muds
THC	total hydrocarbon
GC	gas chromatography
FID	flame ionisation detector
SFS43	synchronous fluorescence scan, $\Delta\lambda$=43nm
PMT	photomultiplier tube
RET	resonance energy transfer
HDF	high-density fluid
IS1	internal standard 1; $C_{20}D_{42}$
IS2	internal standard 2; $C_{30}H_{62}$
BaP	benzo[a]pyrene
a u	arbitrary units
DCM	dichloromethane

Table of contents

1 Objective of this work

This thesis is part of a large project [1] executed on the initiative from the UK Offshore Operators Association (UKOOA), the British organisation corresponding to the Norwegian OLF (oljeindustriens landsforening). The UKOOA cuttings pile initiative is based on the growing appreciation that the decommissioning of offshore oil platforms incorporates more than just structures. Any material residues that may affect North Sea stakeholders or the ambient environment (marine, terrestrial or air) also need to be considered, assessed and abandonment planned. Piles of drilling muds and cuttings, which are the remains of historic drilling activity, are residual materials that require special attention. The aim of the UKOOA project is to decide what is the best environmental option for dealing with cuttings piles. The options are

1. Leave the cuttings in place and
   a) allow natural degradation
   b) apply enhanced bio-remediaton
   c) cover
2. Lift the cuttings to the surface and
   a) reinject them into wells
   b) transport them to shore and treat

The UKOOA project is divided into 2 phases. The first phase was a desktop study. Table 1-1 shows the tasks of the second phase.

Table 1-1. Tasks of the second phase in the UKOOA project.

Task Ref.	**STUDY TITLE**	**CONTRACTOR**
1	Characterisation of cuttings piles	RF Rogaland Research (Norway)
2a	Toxicokinetics of water based mud drill cuttings contaminants in marine sediment	ERT (Scotland) Ltd (Edinburgh)
2b	Assessment of the actual present enviromental impacts of representative oil based mud and water based mud cuttings piles	Cordah Enviromental Management Consultants (Aberdeen) with Akvaplan Niva (Norway)
2c	Water column and food chain impacts	URS-Dames & Moore (Aberdeen) with TNO (Netherlands)
3	**Initiate time series data on factors determining future pile physical size and shape and thus enviromental effect**	**RF Rogaland Research (Norway**) with SINTEF (Norway), ERT (Scotland) Ltd (Edinburgh) and AEA Technology plc (Abingdon)
4	Adapt and update mathematical disturbance model	BMT Marine Information Systems (Southampton)
5a	In-situ solutions: enhanced bio-remediation	AEA Technology plc (Abingdon) with SØRCO and SINTEF (both Norway)

Table 1-1 continued

5b	In-situ solutions: covering	Dredging Researc Ltd (Godalming) with CEFAS /Burnham on Crouch), Enviromental Resources Management (Edinburgh) and Galibraith Consulting (Aberdeen)
6	Feasibility and enviromental impact of offshore lifting	Managed by BP (Aberdeen) with Halliburton Subsea (Aberdeen); SWACO (Aberdeen), CEFAS (Burnham) anf AGR

Rogaland Research is working on the part concerning natural degradation and recovery (phase 2.3). The objective is to indicate time series data on factors determining future pile characteristics from representative OBM (oil-based drilling muds) and WBM (water-based drilling muds) cuttings. The time series data are to be fed into a mathematical model (task 4) that predicts the fate of cuttings piles with time. To generate the time series data samples are examined on for instance sulphide generation, microbial activity, oxygen content, pH and total hydrocarbon (THC) concentration. The examination of THC is a time consuming and expensive piece of work, performed on gas chromatography (GC) with flame ionisation detector (FID). Each run on the GC-FID takes more than 90 minutes. This was the starting point of this thesis. The first part was to examine if fluorescence could be used as a screening method for examination of THC. The main species in oil that give fluorescence are the aromatics.

Figure 1-1. Fluorescence responses of oil compounds [2].

The task was then to examine if there is a correlation between the observed fluorescence due to aromatics and THC measured with GC-FID. If a correlation was observed, and fluorescence could be used to predict the THC content, that would give a large time and cost benefit. A fluorescence measurement is done in a few minutes compared to more than 90 minutes with GC-FID. At the same time as fluorescence was examined as a screening method, a number of fundamentals of fluorescence were investigated. The second part of the thesis was to examine the effect that changes in temperature and addition of nutrients had on the degradation rate. To examine this, samples from one cuttings pile, Beryl A, were incubated at elevated temperature, elevated temperature and nutrients added, and lowered temperature.

2 Materials and methods

2.1 Chemicals and analytical equipment

2.1.1 Experimental work on inner filter effect (chapter 2.3.3.2)

Instrument characteristics:

Fluorescence spectrophotometer
HITACHI, F-4500
Quarts cuvette, light path 10mm

UV/VIS Spectrophotometer
Perkin Elmer, Lambda 15
Quarts cuvette, light path 10mm

Chemicals:

n-hexane,	HPLC quality	(MERCK)
dichloromethane,	HPLC quality	(MERCK)
HDF 200,		(Baroid)

2.1.2 Experimental work on resonance energy transfer (chapter 2.3.4.2)

Instrument characteristics:

Same as for 2.1.1

Chemicals:

n-hexane,	HPLC quality	(MERCK)
dichloromethane,	HPLC quality	(MERCK)
naphthalene,	>99%,	(KeboLab)
antracene,	>98%,	(Sigma)

2.1.3 Experimental work on self-absorption (chapter 2.3.5.2)

Same as for 2.1.2

2.1.4 Extraction of sediment samples (chapter 2.4.2)

Instrument characteristics:

Soxtherm 2000, Gerhardt, Bonn, Germany

- S 306 AK

Technical data Soxtherm extraction unit:

- Width: 550 mm
- Depth: 290 mm
- Height: 350 mm
- Cooling water consumption: 750 L/h
- Cooling water pressure: > 3 bar
- Power consumption: 1000 W

Chemicals:

Internal standard:
0.5g n-eicosane-d_{42}, $C_{20}D_{42}$ 99.2% (Chiron) = IS1
0.25g triacontane, $C_{30}H_{62}$ 99.5% (Fluka) = IS2
Dissolved in, and diluted to 25mL with isooctane, HPLC quality (Merck).

Other analytical equipment:

Extraction Thimbles, 33x80mm, Schleider & Schnell (KeboLab, Bergen)

Visiprep Solid Phase Extraction Vacuum Manifold (Supelco)

Solid Phase extraction tubes, Normal phase packing LC-Si, 3mL, 0.5g (Supelco)

2.1.5 Performance of GC-FID measurements (chapter 2.4.3.1)

Instrument characteristics:

For the analysis of THC a gas chromatograph, HP 5890 series II, with auto sampler, HP7673, was used. Software used was Millennium chromatography manager (1997), Waters.

Column:

- Hewlett Packard Ultra Performance Capillary Column. Ultra 1 (cross linked methyl siloxane)
- Film thickness: 0.33µm
- Length: 50m
- Phase ratio: 150
- Column ID: 0.2mm

This is a non-polar column.

Mobile phase:

Helium. (The Van Deemters plot shows (figure 2.2.1-3) helium has a broad area of flow speeds resulting in high efficiency).

Injector:

Split/splitless; held in a splitless mode for 1 minute.

Temperature program:

• Injector temperature:	290°C	
• Detector temperature:	300°C	
• Ramp:	25°C/min	50-120°C
	3°C/min	120-320°C
• Hold time 320°C:	20min	

Detector:

Flame ionisation detector (FID).

2.1.6 Fluorescence analysis of sediment samples (chapters 2.4.4.1 and 2.4.4.2)

Instrument characteristics:

Luminescence spectrometer
Perkin Elmer, LS50B
Quarts cuvette, light path 10mm

Chemicals:

n-hexane,	HPLC quality	(MERCK)
dichloromethane,	HPLC quality	(MERCK)
benzo[a]pyrene,	>98%	(Fluka)
pyrene,	purity not given	(Sigma)
naphthalene,	>99%	(KeboLab)

2.2 Gas chromatography

2.2.1 Theory of gas chromatography

Chromatography [3,4] is a technique in which the components of a mixture are separated based upon the rates at which they are carried through a stationary phase by a gaseous or liquid phase.

The mobile phase in chromatography is a phase that moves over or through the stationary phase, carrying the analyte with it. When the mobile phase in a chromatographic system is a gas, the technique is called gas chromatography (GC). In contrast to most other types of chromatography, the mobile phase in GC does not interact with molecules of the analyte; its only function is to transport the analyte through the column.

Gas chromatography is always performed as column chromatography, where the stationary phase is held in a narrow tube and the mobile phase is forced through the tube under pressure or by gravity. If the stationary phase is an adsorption medium the term gas-solid chromatography (GSC) is used, and in the case of a non-volatile liquid as stationary phase the term gas-liquid chromatography (GLC) is used.

The species to be analysed on GC have to be volatile and stabile at the temperatures used. The sample is vaporized and injected onto the head of a chromatographic column.

All chromatographic separations are based upon differences in the extend to which solutes are partitioned between the mobile phase and the stationary phase, and each component has a characteristic retention time. The retention time is the time between the injection of a sample and the appearance of a solute peak at the detector of a chromatographic column. A GC analysis can give qualitative as well as quantitative information, qualitative in the way that each component has its characteristic retention time and quantitative by integrating the peaks.

Gas chromatography is performed on a gas chromatograph.

Figure 2.2.1-1. Schematic of a gas chromatograph. 1= high-pressure cylinder with mobile phase, 2= reduction valve, 3= injector, 4= column oven, 5= column, 6= detector, 7= printer.

To be able to separate a mixture of components successfully, it is important to choose the optimum combination of experimental conditions. Such experimental conditions can be the type of stationary and mobile phase, length and diameter of the column as well as pressure, temperature etc.

The purpose of the mobile phase is to transport the analyte through the column. The gaseous mobile phase is to be inert, and not react with the sample or the stationary phase. The most commonly used gases are nitrogen, helium and hydrogen. The choice of the mobile phase will influence the time consume of the analysis and the efficiency. The lower plate height, the better efficiency.

Figure 2.2.1-2. Van Deemters plot for nitrogen, helium and hydrogen.

The Van Deemters plot shows that if the gases are used at optimum flow speed, the efficiency and time consume will decrease as follows: nitrogen>helium>hydrogen. Hydrogen and helium have a larger range of flow speeds resulting in good efficiency, and is thus not so sensitive to changes in flow speed.

Most chromatographs have a vaporization injector. A thermostatic controlled oven heats the injector, and the mobile phase is heated to the selected temperature before it is led to the injector. The temperature should be so high that the sample is vaporized quickly, but not so high that thermo labile components are decomposed. The samples are injected with a syringe. Three injection systems are used; split, split less and on column. A split injection is a customary vaporization injection where the sample is evaporated, but split before it is led to the column. This way most of the sample is ventilated out. This corrects for variations in injected volume.

There are three types of GC-columns; preparative, analytical and capillary columns. Preparative columns are used for isolating species after a gas chromatographic separation and analytical ones are used for ordinary analytical gas chromatography. Capillary columns are columns in which the stationary phase covers the inside wall of the column. The columns are also called “wall-coated open tubular column” (WCOT).

The temperature of the column will affect the retention of the components, and the retention time will decrease as the column temperature is increasing. The column temperature should be high enough to perform the analysis as quickly as possible, but not so high that the

separation is bad. Analysis can be performed isothermally, or with a temperature program where the temperature of the column increases as a function of the time of the analysis. Temperature programming is used for mixtures of components with greatly differing boiling points

Figure 2.2.1-3. Effect of temperature on gas chromatograms. (a) Isothermal at 45°C (b) Isothermal at 145°C (c) programmed at 30°C to 180°C

The higher the temperature is, the shorter is the retention time of the components, but the separation is bad. With temperature programming the best chromatograms are obtained.

Depending on the type of detector being used different information can be obtained. Flame ionisation detector (FID) is the most widely used and generally applicable detector for gas chromatography.

Figure 2.1.1-4. A flame ionisation detector.

The effluent from the column is mixed with hydrogen and air and electrically ignited. Most organic compounds, when pyrolyzed at the temperature of a hydrogen/air flame, produce ions and electrons that can conduct electricity through the flame. The flame ionisation detector responds to the number of carbon atoms entering the detector per unit of time, and is hence a mass sensitive rather than a concentration-sensitive device. As a consequence, this detector has the advantage that changes in flow rate of the mobile phase have little effect on detector response.

It is difficult to inject samples in μL range with a good reproducibility. To compensate for this internal standard is added. The standard calibration curve is made after analysis of solutions with known amount of the analyst of interest, and a constant volume of internal standard added before work up. The relations between the total area and the peak area of the internal standard are plotted against the amount of the analyst of interest.

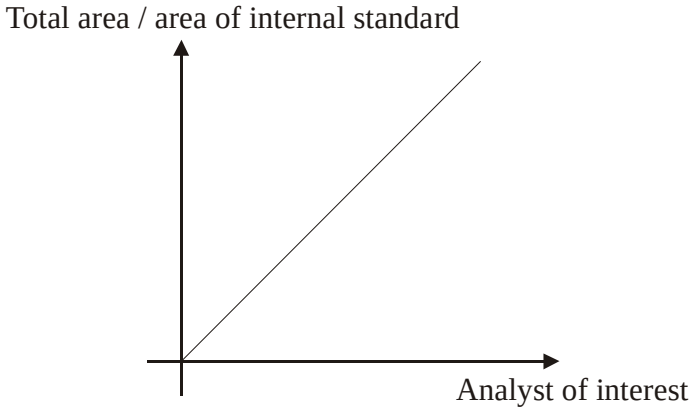

Figure 2.2.1-5. Standard curve

A mathematical expression of the curve is made by linear regression. The area relation in the real samples is decided from integration of the chromatogram, and the amount of the analyst of interest in the sample is decided from the mathematical expression. The internal standard can also correct for variations in the chromatographic system during the analysis. When there is a comprehensive sample work up, such as extraction and evaporation, the internal standard also corrects for variations during work up. An internal standard should ideally fulfil the following requirements:

- it has to be separated from the other compounds in the sample
- its retention time should be near that of the compounds of interest in the sample
- it has to behave like the other compounds during work up

- it must not already be in the sample
- it must be stabile
- it has to be available in pure form
- the response of the internal standard should not be higher then 10 times the lowest signal in the sample, and not smaller then 1/10 of the highest signal.

2.2.2 Application of GC-FID in this work

GC-FID was applied to measure the total hydrocarbon (THC) concentration in extracted sediment samples. THC in this method is defined to be all carbon that can be oxidised, consisting of an n-alkane chain with 12 or more carbon atoms, extracted by the method described in chapter 2.4.2. This analysis takes more than 90 minutes.

2.3 Fluorescence spectroscopy

2.3.1 Theory of fluorescence – in general

Fluorescence spectroscopy [5,6,7] is an optical method in which atoms or molecules of the analyte are excited by the absorption of a beam of electromagnetic radiation. The excited species then relax to the ground state, giving up their excess energy as photons. The resulting emission spectra provide both qualitative and quantitative information.

The energies and wavefunctions of molecules can be separated into different contributions. These are electronic, vibrational and rotational energies.

$$E_{tot} = E_{el} + E_{vib} + E_{rot}$$

Energy levels of a molecule are illustrated in figure 2.3.1-1

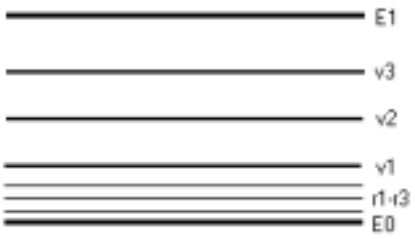

Figure 2.3.1-1. Energy levels of a molecule.

E_0 and E_1 are electronic levels, v_1, v_2 and v_3 are vibrational levels and r_1, r_2 and r_3 are rotational levels.

The excitation in fluorescence spectroscopy is brought about by absorption of a beam of electromagnetic radiation. After absorption the molecule is excited to some higher vibrational level of either E_1 or E_2 (figure 2.3.1-2a).

The excess vibrational energy is then dissipated through vibrational relaxation, or collisions, and the excited molecule is now at the lowest vibrational level of E_2 or E_1 (figure 2.3.1-2 b). This process is called internal conversion and generally occurs in 10^{-12} s or less.

From here the excited molecule may undergo many de-excitation pathways. One possibility is that the excited species return to the ground state still by internal conversion (figure 2.3.1-2 b). This transition does not result in fluorescence. Another possibility is to give up the excess energy as photons. Such a transition is called fluorescence (figure 2.3.1-2 c), and the emitting species are called fluorophores.

Figure 2.3.1-2. Energy-level diagram showing some of the energy changes that occur during a)absorption, b)non-radiative relaxation, and c)fluorescence by molecular species.

Return to the ground state typically occurs to a higher excited vibrational ground-state level. An interesting consequence of emission to higher vibrational ground states is that the emission spectrum is typically a mirror image of the absorption spectrum of the E_0 to E_1 transition (figure 3.1.3-4). The electronic transitions responsible for the fluorescence do not involve a change in the electron spin. Fluorescence is hence short lived, ceasing almost immediately ($<10^{-5}$s). The number of molecules that emit light is relatively small, because fluorescence requires structural features that slow the rate of non-radiative relaxation processes. Typical molecules that fluoresce are aromatics, which are rigid and not able to give up their excess energy as vibrational energy (figure 1-1).

Examination of figure 2.3.1-2 reveals that the energy of the emission is typically less than that of absorption. Hence, fluorescence typically occurs at lower energies or longer wavelengths. This phenomenon is called a Stokes shift, and is due to some energy being lost by non-radiative relaxation. If the wavelength for emission is the same as that for absorption it is called resonance fluorescence.

Fluorescence is measured with a fluorescence spectrophotometer.

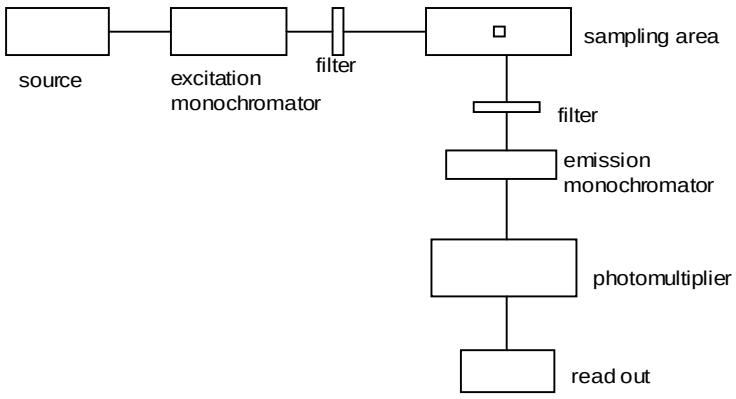

Figure 2.3.1-3. Schematic of a fluorescence spectrophotometer

UV/VIS light is generated at the source, and the light passes through the excitation monochromator, where the wavelength of the excitation beam is selected. The beam then passes through a filter, which transmit all radiation above a specified wavelength and absorbe completely at lower wavelengths. These are used to remove second (and higher) grating radiation and the scattered exciting radiation. As the beam enters the cell in the sampling area, the emitted light is measured at 90° angels to the excitation beam. The emitted light passes through the emission monochromator, which selects the wavelength chosen for measuring the fluorescence. The intensity of the emitted light is measured with a photo multiplier tube.

There are different ways to operate a fluorescence spectrophotometer. These are:

1. Excitation scan
An excitation scan is a scan in which the excitation monochromator is set to vary over a range of excitation wavelengths. The emission monochromator is set at a fixed wavelength.

2. Emission scan
An emission scan is a one in which the excitation monochromator is set at a fixed wavelength, and the emission monochromator is set to vary over a range of emission wavelengths.

3. Synchronous fluorescence scan (SFS)
In a synchronous fluorescence scan the excitation monochromator is set to vary over a range of excitation wavelength, but instead of a fixed emission wavelength the emission and excitation monochromators are allowed to vary simultaneously. The gap between them is called $\Delta\lambda$, and this gap is maintained during the scan. Synchronous spectra generally result in a more structured spectral profile than those obtained in conventional emission spectra with a consequent increased discrimination potential [8].

4. 3D-scan
A 3D-scan is a combination of a number of excitation scans and a number of emission scans, shown as excitation wavelength along one axis, emission wavelength along the second axis and emission intensity along the third axis (see cover page).

2.3.2 Problems correlated to fluorescence measurements

In the beginning of the work on this thesis a lot of previously extracted sediment samples were analysed on a fluorescence spectrophotometer. Both emission scans and synchronous fluorescence scans were taken. It was thought that maybe it could be possible to choose some reference points in the spectra, and simply compare fluorescence intensities at these points in different samples and predict the hydrocarbon content. By dilution of some of the samples it was observed that at some wavelengths there was a non-linear relation between concentration and emission intensity. This led to theoretical and practical investigations on the subjects inner filter effect, resonance energy transfer and self-absorption. These aspects make fluorescence quite difficult for quantitative analysis.

2.3.3 Inner filter effect

2.3.3.1 Theory

The phenomenon of inner filter effect [9] is characterized by decreasing emission intensity, ϕ, with increasing concentration after a certain concentration in the fluorescent species has been reached. According to Lambert Beers law:

$A = \varepsilon\, c\, l$ (eqn. 2.3.3.1-1)

A = absorbance
ε = molar absorptivity ($M^{-1}\ cm^{-1}$)
c = molar concentration (M)
l = path length though medium (cm)

Absorbance is also given as:

$A = -\log_{10}(I / I_0)$ (eqn. 2.3.3.1-2)

I_0 = intensity of the incoming excitation beam
I = intensity of the beam after the cell

Combining the two expressions for absorbance gives:

$-\varepsilon\, c\, l = \log_{10}(I / I_0)$ (eqn. 2.3.3.1-3)

I can be expressed as $I_0\ (10^{-\varepsilon\, c\, l})$. I_a is a measure of the light absorbed, and can be expressed as follows:

$I_a = I_0 - I = I_0 - I_0\ (10^{-\varepsilon\, c\, l}) = I_0\ (1 - 10^{-\varepsilon\, c\, l})$ (eqn. 2.3.3.1-4)

The intensity of fluorescence, ϕ, is given as:

$\phi = q\, I_a$ (eqn. 2.3.3.1-5)

q is a factor quantifying how much of the absorbed light that is capable of generating fluorescence, and is called quantum yield. Theoretically q = 1 and hence:

$\phi = I_a = I_0\ (1 - 10^{-(\varepsilon\, c\, l)})$ (eqn. 2.3.3.1-6)

According to this the fluorescence intensity ϕ should show saturating behavior with increasing concentration of the fluorescent compound (figure 2.3.3.1-1).

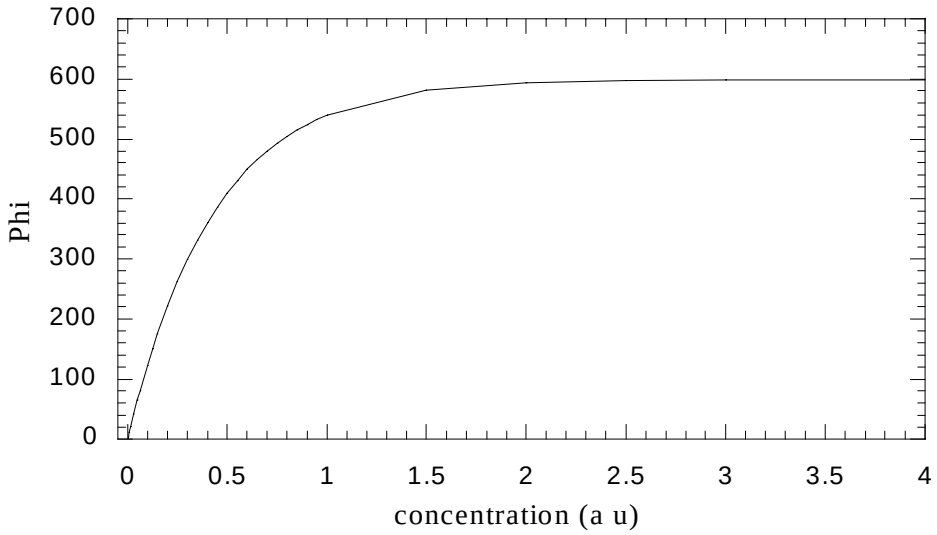

Figure 2.3.3.1-1. Theoretical calibration curve increasing up to $I_0 = 600$.

However, in the case of a standard orthogonal and rectangular beam/cell arrangement, the photomultiplier tube (PMT) senses only part of the emitted fluorescence radiation. For high concentrations of the fluorescent compound, strong absorption (and fluorescence) may occur even before the excitation beam enters the measuring area of the photomultiplier. Thus, as the concentration of the fluorescent compound increases an apparent decrease in fluorescence in the measuring zone may be found.

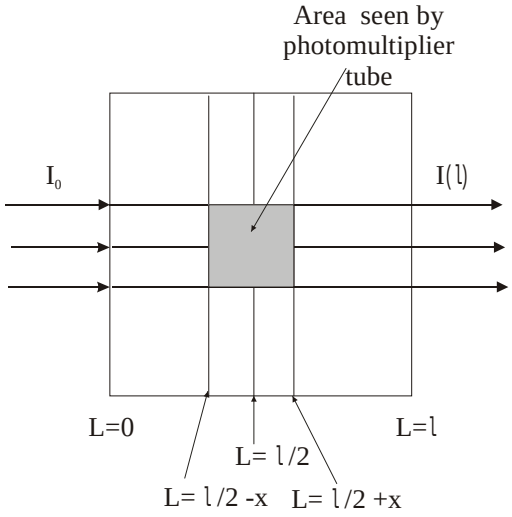

Figure 2.3.3.1-2. Schematic drawing of fluorescent solution inside fluorimetric cell with light path length l. The inner filter effect is due to the fact that only a part of the light path (starting from L=(l/2)-x to L=(l/2)+x) is recognized by the photomultiplier

$I(l) = I_0 (10^{-\varepsilon c l})$ makes it possible to calculate I for any value of l. The photomultiplier is measuring in the area from $l/2 - x$ to $l/2 + x$. The absorption in this area is $I(l/2 - x) - I(l/2 + x)$, and $\phi = q(I(l/2 - x) - I(l/2 + x))$. ϕ can hence be expressed as:

$$\phi = q (I_0 10^{-\varepsilon c (l/2 - x)} - I_0 10^{-\varepsilon c (l/2 + x)}). \qquad \text{(eqn. 2.3.3.1-7)}$$

For different combinations of I_0, x and ε, dissimilar shapes of the calibration curve can be observed. In figure 2.3.3.1-3 some examples are given.

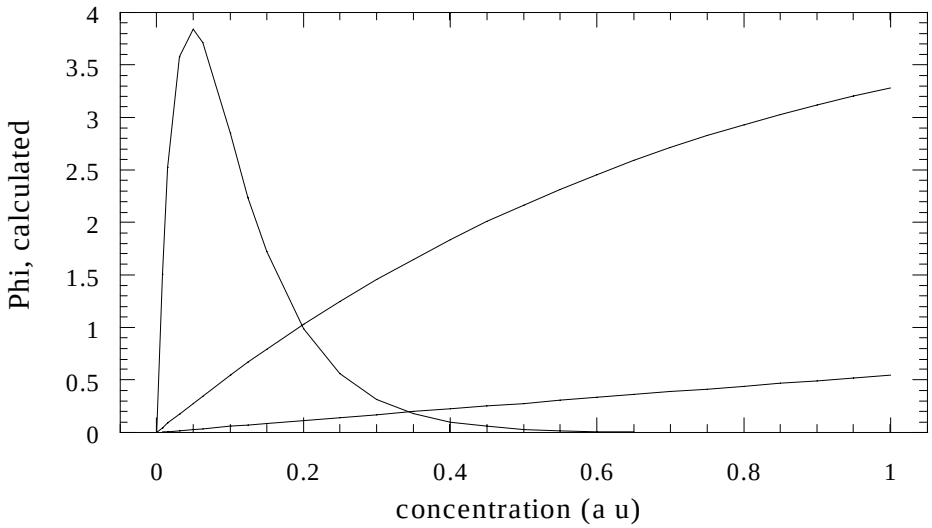

Figure 2.3.3.1-3. Possible shapes of calibration curves based on simulations of ϕ made in mathematical spreadsheet.

2.3.3.2 Experimental work

The first part of the experiments to examine the inner filter effect was simulations made in a mathematical spreadsheet. Based upon the theoretical expression for emission intensity, equation 2.3.3.1-7, simulations were done by keeping two of the parameters constant, varying the third one. The effect that the variations had on the shape of the calibration curve was observed (figures 3.1.1-1 to 3.1.1-3). A calibration curve is a curve showing the relationship between concentration and emission intensity. The effect of changing ε, x and I_0 was investigated. Simulations were also made to see if the theoretical expression could be adjusted to approach an experimental calibration curve (figures 3.1.1-4 to 3.1.1-6).

Based on the observations from the simulations and the experimental calibration curves at different excitation wavelengths, the absorption characteristics of a standard oil were investigated. The standard oil used was HDF 200, an oil with molecular weight of 221g/mole and aromatic content of 3.8%. One standard solution of this oil was made of 0,0221g HDF 200 to 24.4846g solvent. The solvent used throughout all experiments was 1:1 n-hexane: dichloromethane. Absorption measurements were made using a double beam instrument. Absorbance was measured from 200 to 400nm of the standard solution and dilutions of 63.3%, 50.8%, 35.5% and 18.3% relative to the standard solution (figure 3.1.1-7). The dilutions were based on weight, not volume, because it is hard to pipette the solvent due to low surface tension and high volatility. A new, stronger solution was made of 0.4639g HDF 200 to 23.7961g solvent, maximising the absorbance at 281nm. Dilutions of 80,8%, 59,1%, 38,7% and 19,8% relative to the standard solution were made. Absorption spectra from 250 to 400nm were recorded of the standard solution and all dilutions (figure 3.1.1-8). Correspondingly emission scans from 200 to 600nm with excitation wavelength 281 (figure 3.1.1-17), 288 (figure 3.1.1-19), 330 (figure 3.1.1-21), 339, 362 (figure 3.1.1-24) and 386nm were taken of these dilutions.

For a solution of two drops HDF 200 added to the 3mL cuvette containing solvent, a time drive spectrum of absorbance was recorded at 386nm for 500 seconds (figure 3.1.1-15).

2.3.4 Resonance energy transfer

2.3.4.1 Theory

Resonance energy transfer (RET) [10] is a process occurring whenever the emission spectrum of a fluorophore, called the donor, overlaps with the absorption spectrum of another molecule, called the acceptor.

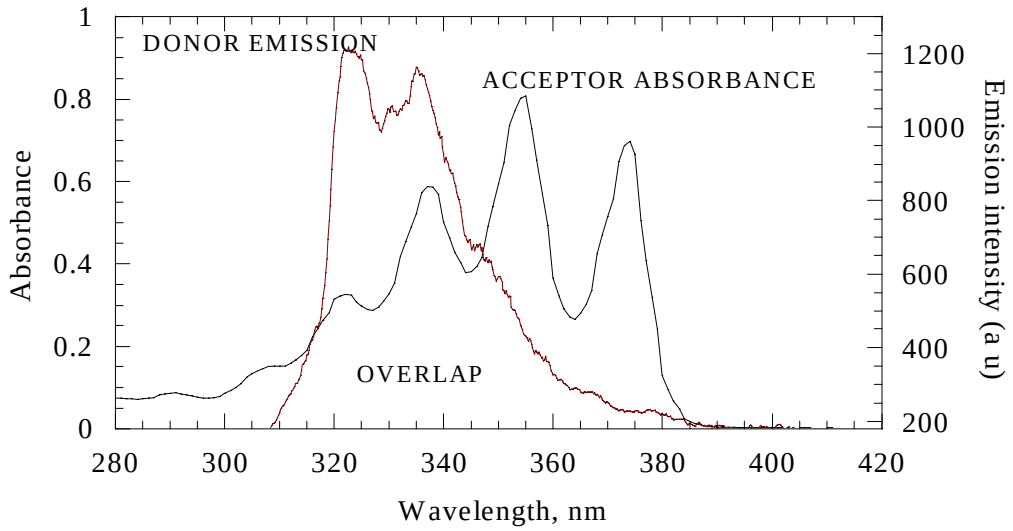

Figure 2.3.4.1-1. Absorbance spectrum of naphthalene and emission spectrum of antracene.

The acceptor does not need to be fluorescent. RET does not involve emission of light by the donor, and is hence not the result of emission from the donor being absorbed by the acceptor. RET is a radiationless transfer of excitation energy from a donor to an acceptor chromophore. There is no intermediate photon in RET, but the donor and acceptor are coupled by dipole-dipole interactions. The distance between the donor and acceptor, and the extent of spectral overlap determines the extent of energy transfer. The transfer of electronic excitation energy from one atom or molecule to another may involve different electronic states of both the donor and acceptor, and may be governed by different mechanisms. In all these mechanisms, the transfer takes place under the condition of conservation of total energy and occurs thus as a resonance process. The conservation of energy requires that the energy of the electronic state of the acceptor molecule must be either the same or less than that of the donor molecule. The excess of electronic energy after transfer has taken place may be dissipated into vibrational energy.

If both the donor and the acceptor are fluorescent RET is seen as the peaks of the donor decreasing and the peaks of the acceptor increasing (until inner filter effect is influencing) with increasing addition of acceptor (figure 3.1.2-3). If the acceptor is not fluorescent RET is only seen as the donor-signal decreasing with increasing addition of acceptor.

RET [11] offers an experimental approach to the determination of molecular distances in the range 10-80 Å, through measurements of the efficiency of energy transfer between a donor and an acceptor located at specific sites. Because of the sensitive inverse sixth power

dependence of the transfer efficiency on the donor-acceptor distance, RET is a sensitive technique for detection of global structure alterations.

2.3.4.2 Experimental work

To examine for resonance energy transfer (RET) solutions of antracene and naphthalene were made. The concentration at this point was not of interest, since this part was qualitative. It was only important to be aware that the solutions were weak enough, otherwise no signal would be observed due to inner filter effect. For both solutions absorption spectra from 200 to 400nm were taken, and emission spectra from 200 to 600nm with excitation wavelength 250nm (figure 3.1.2-1 and 3.1.2-2).

A standard solution of naphthalene was made. This solution was to give a suitably strong signal in an emission scan with excitation wavelength 250nm, so that reduction in peak height could be observed. The solution was finally made of 0.0049g naphthalene and 49.1174g solvent. The density of the solvent was $0.99 g/cm^3$, so the molar concentration of the naphthalene standard was $7,7054\ 10^{-4}$. The standard solution of antracene should have a concentration so that RET could be observed, but not so strong that the naphthalene peak in the emission spectrum disappeared before 4-5 drops had been added the naphthalene standard solution. First one solution of 0.003g antracene and 24.622g solvent was made. Additions of this solution to the naphthalene standard gave too few data points, so the solution was diluted 50% by weighing, and the concentration of the standard solution was hence $3,3835\ 10^{-4}$. To know the volume added, five drops of antracene solution was weighed 20 times, and 2 drops weighed 10 times. Based on the average weight and the density of the solvent, the volume of one drop was calculated. The empty, dry cuvette was weighed, and standard solution of naphthalene added. Emission scan from 200 to 600 with excitation wavelength 250nm of the standard solution was taken. The cuvette was weighed before one drop of antracene standard solution was added to the cuvette and another emission scan taken. This procedure was repeated until a total of 12 drops had been added. Then three and three drops were added, until a total of 40 drops had been added (figure 3.1.2-3). The weighing of the cuvette before addition of antracene was to keep control with evaporation of solvent.

2.3.5 Self-absorption

2.3.5.1 Theory

In RET energy is transferred from one species to another, but in self-absorption [12] energy is transferred within one fluorophore. Self-absorption is expected whenever the absorption spectrum and the emission spectrum of one species are overlapping.

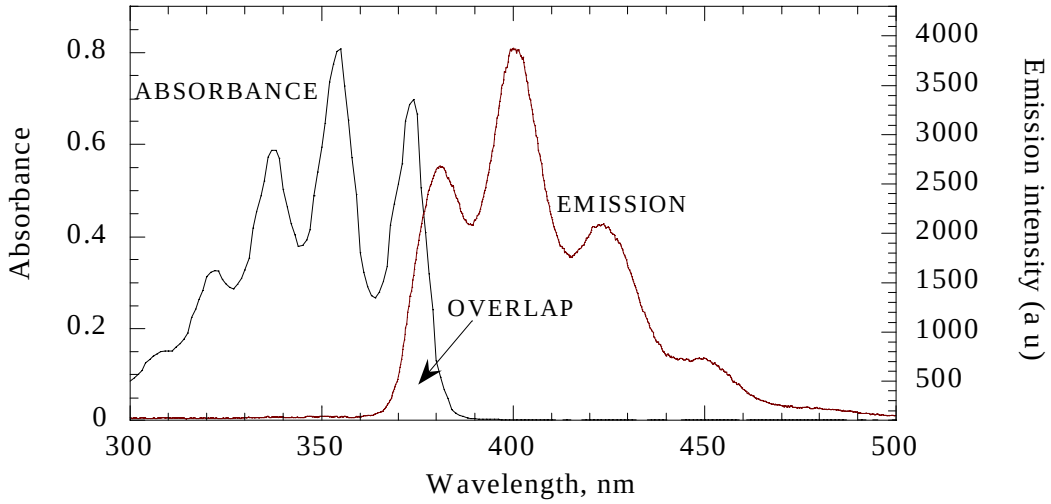

Figure 2.3.5.1-1. Absorption spectrum and emission spectrum of antracene.

The overlap in figure 2.3.5.1-1 is covering the area from 360 to 390nm, and it is the peaks in this area that are expected to disappear. At low concentrations of a fluorescent species a characteristic emission spectrum is observed. In the case of antracene, peaks appear at 381.40, 399.60, 423.60 and 450.40nm (figure 2.3.5.1-2).

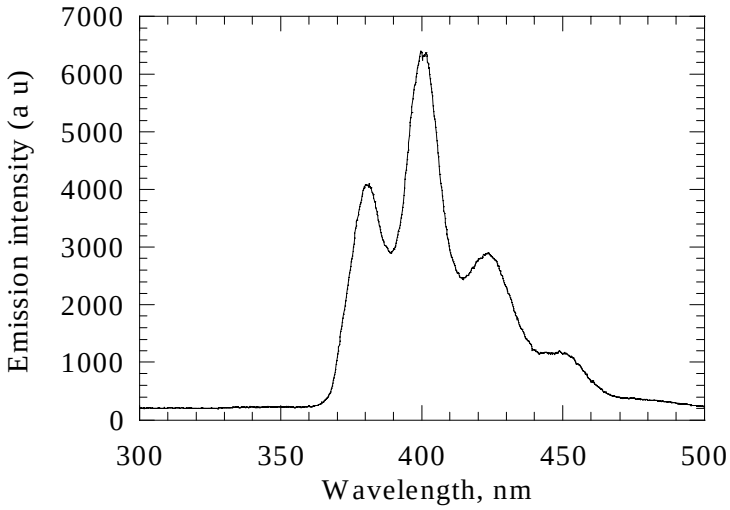

Figure 2.3.5.1-2. Emission spectrum of antracene, 2.49 10^{-5}M.

With increasing concentration of this fluorescent species, however the spectrum is changing, and figure 2.3.5.1-3 shows how the peak at 381.40nm disappears at higher concentration.

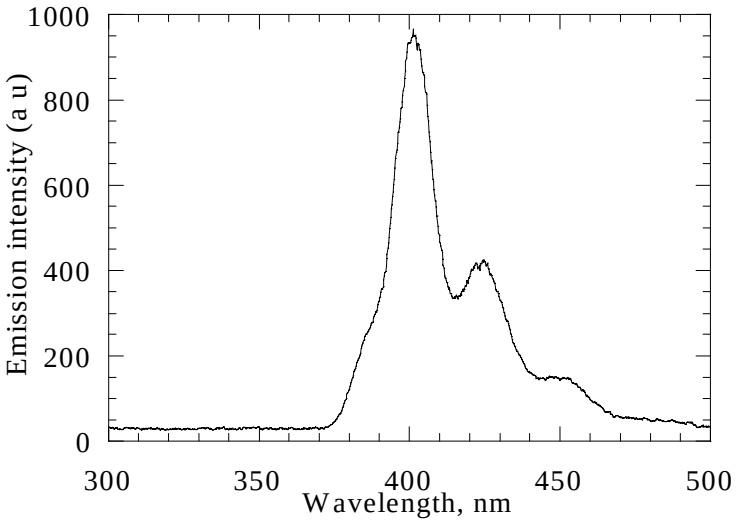

Figure 2.3.5.1-3. Emission spectrum of antracene, 3.371 10^{-4}M.

This is due to energy being transferred from one molecule of antracene to another.

2.3.5.2 Experimental work

The standard solution of antracene from the RET experiments was used. Emission scans from 300 to 500nm with excitation wavelength 250nm were taken of the standard solution and dilutions of 82.76%, 59.79%, 36.95%, 20.6%, 18.37%, 13.44%, 8.68%, 7.39% and 4.63% with respect to standard solution (figure 3.1.3-9). All dilutions were based on weight. The same procedure was followed for the standard solution of naphthalene. Dilutions of 83%, 61.3%, 42.5%, 20.4%, 12.4% and 8.4% were made (figure 3.1.3-2).

The last part of the RET experiment was used to investigate self-absorption of antracene in solution with naphthalene. After the naphthalene peak had disappeared, more and more drops of antracene were added up to a total of 40 drops, where the antracene signal almost disappeared due to inner filter effect (3.1.3-9).

2.3.6 Application of fluorescence in this work

The main species in oil giving fluorescence are the aromatics (figure 1-1). Fluorescence was hence used to analyze sediment samples on aromatics. A fluorescence measurement is done in a few minutes.

2.4 Preparation and analysis of sediment samples

2.4.1 Material and experimental set-up

The scope of the project [1] that this thesis is a part of is to describe the natural processes taking place in cuttings piles in the North Sea. Cuttings piles [13] are accumulations on the seabed of excess material (rock cuttings and muds) that are produced when exploration and production sub sea wells are drilled. The action of the drill bit cuts into the rock, producing fragments, which range in diameter from tens of microns to 1 - 2cm, depending on the nature of the rock. Cuttings in the North Sea are usually composed of shale and sandstone with an asymmetric flake structure. The characteristics of each accumulations varies greatly, according to the types of muds used while drilling, the volumes drilled, cuttings discharge methods, water depth and currents. Cuttings from different piles, both from piles formed from wells drilled with oil- and water based mud, in the Central and Northern North Sea were collected. The cuttings material used are:

- Beryl (OBM)
- Ekofisk 2/4 A (WBM / part ester)
- Ekofisk 2/4 C -96-survey (WBM / part ester)
- Frøy (WBM / part olefins)
- Lille Frigg (WBM)

All batches were mixed and homogenised in a concrete mixer. From each batch samples were collected and transferred to 325mL bottles. The experimental set-up was divided into two tests, one performed at aerobic conditions and one performed at anaerobic conditions.

Test 1 of the experiment was performed at aerobic conditions, and in this part of the project 60g cuttings/reference material and 100mL seawater were added to each bottle. The samples either consisted of 100% cuttings or 20% cuttings and 80% reference sediment. The reference sediment is sediment collected from a known location that is not influenced by drilling activity. Within one cuttings pile one bottle for each incubation time was made, so that sampling at day 1, 28 and 56 was done from unopened bottles. The bottles were incubated laying flat with continuous agitation. The bottles were aerated approximately once a week. The incubation temperature for the samples in the UKOOA-project was 10ºC.

Test 2 of the experiment was performed at anaerobic conditions. 325mL bottles were used incubated standing, no disturbance. The bottles were added 80 g cuttings /reference sediment and 200mL seawater, and incubated at 10ºC. Sampling was done at 1, 28, 56 and 100 days. Table 2.4.1-1 and 2.4.1-2 show the experimental set-ups.

Table 2.4.1-1. Schematic of samples and sample numbers in test 1. Samples in cursive are the samples treated in the thesis.

Sample	**Day 1**	**Day 28**	**Day 56**
Reference sediment, 10°C	1.1	1.2	1.3
Beryl A 20%, 10°C	2.1	2.2	2.3
Beryl A, 10°C	3.1	3.2	3.3
Beryl A, 10°C	4.1	4.2	4.3

Table 2.4.1-1 continued

Beryl A, 10°C	5.1	5.2	5.3
Ekofisk 2/4 A 20%, 10°C	6.1	6.2	6.3
Ekofisk 2/4 A, 10°C	7.1	7.2	7.3
Frøy 20%, 10°C	8.1	8.2	8.3
Frøy, 10°C	9.1	9.2	9.3
Lille-Frigg 20%, 10°C	10.1	10.2	10.3
Lille-Frigg, 10°C	11.1	11.2	11.3
Ekofisk 2/4 C 20%, 10°C	12.1	12.2	12.3
Ekofisk 2/4 C, 10°C	13.1	13.2	13.3
Beryl A 20ºC	*15.1*	*15.2*	*15.3*
Beryl A 20ºC	*16.1*	*16.2*	*16.3*
Beryl A 20ºC +N+P	*17.1*	*17.2*	*17.3*
Beryl A 20ºC +N+P	*18.1*	*18.2*	*18.3*
Beryl A 5ºC	*19.1*	*19.2*	*19.3*
Beryl A 5ºC	*20.1*	*20.2*	*20.3*

Table 2.4.1-2. Schematic of samples and sample numbers in test 2. Samples in cursive are the samples treated in the thesis.

Sample	**Day 1**	**Day 28**	**Day 56**	**Day 100**
Reference sediment, 10°C	B1.1	B1.2	B1.3	B1.4
Beryl A 20%, 10°C	B2.1	B2.2	B2.3	B2.4
Beryl A, 10°C	B3.1	B3.2	B3.3	B3.4
Beryl A, 10°C	B4.1	B4.2	B4.3	B4.4
Beryl A, 10°C	B5.1	B5.2	B5.3	B5.4
Ekofisk 2/4 A 20%, 10°C	B6.1	B6.2	B6.3	B6.4
Ekofisk 2/4 A, 10°C	B7.1	B7.2	B7.3	B7.4
Frøy 20%, 10°C	B8.1	B8.2	B8.3	B8.4
Frøy, 10°C	B9.1	B9.2	B9.3	B9.4
Lille-Frigg 20%, 10°C	B10.1	B10.2	B10.3	B10.4
Lille-Frigg, 10°C	B11.1	B11.2	B11.3	B11.4
Ekofisk 2/4 C 20%, 10°C	B12.1	B12.2	B12.3	B12.4
Ekofisk 2/4 C, 10°C	B13.1	B13.2	B13.3	B13.4
Beryl A 20ºC	*B15.1*	*B15.2*	*B15.3*	*B15.4*
Beryl A 20ºC	*B16.1*	*B16.2*	*B16.3*	*B16.4*
Beryl A 20ºC +N+P	*B17.1*	*B17.2*	*B17.3*	*B17.4*
Beryl A 20ºC +N+P	*B18.1*	*B18.2*	*B18.3*	*B18.4*
Beryl A 5ºC	*B19.1*	*B19.2*	*B19.3*	*B19.4*
Beryl A 5ºC	*B20.1*	*B20.2*	*B20.3*	*B20.4*

All samples incubated at 10°C were treated and analysed by participants in the UKOOA project. In addition to the UKOOA samples incubated at 10°C, the experimental set up was increased with samples incubated at 20°C, 20°C and nutrients as nitrogen and phosphorus added and incubated at 5°C. These are the samples collected, extracted, analysed and discussed in the thesis.

At sampling days sediment was collected by gravitational filtration of the mixture of sediment and seawater. The sediment was frozen in scintillation glass until extraction.

2.4.2 Extraction of sediment samples

The following is the procedure for extraction of oil from sediment samples, to get extracts for fluorescence analysis and GC-FID analysis.

The frozen sediment samples were thawed standing still. The layer of water forming on top of the sediment was removed using a pipette, and the sediment was shaken carefully to get a homogenous sample.

To make analysis of water content in sediment samples, a few grams (exact weight recorded) of sediment were transferred to a previously weighted beaker, left for drying at 110°C overnight. Then the beaker was weighed again and water content calculated.

Approximately (exact weight recorded) 10g sediment was transferred to an extraction thimble, one spatula was left in each thimble. 25µL internal standard and 40mL methanol was added and stirred cautiously. The internal standard was stored at a dark place, and sonicated before use. This was done to dissolve what might have precipitated. The methanol was added to wash out the remaining water from the sediment. In addition this ensured good contact between the solvent and the oil containing sediment. 100mL dichloromethane, which is the solvent, was added. It was ensured that the sediment in the extraction thimble was completely covered with solvent. Boiling stones are added to the extraction beakers before the extraction is started.

For the extraction a Soxtherm 2000 was used, and the extraction characteristics are:

- Extraction temperature: 150 °C
- Boiling time: 30 minutes
- Solvent reduction A: 5 x 15 mL
- Extraction time: 60 minutes
- Solvent reduction B: 8 minutes
- Solvent reduction C: 5 minutes

During the boiling phase the sample was placed in boiling solvent, which brought a large part of the extract into solution. For a complete extraction the solvent level was reduced to a point where there was a clear gap between the solvent and the extraction thimble (Reduction A). The evaporated solvent was cooled in the condenser and dropped back into the form tube middle part, where 15mL was collected before it was brought together with the sample. For the reduction compressed air was led through the condenser, which pressed the solvent into the built-in collecting vessel. After the reduction was finished the solvent was evaporating during reduction phase B, but not upon drying, to avoid a change of the extract. During reduction phase C the extraction beakers were raised away from the heating plates. Heating and cooling water was still turned on. The evaporation was minimal. The extract was not endangered, as the extraction beakers were based only in the hot air current.

After cooling, the samples were transferred to 250mL beakers. The extraction beakers were washed with portions of DCM, and the extract dried overnight. If there was problems to get it completely dry, some nitrogen was carefully blew at the surface of the extract.

The next step was a clean up of the dried extracts. Equipment needed for this was a vacuum manifold and solid phase extraction tubes. For the cleanup 1:1 n-hexane: dichloromethane was used as solvent. 10-15mL tubes were placed in the vacuum manifold. 50mg anhydrous Na_2SO_4 were placed on top of the silica column, and the column was conditionated with 3 portions of 3mL solvent. The anhydrous sodium sulphide was used to remove any traces of water. The vacuum was adjusted until the solution was running through the column with 4-5 drops/sec. The packing material must never get dry. The vacuum was closed, and a clean 10mL tube was placed inside the manifold. The beakers with dry extract were added 3mL solvent, and were then transferred to the silica columns. The vacuum was turned on, and appropriate extraction speed was 1-3 drops/sec. The cleaning procedure was repeated with 3mL portions of solvent until the beakers were clean. This clean up was done to remove polar contamination possibly interfering with the GC analysis.

After clean up there was approximately 10mL eluate in the tube. The total volume of the cleaned up eluate was recorded, and a 0.5mL sample was collected for fluorescence analysis. The eluate was then evaporated to approximately 0.5mL, and transferred to suitable vials for GC-analysis.

2.4.3 Measurements of total hydrocarbon content

2.4.3.1 Performance of GC-FID measurements on extracted sediment samples

All samples in cursive in table 2.4.1-1 and 2.4.1-2 were extracted and analysed on GC-FID, according to the description given in chapter 2.4.2 (extraction procedure), 2.1.5 (chemicals and analytical equipment) and 2.4.3.2 (calculation of THC). For Beryl A, test 1, incubation temperature 20°C and incubation time 28 days; three injections and calculations were made. For three of the samples three parallel extractions, measurements and calculations were made. The three samples were:

1) Beryl A, test 1, incubation temperature 20°C and incubation time 28 days
2) Beryl A, test 2, incubation temperature 5°C and incubation time 56 days
3) Beryl A, test 2, incubation temperature 20°C, nutrients added and incubation time 1 day

2.4.3.2 Calculation of THC from gas chromatograms

THC in this method is defined to be all extractable (see 2.4.2) carbon-compounds that can be oxidized, and thus determined by FID, with retention time equal to or exceeding the retention time of C_{12} n-alkane (dodekane). A standard calibration curve had been made using non-contaminated sediment that was added various amounts of HDF 200, a standard oil proposed by Statens forurensnings tilsyn (SFT) [14] in "guidelines 99:01; Environmental monitoring of petroleum activities on the Norwegian shelf", and a known, constant amount of internal standard. The calibration standards were extracted and cleaned up the same way as described for the sediment samples. The total area of all peaks with retention time between 10 and 74 minutes was integrated (appendix 7.1). The area of internal standards, appearing at 41.5 minutes and 70.2 minutes, was subtracted from the total area. The relation (total area – area of internal standards) / area of $C_{20}D_{42}$ was calculated for each standard. $C_{20}D_{42}$ was used as internal standard for the calculations of THC because problems with precipitation of $C_{30}H_{62}$ occurred. The standard calibration curve was constructed with the amounts of HDF 200 added (mg) along the x-axis, and the corresponding relation between (total area – area of internal standards) / area of $C_{20}D_{42}$ along the y-axis. The equation representing this relation was:

$x = (y+1.30656)/1.885332$ (eqn. 2.4.3.2-1)

The curve was made from 7 calibration standards, and the correlation coefficient was 0.96671.

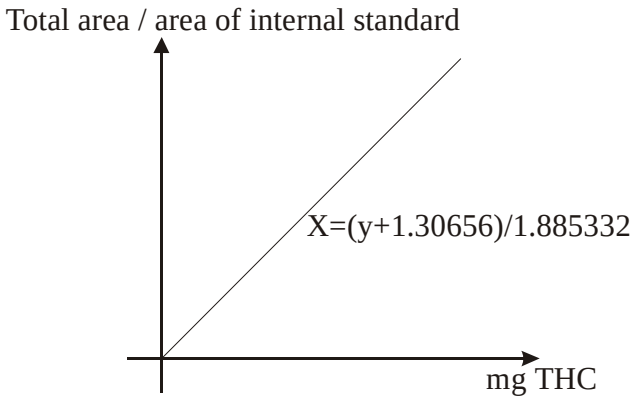

Figure 2.4.3.2-1. Standard curve for THC.

For decision of THC in sediment samples, the chromatograms were integrated the same way as for the calibration standards. The relation (total area – area of internal standards) / area of $C_{20}D_{42}$ was calculated, and the amount of THC was then calculated from the equation representing the standard calibration curve.

Example: Beryl A, 20°C, test 1, day 1.

The total area of all peaks in the chromatogram was 3966286 and the area of the internal standards was 290620. Total area - area of internal standards was hence 3675666, and the area of $C_{20}D_{42}$ was 202318. The relation (total area – area of internal standards) / area of $C_{20}D_{42}$ was then 18.17. From equation 2.4.3.2-1 the amount of THC was calculated to be 10.33mg.

A blank, a calibration standard with no HDF 200 added, was measured three times indicating an amount of 0.84mg THC. For all samples 0.84mg was subtracted, and the amount of THC in this case was hence 9.49mg.

Based on the amount of wet sediment extracted, and the water content in the samples, the concentration of THC in sediment samples were calculated. The results are given as mg THC/kg wet sediment or mg THC/kg dry sediment. For Beryl A 20°C, test 1, day 1, 8.33g wet sediment was extracted. The water content was 38.81 %, and the concentration of THC was then 9.49 / 8.33 = 1139mg/kg wet sediment and 9.49 / 5.09 =1861mg/kg dry sediment.

2.4.4 Measurements of aromatics

2.4.4.1 Procedure to choose operational parameters for SFS

Solutions of a selection of aromatics were made. Naphthalene was chosen to represent the 2-ring aromatics, because naphthalene and its alkylated homologues are the main aromatic components in crude oil.

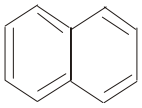

Figure 2.4.4.1-1. Structure of naphthalene

Pyrene was chosen to represent the 4-ring aromatics, because it is known to give a strong signal in fluorescence.

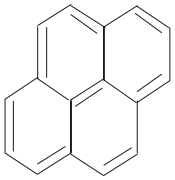

Figure 2.4.4.1-2. Structure of pyrene

Benzo[a]pyrene was chosen to represent the 5-ring aromatics, because it is interesting due to its carcinogenic effects.

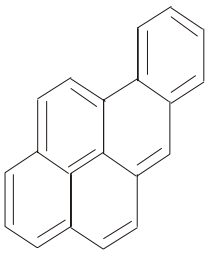

Figure 2.4.4.1-3. Structure of benzo[a]pyrene

The substances were dissolved in dichloromethane and n-hexane (1:1). The following procedure was followed for each of the components.

The first step was to run an excitation scan with a broad range for the excitation wavelengths. The emission was recorded 40nm higher then the highest excitation wavelength in the scan. Then the range of the scan was reduced at the upper end, and hence the intensity of the emission was recorded at shorter wavelengths. The range was reduced until emission was recorded at a wavelength were a characteristic spectrum was observed. At very high wavelengths no emission is observed, except from scattering light, which is light appearing at multiples of the wavelength chosen for recording emission.

The second step was to run an emission scan, where the fixed excitation wavelengths were chosen to be the wavelengths of the peaks in the excitation scan (step 1). The wavelengths of the peaks in the emission scan are denoted λ_{em}.

The third step was to run another excitation scan at fixed emission wavelengths of λ_{em}. The wavelengths of the peaks in the excitation scans are denoted λ_{ex}.

The fourth step was to run a synchronous scan. $\Delta\lambda=\lambda_{em}-\lambda_{ex}$ To choose the best $\Delta\lambda$ for the runs, the samples have to give a good signal at the chosen $\Delta\lambda$, and the signals for the different components should ideally be separated.

Example: benzo[a]pyrene.

The excitation scans with emission intensity recorded at 540 and 500 nm showed no emission except from scattering light at (540/2) 270nm and (500/2) 250nm. The excitation scan with emission intensity recorded at 450nm, however, showed a characteristic spectrum with peaks appearing at 265, 285, 297, 348, 362 and 386nm.

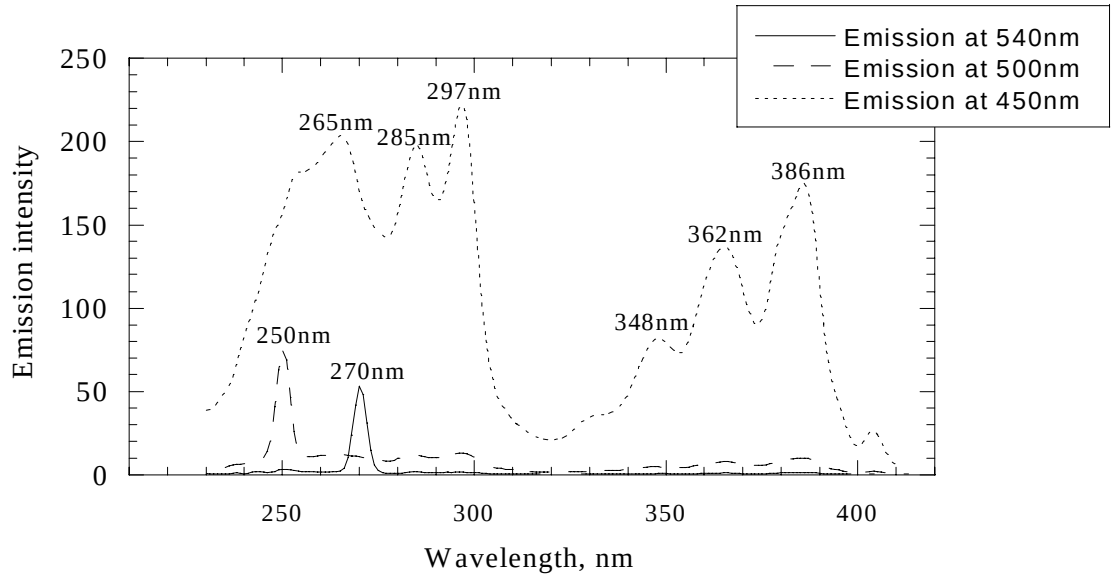

Figure 2.4.4.1-4. Excitation scans of BaP with fixed emission at 540, 500 and 450nm.

The second step was then to run emission scans with fixed excitation at 265, 285, 297, 348, 365 and 386nm. Only a selection of the emission scans is shown in figure 2.4.4.1-5 to make it well arranged. In all the scans peaks were appearing at 405nm, 429nm and 456nm.

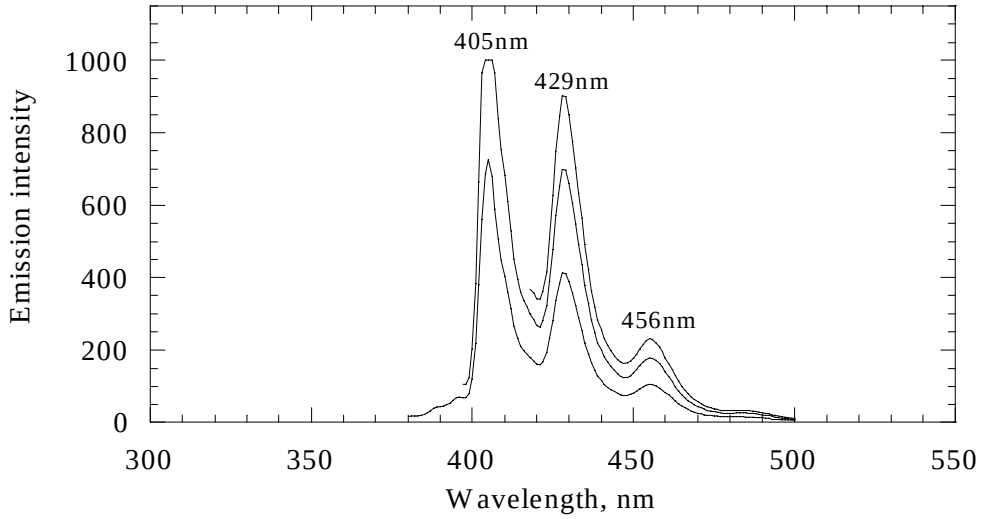

Figure 2.4.4.1-5. Emission scans of BaP with fixed excitation at 348, 365 and 386nm.

Increasing wavelengths resulted in lower emission intensities. Figure 2.4.4.1-5 shows that the shape of the emission spectrum of a component is independent of the wavelength used for excitation. λ_{em} is 405, 429 and 456nm. The third step was then to run excitation scans with fixed emission at 405, 429 and 456nm. The emission spectrum with excitation wavelength 429nm is sown in figure 2.4.4.1-6.

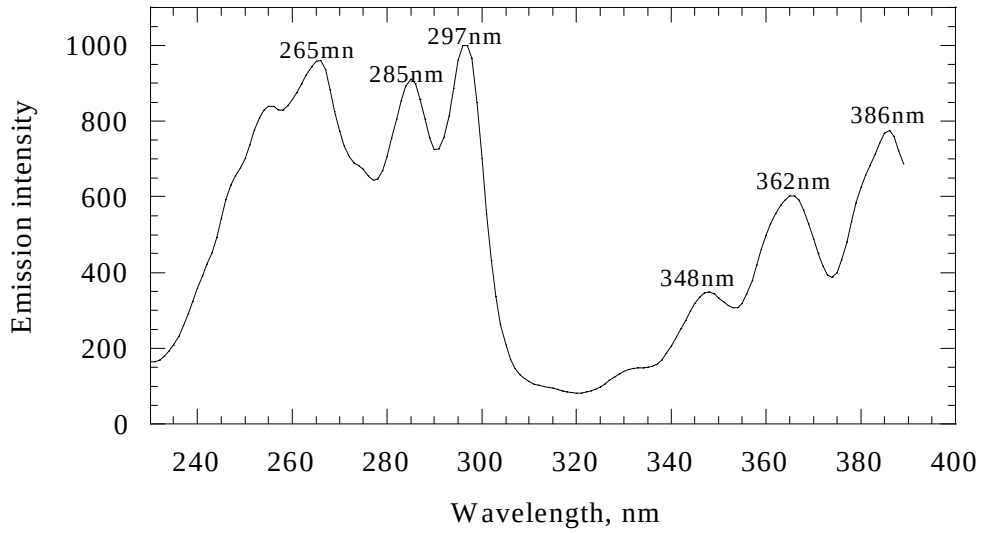

Figure 2.4.4.1-6. Emission scan of BaP with fixed excitation at 429nm.

This emission spectrum was identical to that in step 1. λ_{ex} was then 265, 285, 297, 348, 362 and 386nm, and possible $\Delta\lambda$ for BaP were:

$\Delta\lambda_1$=429-265=164
$\Delta\lambda_2$=429-285=144
$\Delta\lambda_3$=429-297=132
$\Delta\lambda_4$=429-348=81

$\Delta\lambda_5$=429-362=67
$\Delta\lambda_6$=429-386=43

The fourth step was then to run a synchronous scan for all the different $\Delta\lambda$. In figure 2,4,4,1-7 the synchronous scans for $\Delta\lambda$ = 132 and 43 are shown.

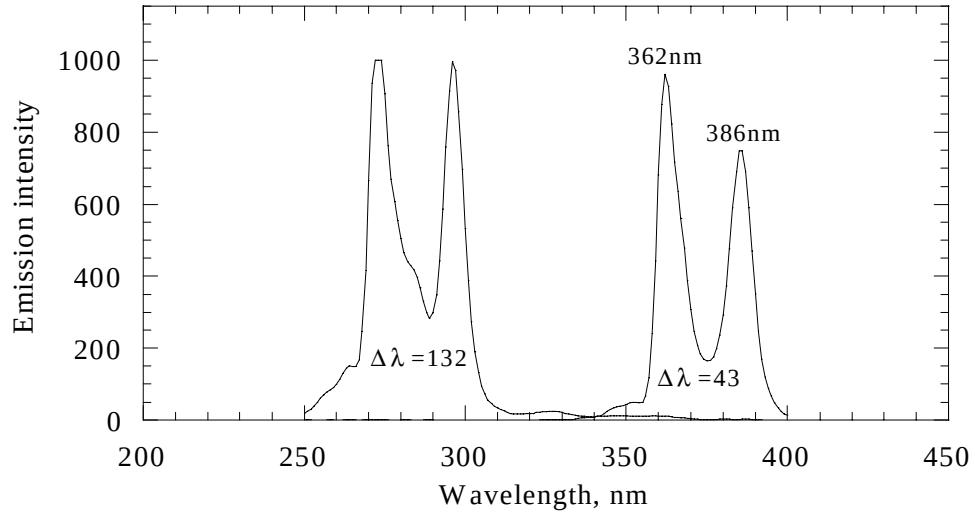

Figure 2.4.4.1-7. Synchronous scan of BaP with $\Delta\lambda$ = 132 and 43.

To choose the best $\Delta\lambda$ for the synchronous scans, the samples should give a good signal at the chosen $\Delta\lambda$, and the peaks of the components of interest should be separated. This was the case for $\Delta\lambda$ = 43, for which naphthalene showed peaks at λ = 281 and 288nm (figure 2.4.4.1-8), pyrene at 330 and 339nm (figure 2.4.4.1-9) and benzo[a]pyrene at 362 and 386nm (figure 2,4,4,1-7). These wavelengths were chosen to represent the 2-, 4- and 5-ring aromatics respectively.

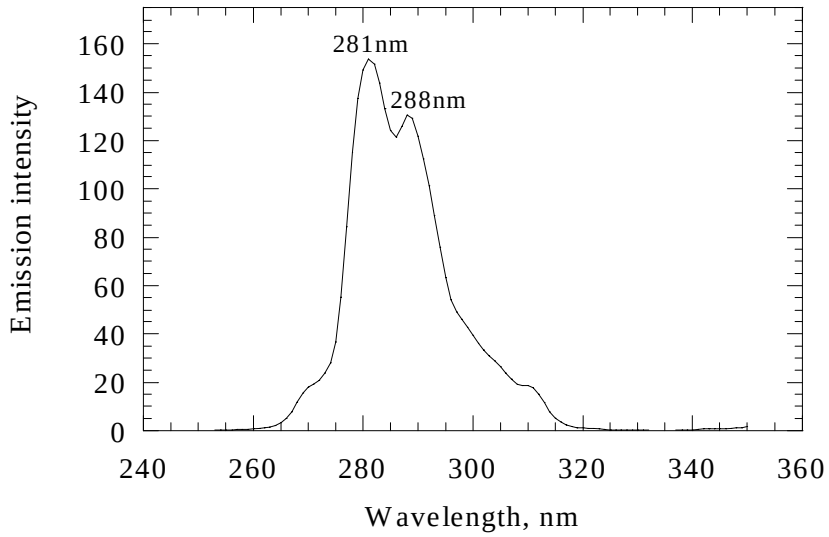

Figure 2.4.4.1-8. Synchronous scan of naphthalene with $\Delta\lambda$ =43.

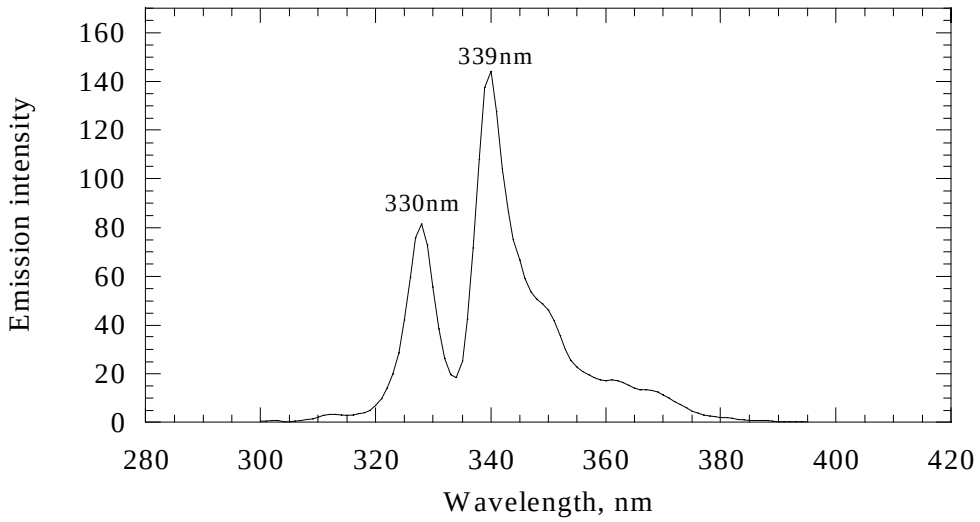

Figure 2.4.4.1-8. Synchronous scan of naphthalene with $\Delta\lambda$ =43.

2.4.4.2 Performance of fluorescence measurements on extracted sediment samples

The volume of the cuvette used for fluorescence measurements was 3000µL. The extracted sediment samples were then diluted to a total volume of 2900µL. The dilutions were based on the relation between the amount of dry sediment extracted and the volume after clean up. The dry weight was used to correct for variations in water content. After trial and fail, all samples were diluted 15 times because this gave suitable signal intensity.

For the fundamental investigations all dilutions were based on weight. That was impractical in this case, and a pipette was used for preparation of initial solutions (15 times dilution) and dilutions. To quantify the uncertainty correlated to this, the pipette was calibrated to 885µL with distilled water. 885µL solvent was pipetted, without wetting the pipette tip, into a previously weighted volumetric flask with glass stopper. The weight was recorded, and this was repeated ten times. Then the pipette tip was wetted one, two, three and four times before the weight of the pipetted solvent was recorded. In the practical work the pipette tip was always wetted three times before use, because this was found to give satisfyingly reproducibility (3.3-2).

Each day fluorescence measurements were made, an instrument check up was done by measuring a standard solution of pyrene, 20ppm. The bottle was covered with aluminum foil and stored in the refrigerator. In the SFS43 emission intensity was recorded at excitation wavelengths 328.42nm and 340.47nm (the two emission maxima in the spectrum) (figure 3.3-1).

Example of how to calculate initial solution:
For Beryl A, 20°C, day 1, test 1, 8.33g wet sediment was extracted. The water content was 38.81%, and the amount of dry sediment was hence 5.097g. The volume after clean up was 9.9mL, and dry sediment (g) per volume (mL) was 0.1549. 15 times dilution (0.1549*15 = 7.723) and a total volume of 2900µL means a volume of 2900/7.723 = 375.5µL extract. For practical reasons all volumes were rounded to nearest 5. In this case the volume of extract was 375µL and the volume of solvent was 2525µL.

For all samples a synchronous fluorescence scan from 250-400 nm with $\Delta\lambda$ = 43nm was taken, and emission intensity recorded at excitation wavelengths 281, 288, 330, 339, 362 and 386.

To get information about the shape of the calibration curve for the Beryl samples, Beryl A, 20°C, day 1, test 1, was diluted 1/2, 1/4, 1/8, 1/16, 1/32 and 1/64 relative to the initial concentration (15 times diluted) (figures 3.3-2 to 3.3-7).

The same samples as those analysed on GC-FID were analysed on fluorescence.

3 Results

3.1 Effects affecting fluorescence analysis

Many factors and effects influence and make fluorescence analysis difficult to use. Among these are inner filter effect, resonance energy transfer and self-absorption. It is very important to be aware of these effects, otherwise use of fluorescence data might lead to wrong conclusions.

3.1.1 Inner filter effect

Simulations made in mathematical spreadsheet to examine the effect of changing the parameters in the theoretical expression of ϕ, showed that ε is the parameter affecting the shape of the calibration curve with respect to linearity contra curving. A high value of ε results in a curve reaching maximum emission intensity at low concentration. The emission intensity decreases rapidly after the maximum, giving a sharp peak. Decreasing the value of ε, keeping the other parameters constant, moves the maximum emission intensity towards higher concentration. Decreasing the value of ε also makes the emission intensity decrease slower after the maximum has been reached, resulting in a less sharp peak. Finally at very low values of ε the calibration curve is getting linear.

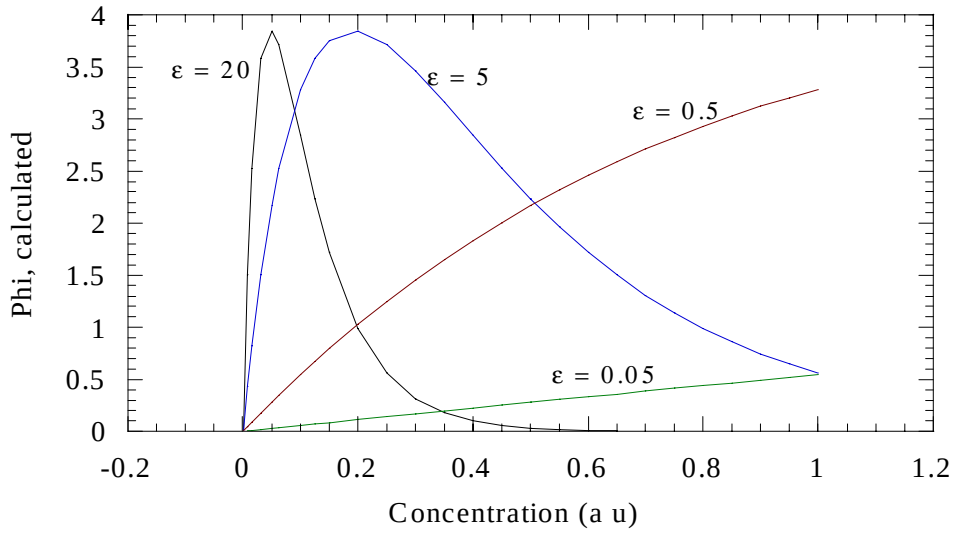

Figure 3.1.1-1.Changes in epsilon affecting the shape of the calibration curve. l, x and I_0 are kept constant at 1, 0.25 and 10 respectively.

The deviations from linearity are due to the inner filter effect. The inner filter effect will be most apparent at low concentrations for species with relatively high ε.

Independent on the value of I_0, the concentration for maximum emission intensity is the same. Increasing the value of I_0, keeping the values of ε and x constant, only moves the calibration curve up along the emission intensity axis. The shape with respect to linearity or curving is not affected. The concentration for maximum intensity for all calibration curves is the same, they all start at zero intensity for zero concentration and they all terminate at the same concentration. This results in steeper curves for higher values of I_0.

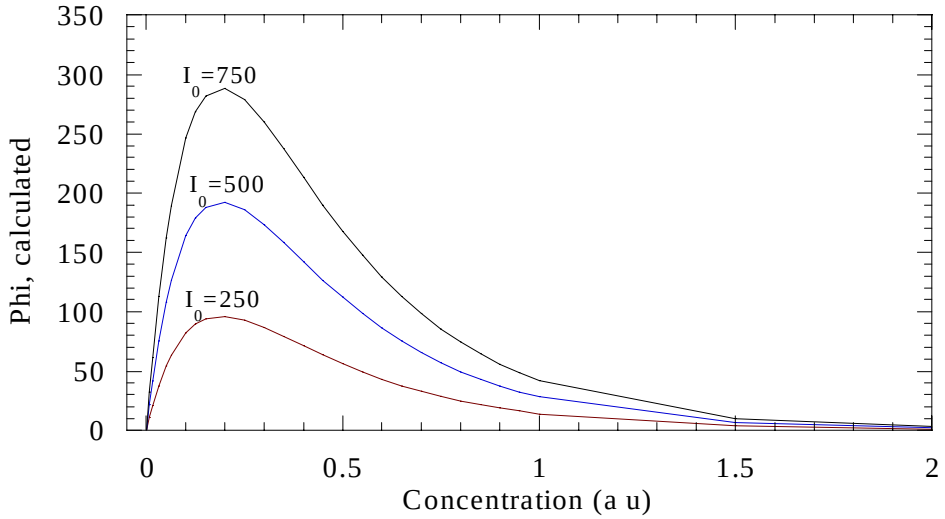

Figure 3.1.1-2. Changes in I_0. ε and x kept constant at 5 and 0,25 respectively

Increasing x, keeping ε and I_0 constant, seems to result in an overall increase in emission intensity. The concentration for maximum emission intensity seems to be slightly higher for higher values of x. The emission intensity is also decreasing less at the right side of the maximum emission intensity than for lower values of x.

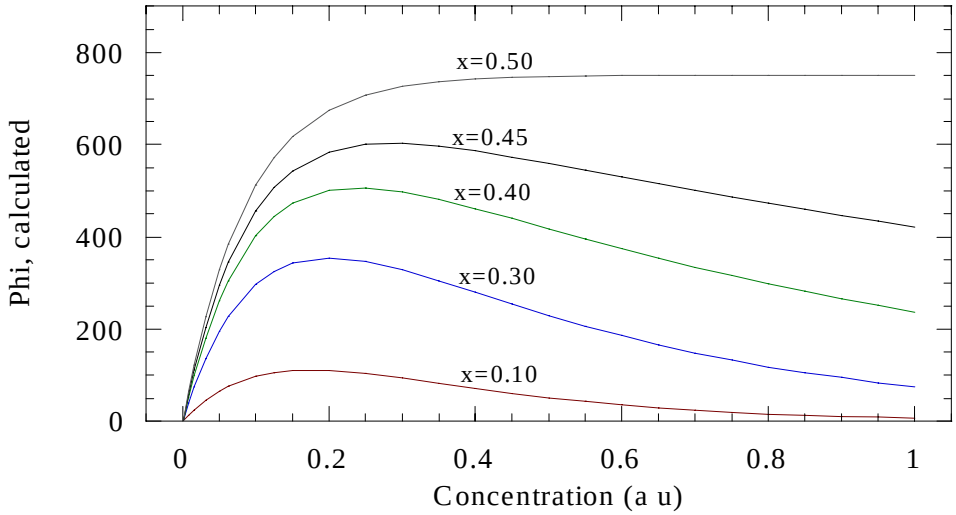

Figure 3.1.1-3. Changes in x. ε and I_0 kept constant at 5 and 750 respectively.

Simulations also show that the theoretical expression of ϕ can be adjusted to approach experimental values of a calibration curve pretty good. In figures 3.1.1-4 to 3.1.1-6, relative concentration=1 refers to the initial solution (15 times dilution) described in chapter 2.4.4.2

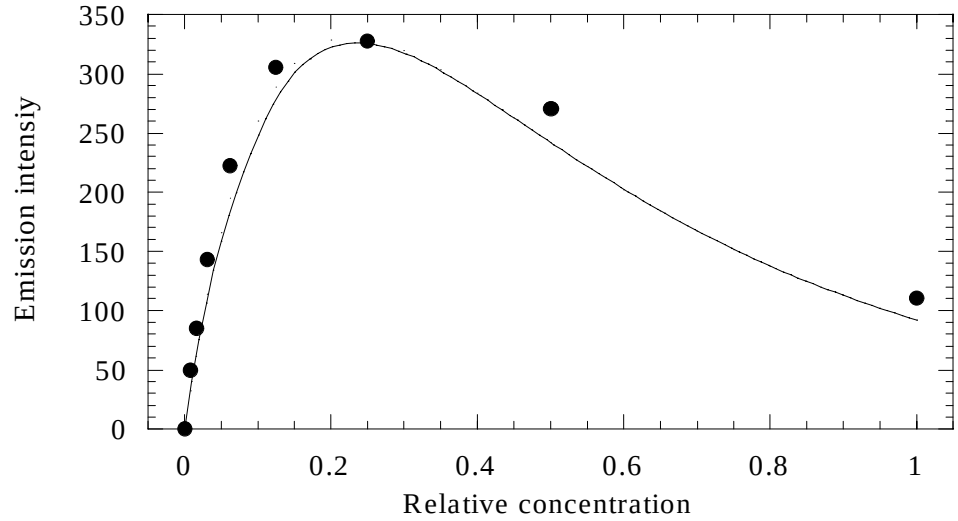

Figure 3.1.1-4. Experimental data (black dots) collected from synchronous fluorescence scan, $\Delta\lambda$ =43nm, of extracted sediment sample from UKOOA-project. **Excitation wavelength 281nm**. Emission intensity recorded 43 nm higher than excitation wavelength. Phi is calculated (black curve) from the theoretical expression. ε=4.4, x=0.3 and I_0=700.

The root mean square deviation of the approach for excitation at 281nm is 63.3.

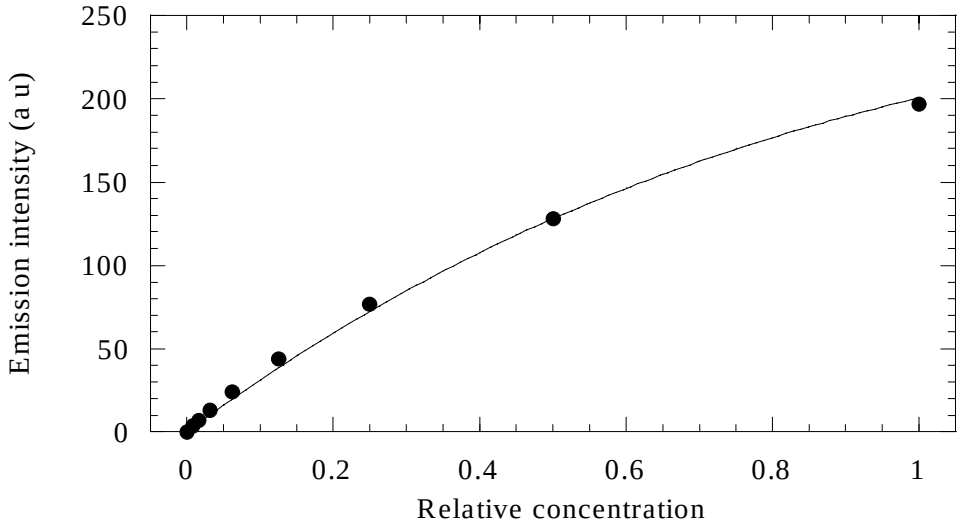

Figure 3.1.1-5. Experimental data (black dots) collected from synchronous fluorescence scan, $\Delta\lambda$ =43nm, of extracted sediment sample from UKOOA-project. **Excitation wavelength 330nm**. Emission intensity recorded 43 nm higher than excitation wavelength. Phi is calculated (black curve) from the theoretical expression. ε=0.44, x=0.25 and I_0=650

The root mean square deviation of the approach for excitation at 330nm is 9.5, and that for excitation at 386nm is 2.0.

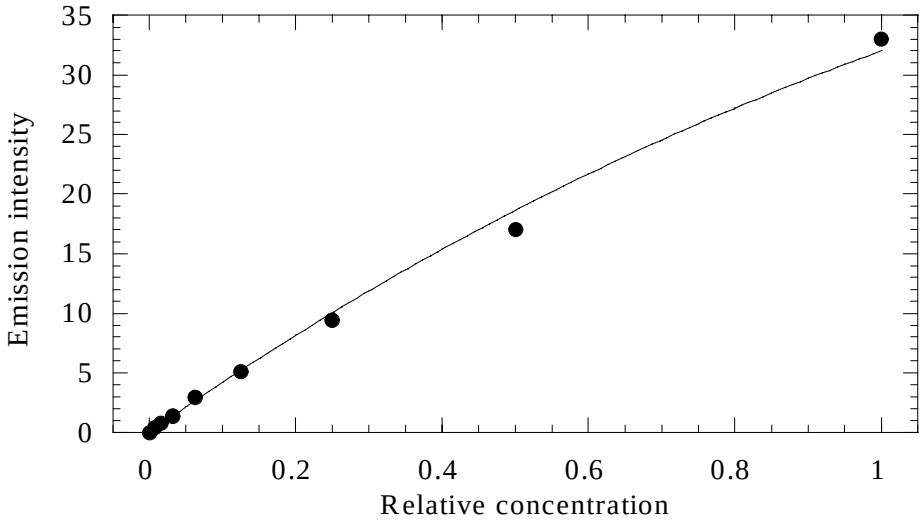

Figure 3.1.1-6. Experimental data (black dots) collected from synchronous fluorescence scan, $\Delta\lambda$ =43nm, of extracted sediment sample from UKOOA-project. **Excitation wavelength 386nm**. Emission intensity recorded 43 nm higher than excitation wavelength. Phi is calculated (black curve) from the theoretical expression. ε=0.27, x=0.25 and I_0=140.

All together there is a good correlation between the experimental calibration curves and those based on the theoretical expression. Since ε is the parameter affecting the shape of the curve with respect to linearity, and the experimental values from SFS43 showed more linear curves at higher wavelengths of excitation within one sample, these simulations lead to the idea that ε is changing with wavelength. The calibration curve for 281nm (figure 3.1.1-4) is similar to that of epsilon = 5 in figure 3.1.1-1, and that of 330nm (3.1.1-5) is similar to epsilon = 0.5. That is a decrease by one factor going from excitation of 281nm to excitation of 330nm. The standard oil HDF 200 was used to investigate this. The first solution and its dilutions gave strong absorption at short wavelengths, but very low absorption at the wavelengths of interest (figure 3.1.1-7). Wavelengths of interest are 281, 288, 330, 339, 362 and 386nm, based on the observations that the shape of the experimental calibration curves at these wavelengths were different. Calibration curves at 281 and 288nm are usually strongly affected by the inner filter effect, 330 and 339nm less affected, and 362 and 386nm are usually linear.

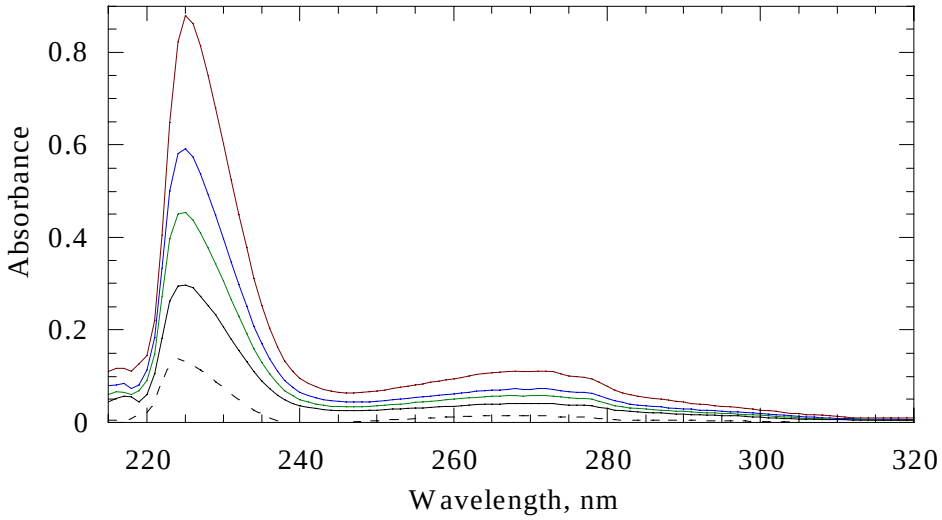

Figure 3.1.1-7. Absorption spectra from 210-350nm of different amounts of standard solution. 100%=standard solution made of 0.0221g HDF200 and 24.4846g solvent (1:1 n-hexane and dichloromethane). Red curve; 100%, dark blue curve; 63.3%, blue curve; 50.8%, black curve; 35.5% and black stipulated curve; 18.3%.

The absorption spectra from 250 to 400nm of the second and stronger HDF solution, and its dilutions, are shown in figure 3.1.1-8.

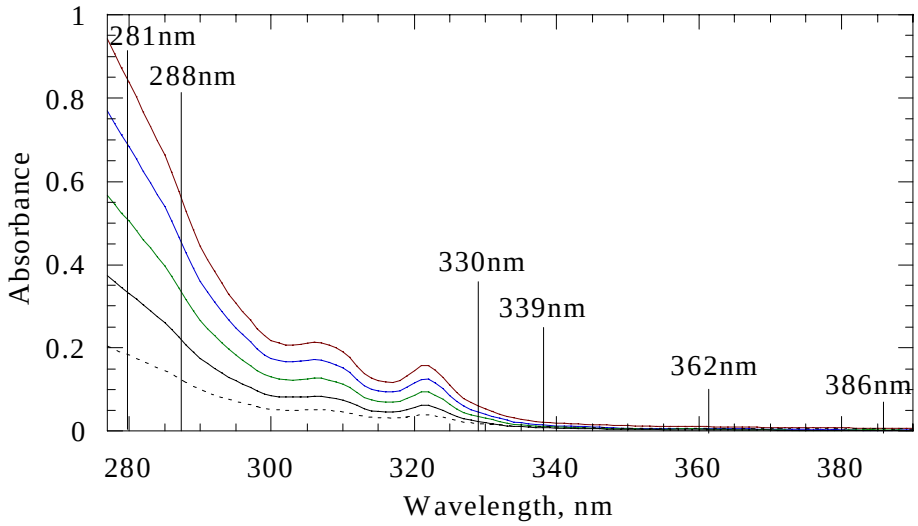

Figure 3.1.1-8. Absorption spectra from 280-390nm of different amounts of standard solution. 100%=standard solution made of 0.4639g HDF200 and 23.7961g solvent (1:1 n-hexane and dichloromethane). Red curve; 100%, dark blue curve; 80.8%, blue curve; 59.1%, black curve; 38.7% and black stipulated curve; 19.8%.

By viewing the absorption spectra it is apparent that the absorption at 281, 288, 330, 339, 362 and 386nm is decreasing respectively. Before Lambert Beers law could be used to estimate ε at different wavelengths, it was necessary to control if Lambert Beers law was applicable at the wavelengths of interest. For Lambert Beers law to be applicable there has to be a linear relation between concentration and absorbance. For all dilutions of the standard solution the absorbance was measured at 281, 288, 330, 339, 362 and 386nm. Only calibration curves for excitation at 281, 330, 362 and 386nm are shown here, because 288 is identical to 281 and

339 identical to 330nm. In figures 3.1.1-9 to 3.1.1-14, relative concentration=1 refers the standard solution of HDF 200 described in chapter 2.3.3.2.

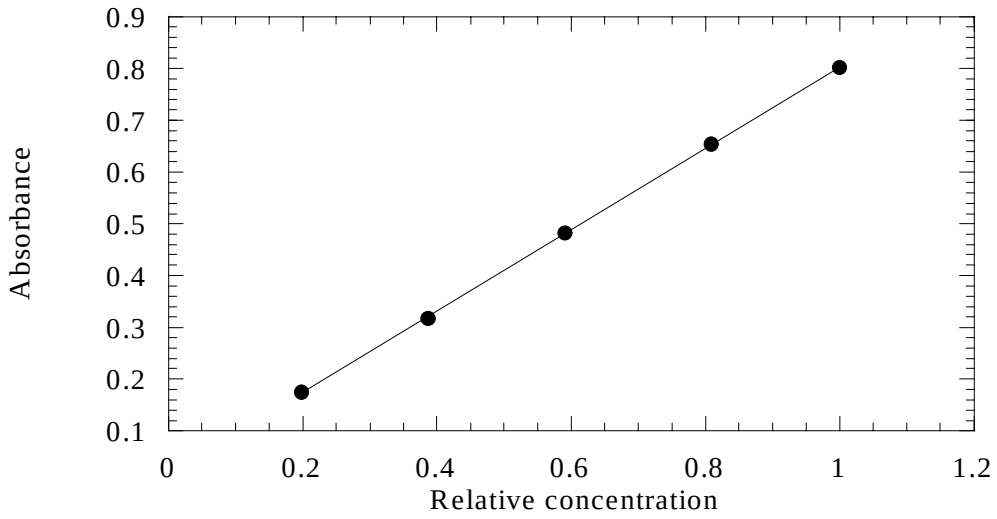

Figure 3.1.1-9. Control to see if Lambert Beers law is applicable at **281nm**. Black dots are experimental values. Black curve is linear curve fit, correlation coefficient 0.99995.

The relationship between concentration and absorbance is linear at both 281 (figure 3.1.1-9) and 288nm. At 330 (figure 3.1.1-10) and 339nm the relationship is also linear, only a small indication of deviation at low concentration and very low absorbance.

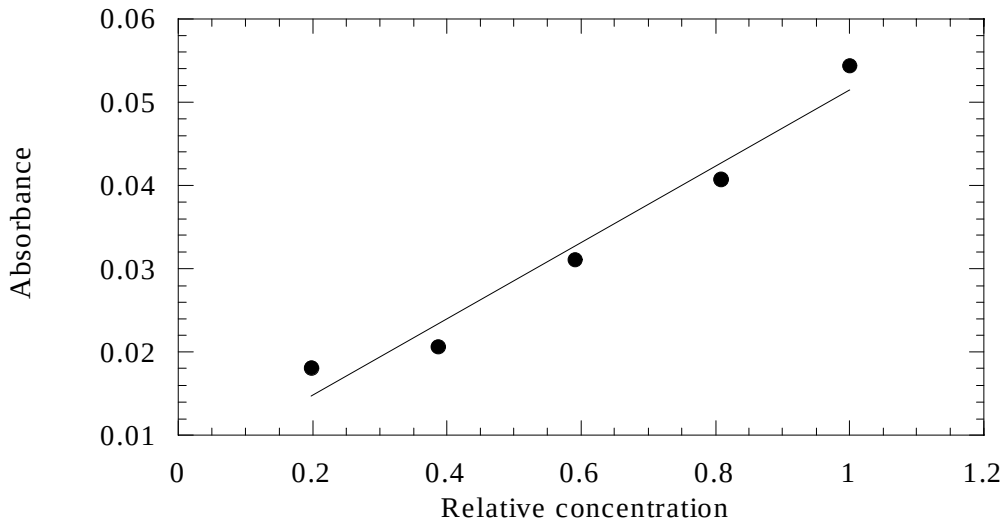

Figure 3.1.1-10. Control to see if Lambert Beers law is applicable at **330nm**. Black dots are experimental values. Black curve is linear curve fit, correlation coefficient 0.98095.

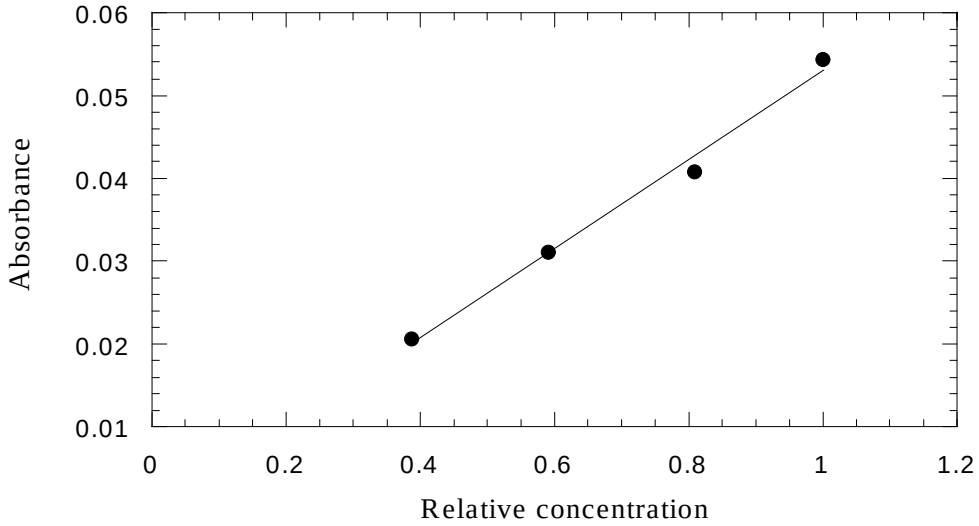

Figure 3.1.1-11. Control to see if Lambert Beers law is better applicable at **330nm when the lowest concentration is excluded**. Black dots are experimental values. Black curve is linear curve fit, correlation coefficient 0.99532.

Since the relationship between concentration and absorbance for excitation at 330 and 339 is more linear for the highest concentrations (figure 3.1.1-11), the lowest concentration is excluded in the following calculations of ε.

The pattern for excitation at 362nm (figure 3.1.1-12) is quite similar to that of 330 and 339.

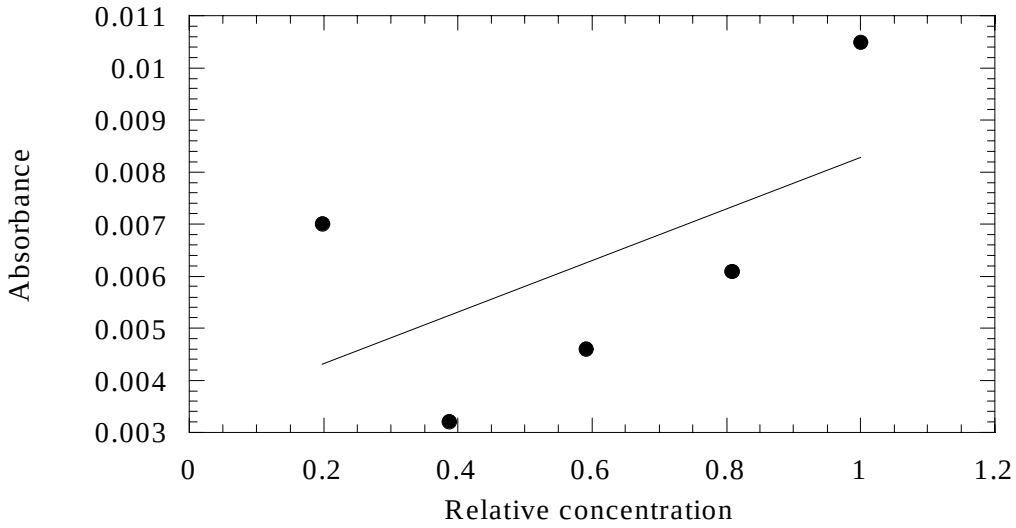

Figure 3.1.1-12. Control to see if Lambert Beers law is applicable at **362nm**. Black dots are experimental values. Black curve is linear curve fit, correlation coefficient 0.57294

The lowest concentration is excluded, and the relationship becomes more linear (figure 3.1.1-13). The correlation coefficient goes from 0.57297 to 0.94905.

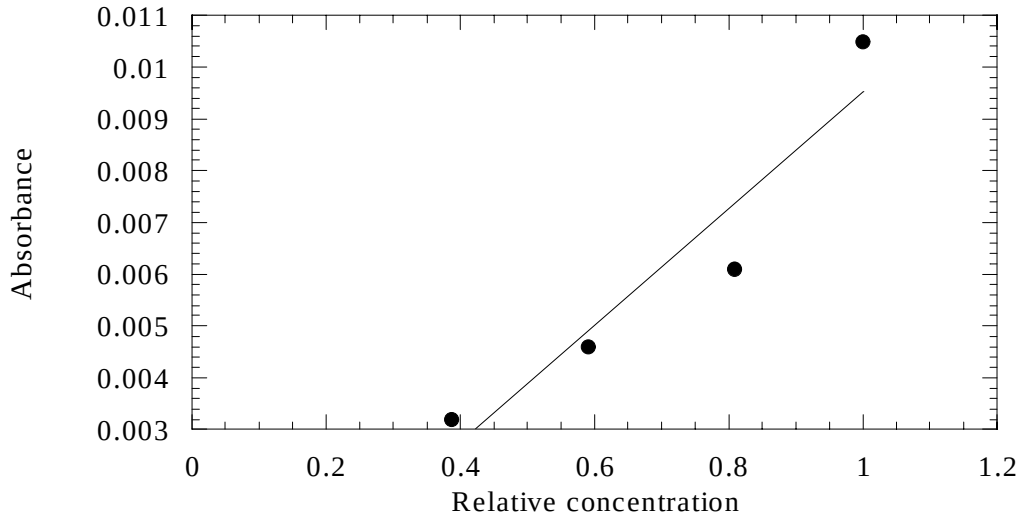

Figure 3.1.1-13. Control to see if Lambert Beers law is better applicable at **362nm, when the lowest concentration is excluded**. Black dots are experimental values. Black curve is linear curve fit, correlation coefficient 0.94905

For absorbance at excitation 386nm however, the absorbance is varying without a pattern (figure 3.1.1-14).

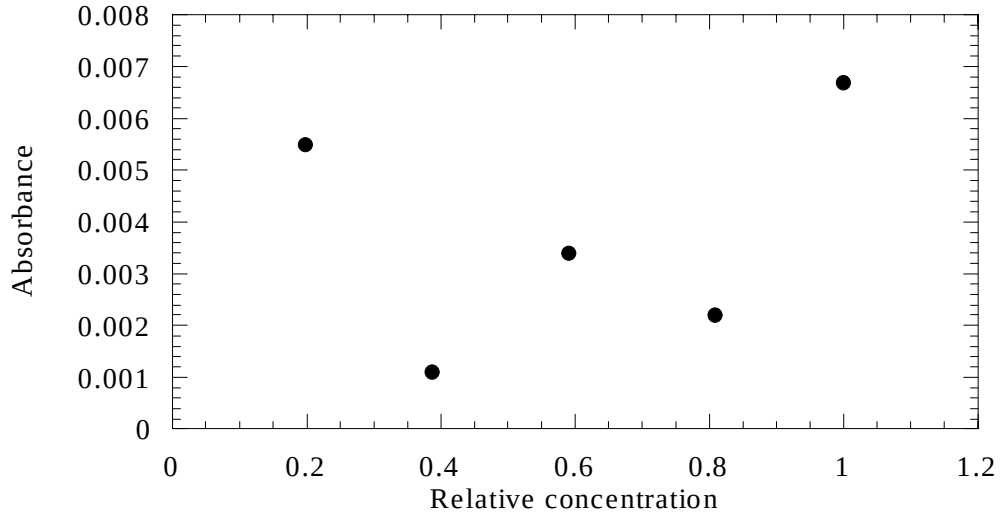

Figure 3.1.1-14. Control to see if Lambert Beers law is applicable at **386nm**. Black dots are experimental values.

The absorbance for these measurements is very low, and examination of noise was performed. Analysis of absorption over time for excitation at 386nm showed that absorbance in this region varies from 0.0012 to 0.0054 (figure 3.1.1-15).

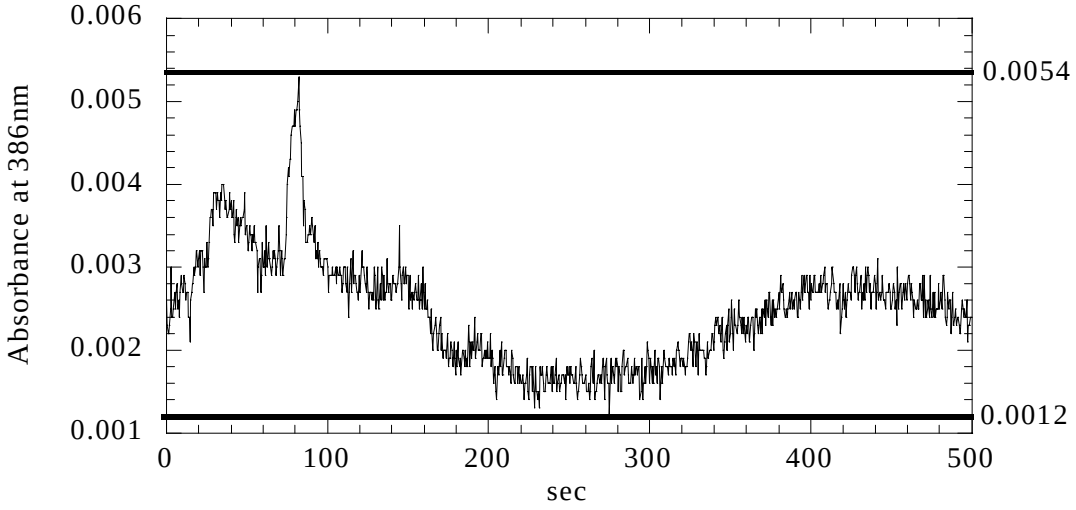

Figure 3.1.1-15. Absorbance of two drops of HDF 200 in a 3mL cuvette filled with solvent, measured at 386nm for 500 seconds.

On the basis of these observations all values for absorbance, at excitation wavelength 386nm, below 0,0054 were excluded. According to Lambert Beers law, $A=\varepsilon l c$, ε is calculated at 281, 288, 330, 339, 362 and 386nm.

Table 3.1.1-1. Calculation of ε. l=1.

Wavelength, nm	Absorbance	Concentration (relative)	Epsilon calculated	Average epsilon
281	0.8026	1	0.8026	0.8268
281	0.6537	0.808	0.8090	
281	0.4825	0.591	0.8164	
281	0.3172	0.387	0.8196	
281	0.1755	0.198	0.8864	
288	0.5277	1	0.5277	0.5443
288	0.4282	0.808	0.5300	
288	0.3154	0.591	0.5337	
288	0.2077	0.387	0.5367	
288	0.1175	0.198	0.5934	
330	0.0544	1	0.0544	0.0527
330	0.0408	0.808	0.0505	
330	0.0311	0.591	0.0526	
330	0.0206	0.387	0.0532	
330	excluded			
339	0.0215	1	0.0215	0.0202
339	0.0144	0.808	0.0178	
339	0.0115	0.591	0.0195	
339	0.0085	0.387	0.0220	
339	excluded			
362	0.0105	1	0.0105	0.0085
362	0.0061	0.808	0.0075	
362	0.0046	0.591	0.0078	
362	0.0032	0.387	0.0083	
362	excluded			

Table 3.1.1-1 continued

386	0.0067	1	0.0067	0.0067
386	excluded	0.808		
386	excluded	0.591		
386	excluded	0.387		
386	excluded	0.198		

ε was calculated for all the different dilutions, and the results are given as the average of these.

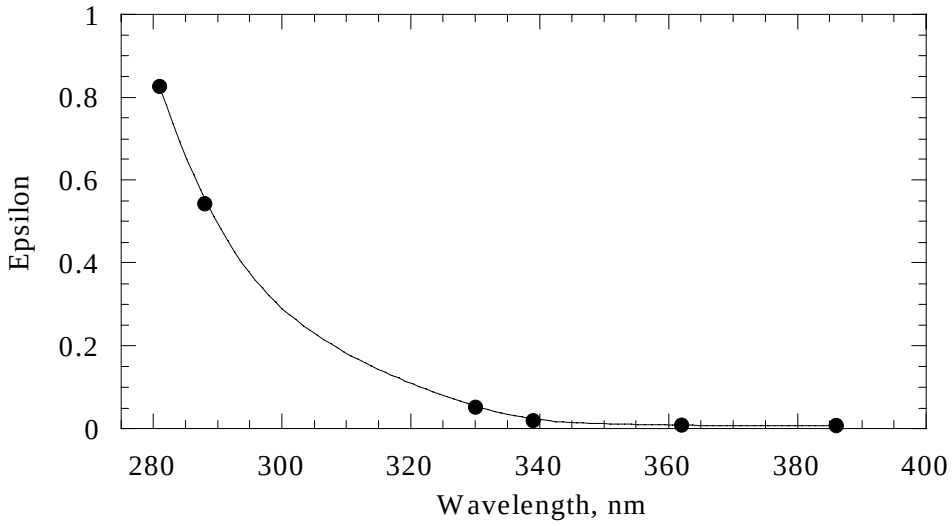

Figure 3.1.1-16. Relationship between calculated epsilon at 281, 288, 330, 339, 362, 386nm and wavelength. Smooth curve fit (black curve).

For the wavelengths of interest the value of ε is decreasing with increasing wavelength. The results from the simulations in the mathematical spreadsheet showed that ε was decreasing by one factor from excitation at 281 to 330. Comparing the experimentally obtained values for ε, a decrease from 0.8268 to 0.0527 is observed going from excitation at 281nm to excitation at 330nm. This is a decrease by one factor, which is identical to the observations made in the mathematical spreadsheet.

The emission scans of the same dilutions as those used for absorption measurements, show the tendencies expected with respect to changes in the shape of the calibration curve with changes in excitation wavelength.

The emission scan of HDF 200 with excitation wavelength 281nm, is shown in figure 3.1.1-17.

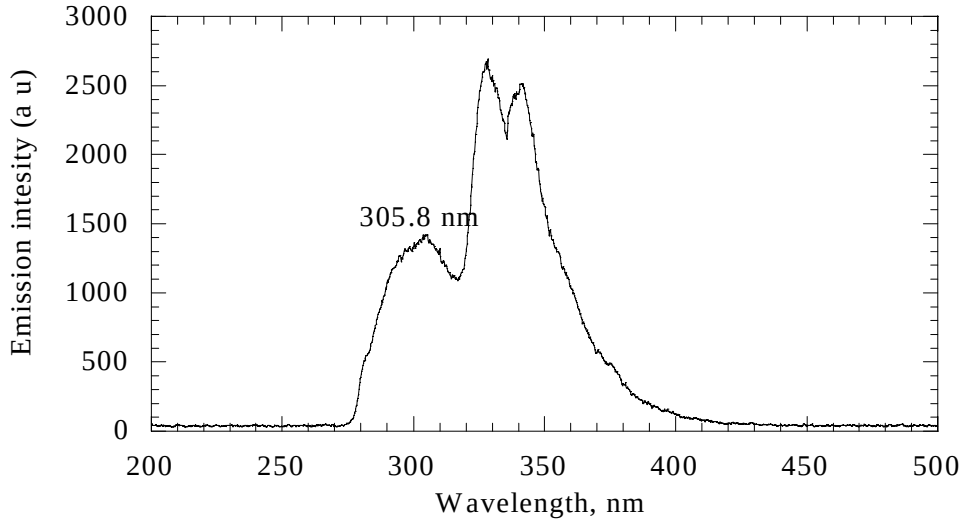

Figure 3.1.1-17. Emission spectrum of HDF 200, excitation wavelength **281nm**.

Emission intensity of the peak at 305.8nm was chosen to construct the calibration curve for excitation wavelength 281nm. This calibration curve is shown in figure 3.1.1-18, and reaches emission maximum at relative concentration 0.4. In figures 3.1.1-18, 20, 22 and 23, relative concentration=1 refers to the standard solution described in chapter 2.3.3.2

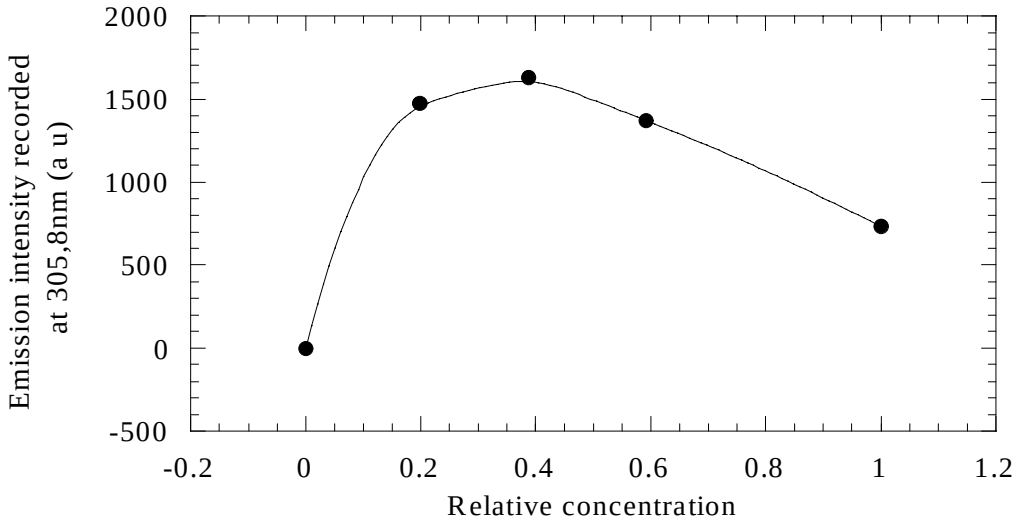

Figure 3.1.1-18. Shape of calibration curve at excitation wavelength **281nm** corresponding to ε=0.8268.

To construct the calibration curve for excitation wavelength 288nm, the emission intensity at 329.8nm was used.

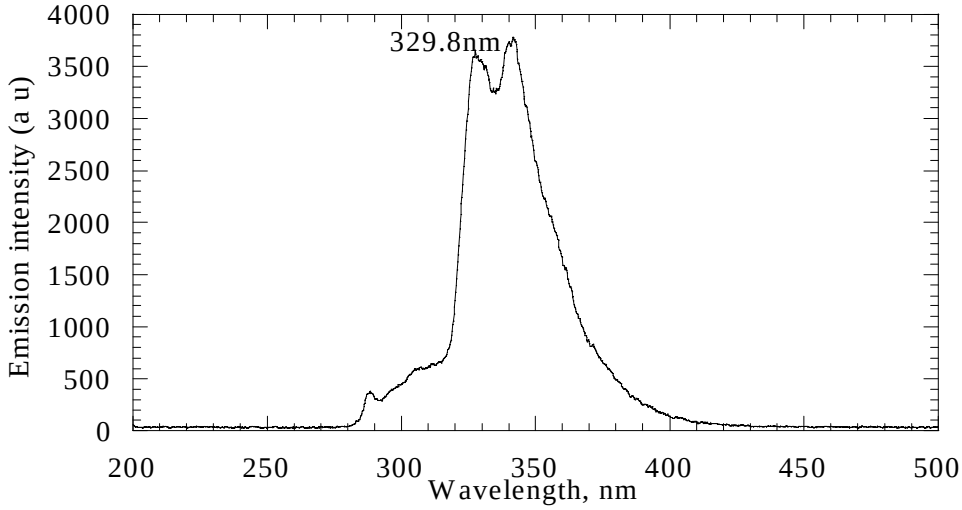

Figure 3.1.1-19. Emission spectrum of HDF 200, excitation wavelength **288nm**.

The calibration curve for excitation at 288nm reaches emission maximum at a higher relative concentration than that of 281nm, approximately 0.6. The curve is also decreasing slower after maximum has been reached.

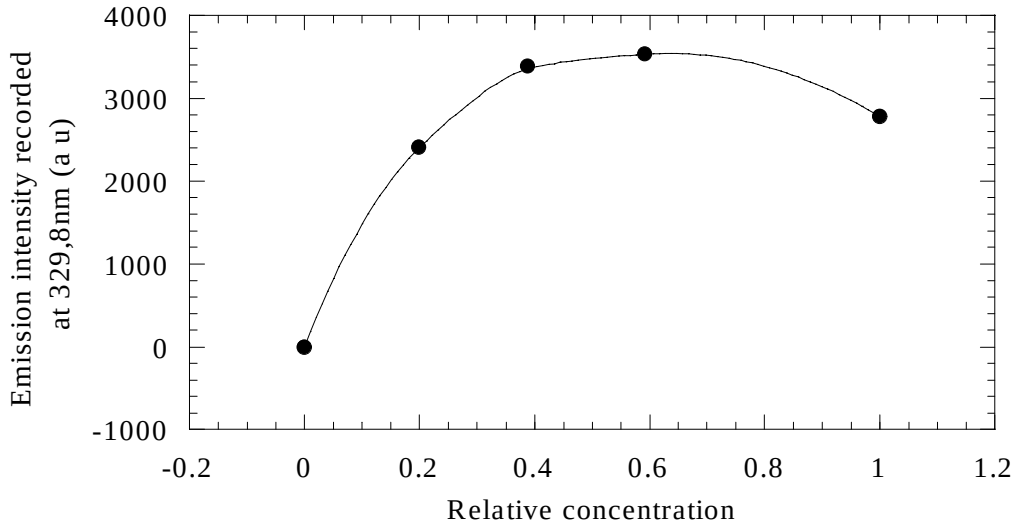

Figure 3.1.1-20. Shape of calibration curve at excitation wavelength **288nm** corresponding to ε=0.5443.

For excitation wavelength 330nm emission intensity was recorded at 346.2nm to construct the calibration curve, and for 339nm 376.0nm was used. The peak appearing at 330nm in figure 3.1.1-21 is scattering light, which is the light appearing at the excitation wavelength.

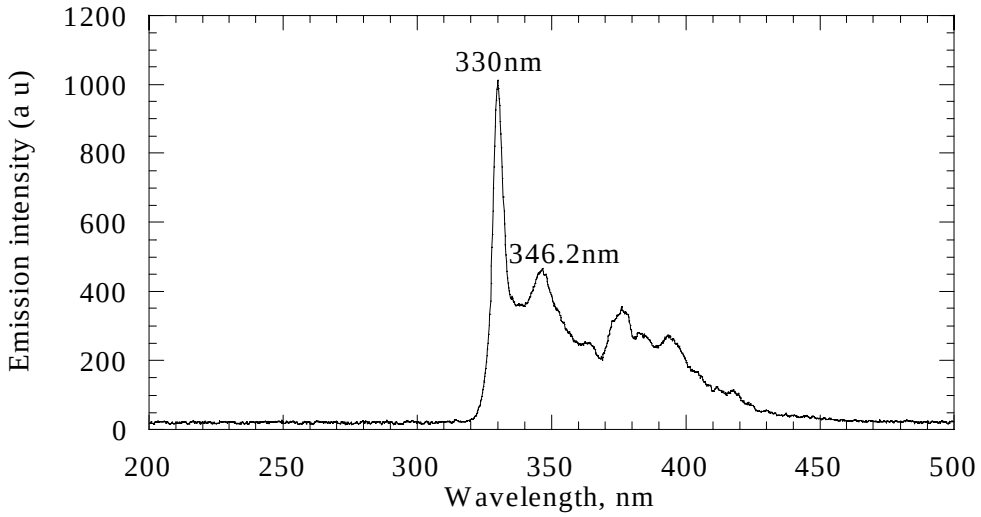

Figure 3.1.1-21. Emission spectrum of HDF 200, excitation wavelength **330nm**.

The calibration curves for excitation at 330 and 339nm are almost linear, only showing a small deflection.

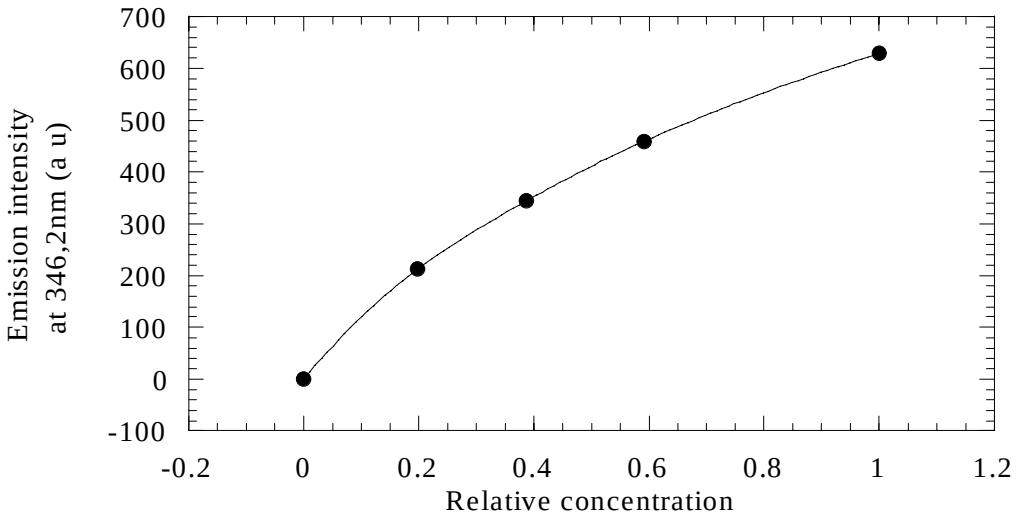

Figure 3.1.1-22. Shape of calibration curve at excitation wavelength **330nm** corresponding to ε=0.0527.

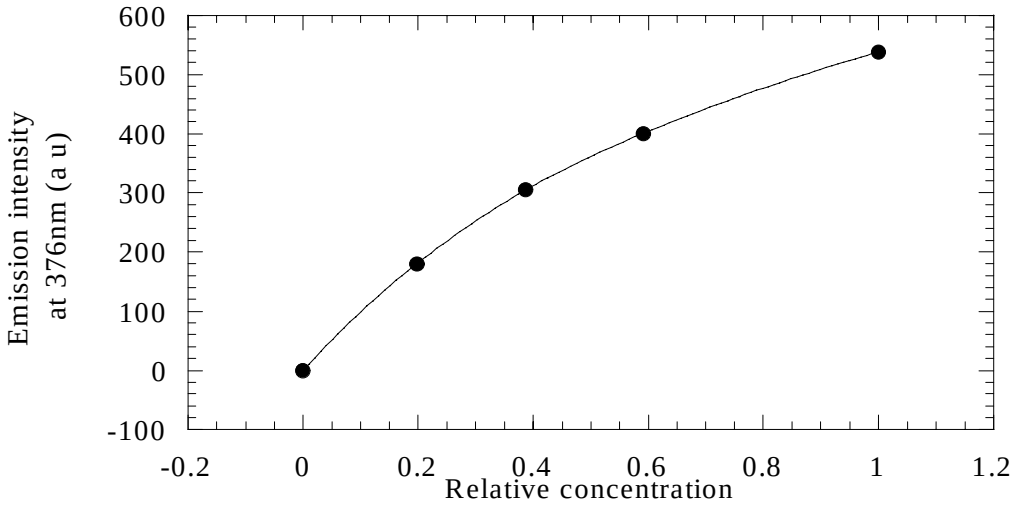

Figure 3.1.1-23. Shape of calibration curve at excitation wavelength **339nm** corresponding to ε=0.0207

Excitation at 362 and 386nm showed no emission except from scattering light.

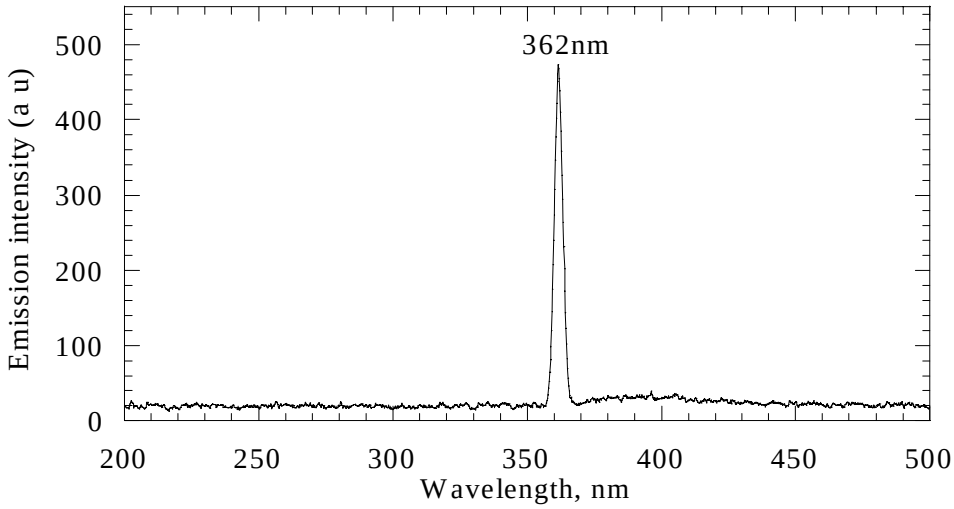

Figure 3.1.1-24. Emission scan of HDF 200, excitation wavelength **362nm**.

This was expected due to very low ε and hence very low absorption and emission.

The observations from figures 3.1.1-18, 20 22 and 23 confirms the presumption that ε is changing with the wavelength of excitation. The calibration curves are less affected by the inner filter effect at higher wavelength of excitation and lower value of ε.

3.1.2 Resonance energy transfer

For resonance energy transfer to occur the emission spectrum of a fluorophore has to overlap with the absorption spectrum of another molecule. There was no overlap between the absorption spectrum of naphthalene and the emission spectrum of antracene, and it was not expected to observe resonance energy transfer from antracene to naphthalene.

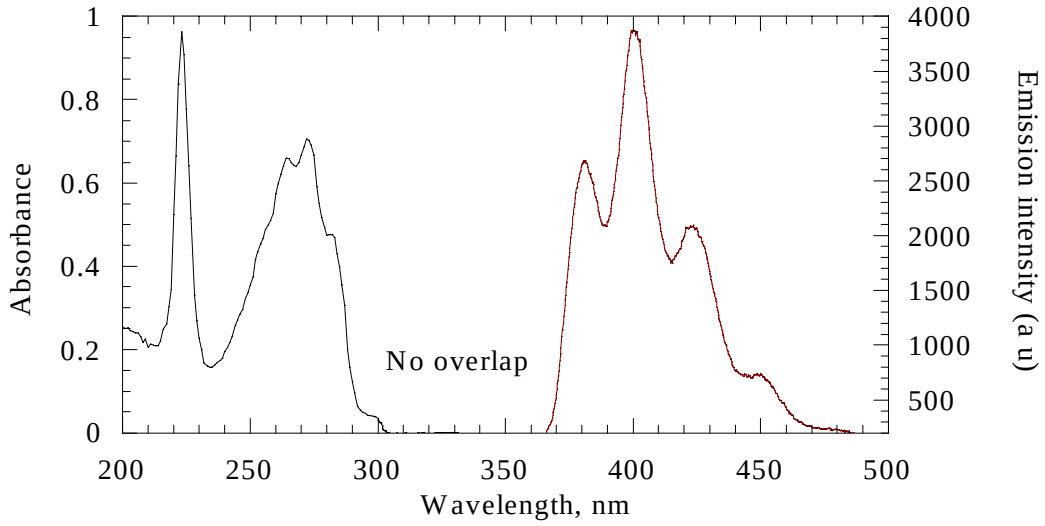

Figure 3.1.2-1. Absorbance spectrum of naphthalene and emission spectrum of antracene.

An overlap between the absorption spectrum of antracene and the emission spectrum of naphthalene was however observed.

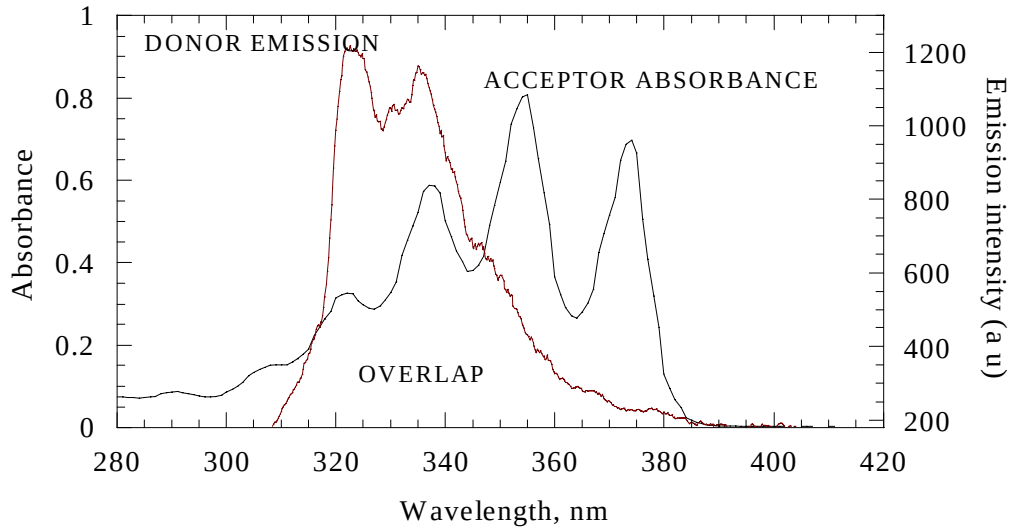

Figure 3.1.2-2. Absorbance spectrum of antracene and emission spectrum of naphthalene.

This indicates that RET with naphthalene as donor and antracene as acceptor will be expected. The experiment with adding drops of antracene to a solution of naphthalene confirms this

expectation. Figure 3.1.2-3 shows qualitatively how the intensity of the naphthalene signal is decreasing as more and more drops of antracene are added.

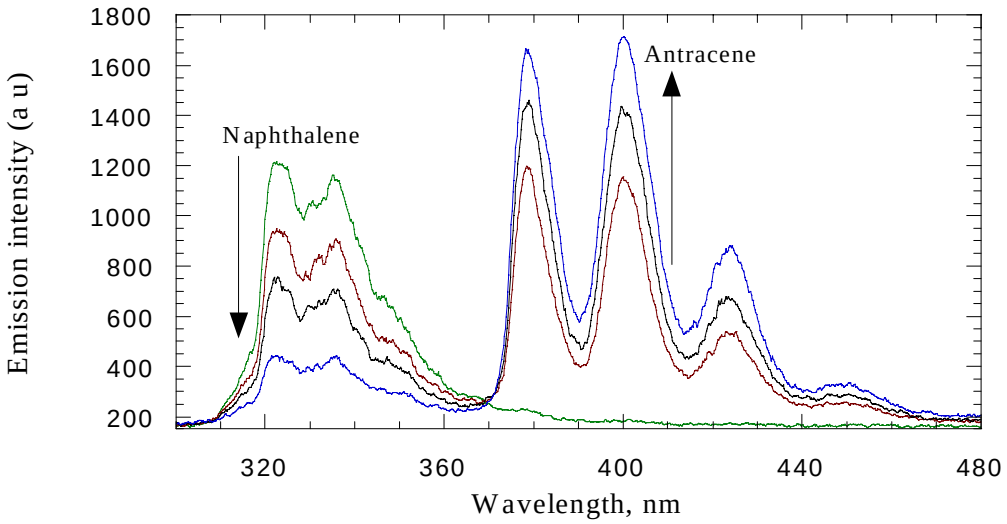

Figure 3.1.2-3. Emission scans of pure naphthalene solution, and naphthalene added different amounts of antracene. Blue curve is naphthalene standard, red curve is naphthalene standard in the 3mL cuvette added 1 drop antracene, black curve 2 drops antracene and dark blue curve 5 drops antracene.

Based on the volume of antracene added, and the total volume in the cuvette, the molar concentration of antracene and naphthalene in each measurement was calculated.

Table 3.1.2-1. Calculations of naphthalene and antracene concentration in cuvette.

Number of drops added	Calculated volume (L) of antracene added	Calculated volume (L) before antracene added	Calculated total volume (L) in cuvette	Concentration naphthalene (M)	Concentration of antracene (M)
0	0	0	0	$7.7055\ 10^{-4}$	0
1	$8.2071\ 10^{-6}$	$3.2111\ 10^{-3}$	$3.2193\ 10^{-3}$	$7.6858\ 10^{-4}$	$8.6255\ 10^{-7}$
2	$1.6414\ 10^{-5}$	$3.1667\ 10^{-3}$	$3.1749\ 10^{-3}$	$7.6855\ 10^{-4}$	$1.7493\ 10^{-6}$
3	$2.4621\ 10^{-5}$	$3.1253\ 10^{-3}$	$3.1335\ 10^{-3}$	$7.6853\ 10^{-4}$	$2.6586\ 10^{-6}$
4	$3.2828\ 10^{-5}$	$3.0859\ 10^{-3}$	$3.0941\ 10^{-3}$	$7.6850\ 10^{-4}$	$3.5899\ 10^{-6}$
5	$4.1035\ 10^{-5}$	$2.9677\ 10^{-3}$	$2.9759\ 10^{-3}$	$7.6842\ 10^{-4}$	$4.6656\ 10^{-6}$
6	$4.9242\ 10^{-5}$	$2.9263\ 10^{-3}$	$2.9345\ 10^{-3}$	$7.6839\ 10^{-4}$	$5.6777\ 10^{-6}$
7	$5.7449\ 10^{-5}$	$2.8737\ 10^{-3}$	$2.8819\ 10^{-3}$	$7.6835\ 10^{-4}$	$6.7447\ 10^{-6}$
8	$6.5657\ 10^{-5}$	$2.8303\ 10^{-3}$	$2.8385\ 10^{-3}$	$7.6832\ 10^{-4}$	$7.8262\ 10^{-6}$
9	$7.3864\ 10^{-5}$	$2.8020\ 10^{-3}$	$2.8102\ 10^{-3}$	$7.6830\ 10^{-4}$	$8.8931\ 10^{-6}$
10	$8.2071\ 10^{-5}$	$2.7586\ 10^{-3}$	$2.7668\ 10^{-3}$	$7.6826\ 10^{-4}$	$1.0036\ 10^{-5}$
11	$9.0278\ 10^{-5}$	$2.7030\ 10^{-3}$	$2.7112\ 10^{-3}$	$7.6821\ 10^{-4}$	$1.1266\ 10^{-5}$
12	$9.8485\ 10^{-5}$	$2.6727\ 10^{-3}$	$2.6809\ 10^{-3}$	$7.6819\ 10^{-4}$	$1.2429\ 10^{-5}$
15	$1.2311\ 10^{-4}$	$2.6273\ 10^{-3}$	$2.6519\ 10^{-3}$	$7.6339\ 10^{-4}$	$1.5707\ 10^{-5}$
18	$1.4773\ 10^{-4}$	$2.5899\ 10^{-3}$	$2.6145\ 10^{-3}$	$7.6329\ 10^{-4}$	$1.9118\ 10^{-5}$
21	$1.7235\ 10^{-4}$	$2.5657\ 10^{-3}$	$2.5903\ 10^{-3}$	$7.6322\ 10^{-4}$	$2.2513\ 10^{-5}$
25	$2.0518\ 10^{-4}$	$2.5384\ 10^{-3}$	$2.5812\ 10^{-3}$	$7.5777\ 10^{-4}$	$2.6999\ 10^{-5}$
28	$2.2980\ 10^{-4}$	$2.5273\ 10^{-3}$	$2.5519\ 10^{-3}$	$7.6311\ 10^{-4}$	$3.0468\ 10^{-5}$
31	$2.5442\ 10^{-4}$	$2.4960\ 10^{-3}$	$2.5206\ 10^{-3}$	$7.6302\ 10^{-4}$	$3.4152\ 10^{-5}$

Table 3.1.2-1 continued

35	$2.8725\ 10^{-4}$	$2.4424\ 10^{-3}$	$2.4753\ 10^{-3}$	$7.6033\ 10^{-4}$	$3.9264\ 10^{-5}$
40	$3.2828\ 10^{-4}$	$2.4535\ 10^{-3}$	$2.4946\ 10^{-3}$	$7.5787\ 10^{-4}$	$4.4526\ 10^{-5}$

Based on these calculations the relationship between concentration of antracene and the emission intensity of the two antracene peaks is illustrated in figures 3.1.2-4 and 3.1.2-5.

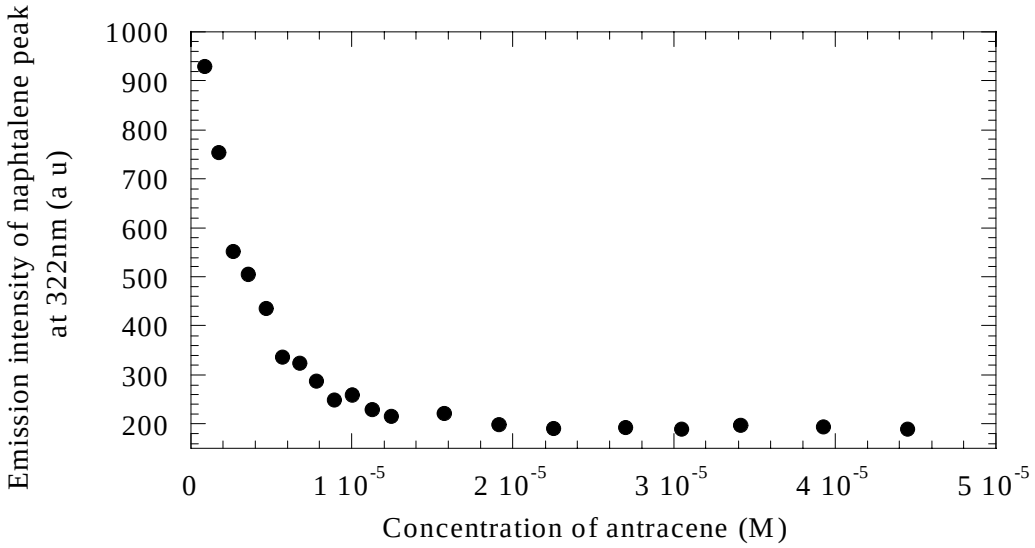

Figure 3.1.2-4. Emission scans of naphthalene with different amounts of antracene added. Excitation 250nm. Intensity of the naphthalene peak at 322nm recorded.

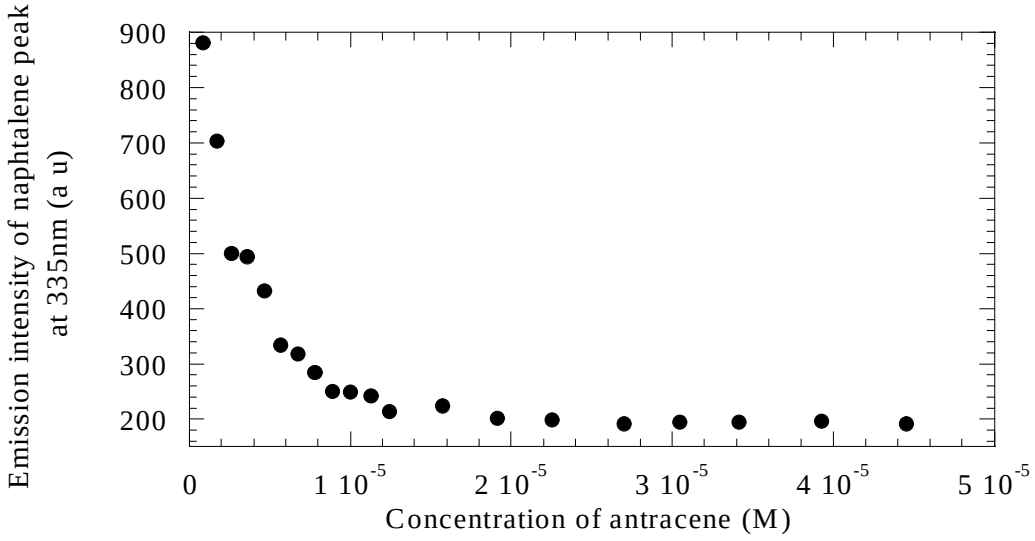

Figure 3.1.2-5. Emission scans of naphthalene with different amounts of antracene added. Excitation 250nm. Intensity of the naphthalene peak at 335nm recorded.

The concentration of naphthalene is almost constant, only a small variation due to evaporation. Despite of this the emission intensity, for both naphthalene peaks, is decreasing with increasing concentration of antracene. Naphthalene is clearly transferring energy from itself to antracene.

3.1.3 Self-absorption

For any energy transfer to occur, either between two different molecules or within a molecule, there has to be an overlap of the emission spectrum and the absorption spectrum. That was not the case for naphthalene.

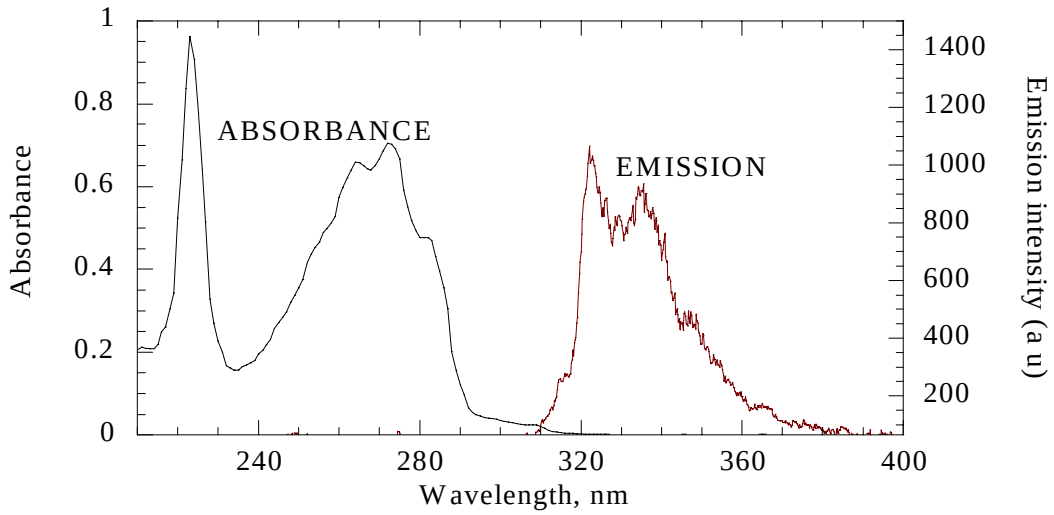

Figure 3.1.3-1. Absorption and emission spectrum of naphthalene.

To check this, emission spectra were recorded of different dilutions of the naphthalene standard solution. Only a limited number of the dilutions are shown in figure 3.1.3-2, to make it well arranged.

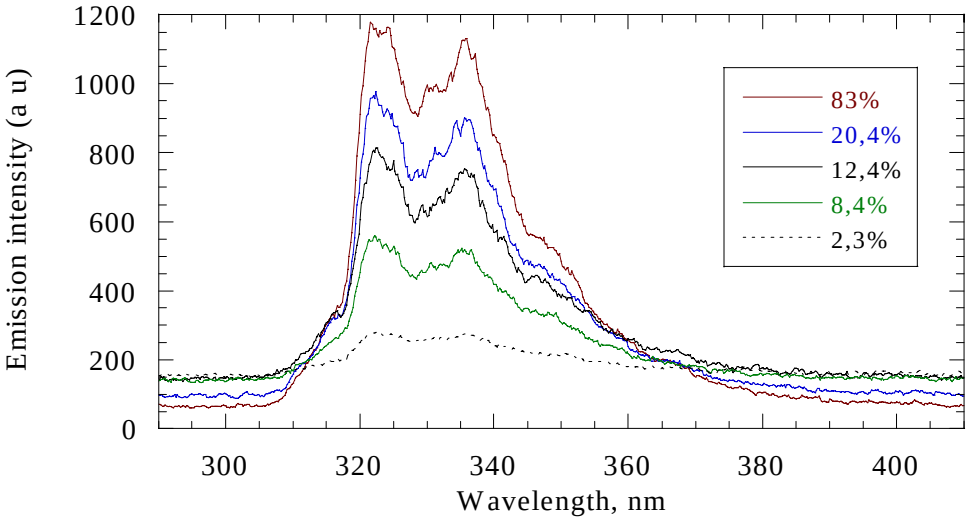

Figure 3.1.3-2. Emission spectra of different dilutions of the standard solution (100%) of naphthalene. Excitation wavelength 250nm.

These spectra show a constant relation between the peak at 323nm and the one at 335.6nm. In figure 3.1.3-3, relative concentration=1 refers to the standard solution of naphthalene described in chapter 2.3.4.2.

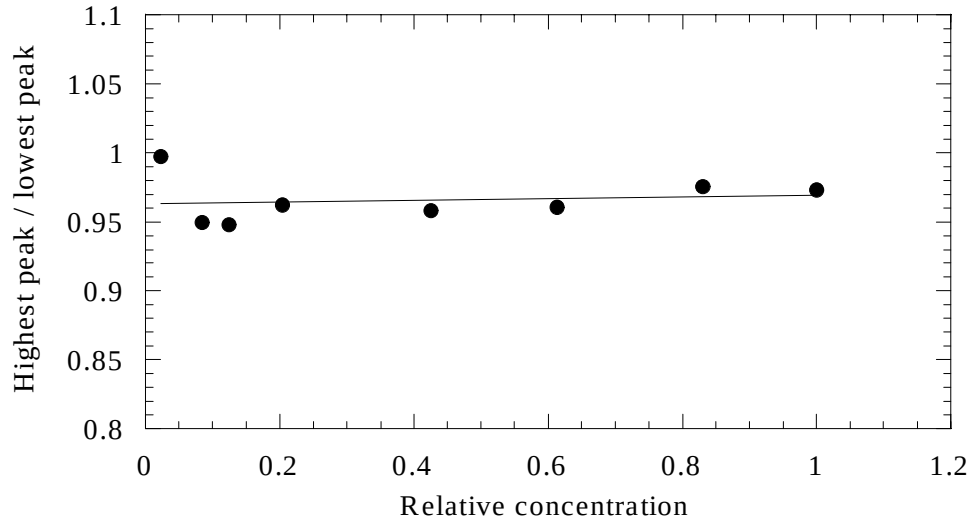

Figure 3.1.3-3. Relationship between the peak at 323nm and the peak at 335,6nm in the emission spectra of naphthalene. Black line indicating linear curve fit.

The absorption spectrum of antracene (figure 3.1.3-4) shows significant structure due to the individual vibrational energy levels of the ground state and the excited states. The absorption spectrum of naphthalene however (figure 3.1.3-1) shows less vibrational structure. For antracene the absorption and emission spectra are mirror images, meaning that these spectra are a result of the same transitions being involved for both absorption and emission. An overlap between the absorption and the emission spectrum of antracene was observed, indicating that energy transfer within the antracene molecule would be expected.

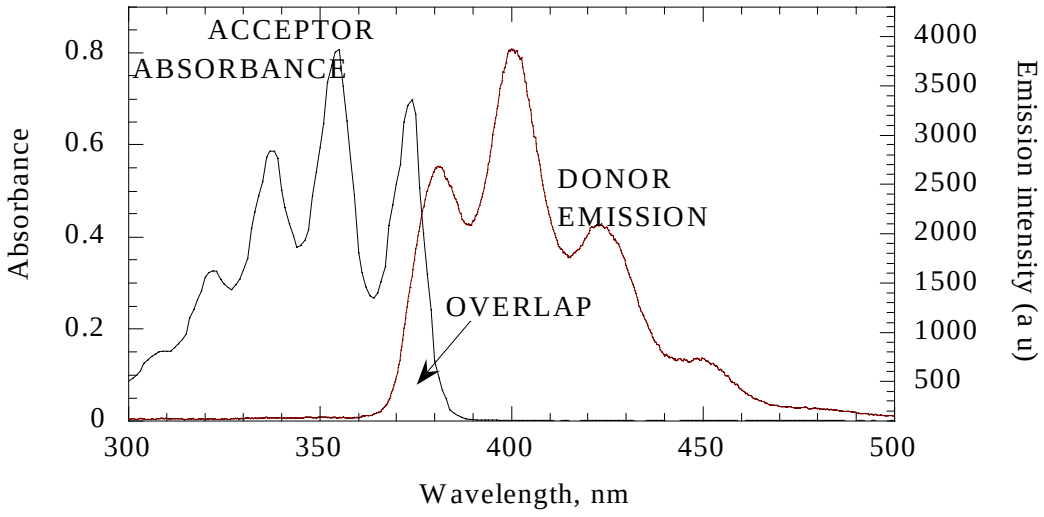

Figure 3.1.3-4. Absorption and emission spectrum of antracene.

To check this, emission spectra were recorded of different dilutions of the antracene standard solution. A limited number of the dilutions are shown in figure 3.1.3-5, to make the illustration clearly set out.

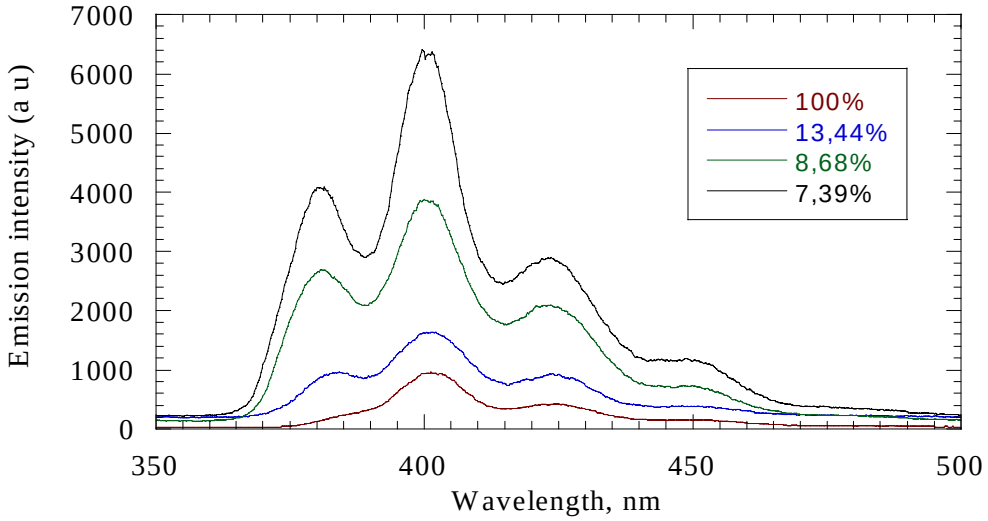

Figure 3.1.3-5. Emission spectra of different dilutions of the standard solution (100%) of antracene. Excitation wavelength 250nm.

These emission spectra show emission maximum at 381.4, 399.6, 423.6 and 450.4nm. Examination of the emission spectra of these dilutions, show that the peak at 381.40nm is decreasing more than the others. In figures 3.1.3-6 to 3.1.3-8, relative concentration=1 refers to the standard solution of antracene described in chapter 2.3.4.2.

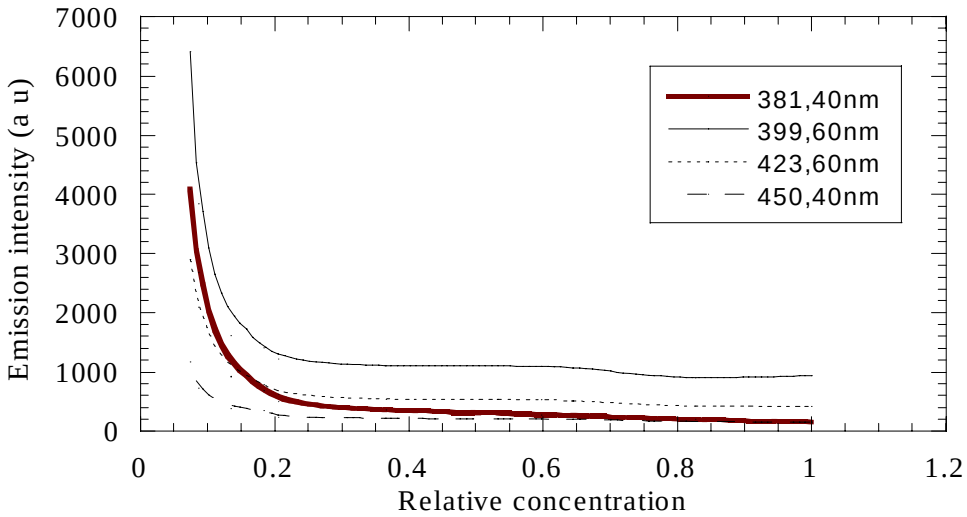

Figure 3.1.3-6. Reduction in emission intensity of the different peaks in the emission spectra in fig 3.1.3-5.

The peak at 381.40nm is the second highest peak at relative concentrations up to 0.15. From 0.15 to 0.75 the peak height of 381.40nm is decreasing more than the others until it after 0.75 becomes the lowest peak.

The peak at 381.40nm is also the peak being reduced most with respect to itself. In figure 3.1.3-7 the peak height of all dilutions at 381.40nm has been divided by the peak height of the highest peak at this wavelength. The same has been done for the other wavelengths.

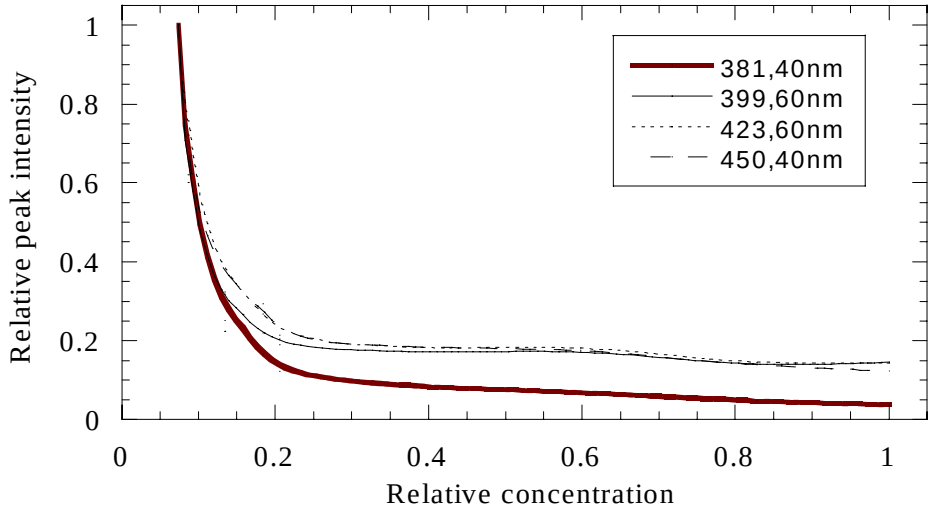

Figure 3.1.3-7. Reduction in peak height at 381,40nm, 399,60nm, 423,60nm and 450,40nm

The reduction in peak height at 399.60nm, 423.60nm and 450.40nm with increasing concentration is due to the inner filter effect. The peak at 381.40nm is in addition reduced due to self-absorption.

Examination of the peak heights for different dilutions relative to the peak height at 399.60nm shows that for relative concentrations higher than 0.25, the relation between the peak at 423.60nm and 450.40 relative to the peak at 399.60 is almost constant. The peak at 381.40nm, however, is decreasing more than the peak at 399.60nm.

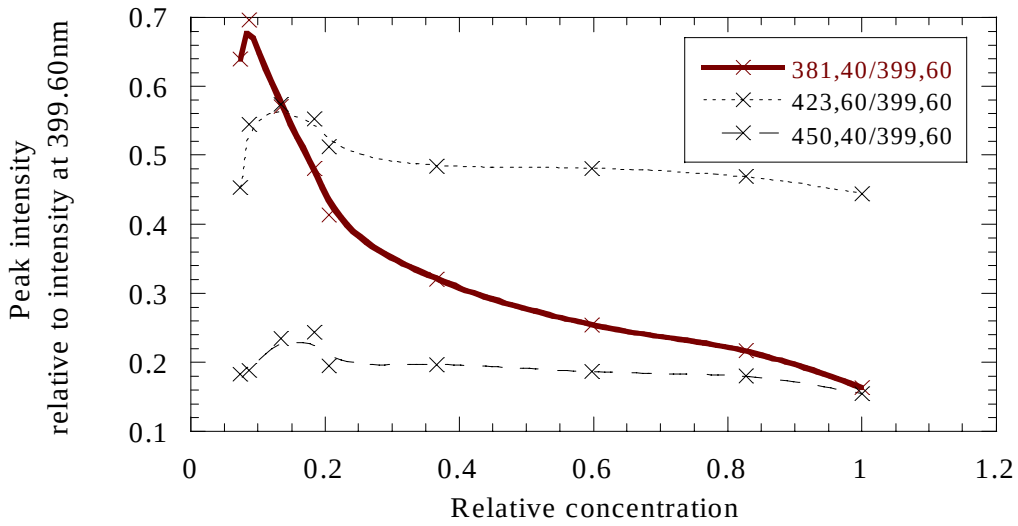

Figure 3.1.3-8. Peak intensity relative to peak intensity at 399,60nm.

In the case of antracene in solution with naphthalene, the same pattern is not observed. With a nearly constant concentration of naphthalene, and increasing concentration of antracene the peak at 381.40 nm does not disappear the same way as when antracene is alone.

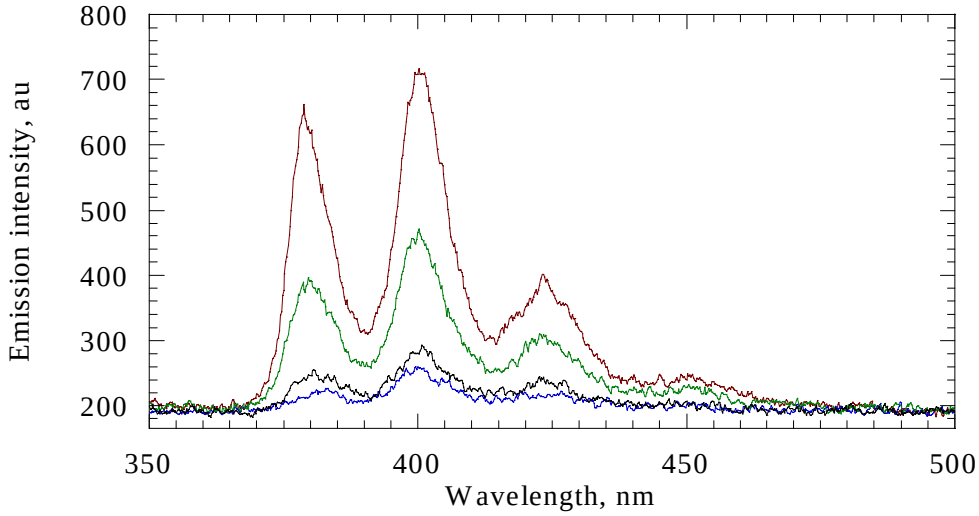

Figure 3.1.3-9. Increasing concentration of antracene in solution with naphthalene. Only the antracene part of the spectrum is shown. Concentration of antracene in red spectrum is 1.2429 10^{-5}M, blue spectrum 1.9118 10^{-5}M, black spectrum 3.0468 10^{-5}M and dark blue spectrum 4.4526 10^{-5}M.

This is probably because there still is an energy transfer to naphthalene, even if the naphthalene peak has disappeared. This means that naphthalene in a sample can influence the spectrum of other components, even when it is not possible form the spectrum to detect naphthalene.

3.2 TCH from gas chromatography

The variation for the GC-analysis was investigated by performing three parallel injections and calculations of one sample: Beryl A, test 1, incubation temperature 20°C and incubation time 28 days; three injections and calculations were made.

Table 3.2-1. Calculation of uncertainty in injection and integration

Injection	mg THC / kg wet sediment	mg THC / kg dry sediment
No 1	725	1695
No 2	706	1649
No 3	728	1702
Average	720	1682
Standard deviation (absolute)	12	29
Standard deviation (%)	1.72%	1.72%

The variation of THC for both wet and dry sediment, due to variations in injection and integration is very small, only 1.72%.

The variation of the overall THC-method was investigated as follows: For three of the samples three parallel extractions, measurements and calculations were made. The three samples were:

1) Beryl A, test 1, incubation temperature 20°C and incubation time 28 days
2) Beryl A, test 2, incubation temperature 5°C and incubation time 56 days
3) Beryl A, test 2, incubation temperature 20°C, nutrients added and incubation time 1 day

Table 3.2-2. Calculation of uncertainty in extraction. THC is given as mg THC/kg wet sediment.

Parallel	THC in sample 1)	THC in sample 2)	THC in sample 3)
No 1	720	1933	2799
No 2	887	2197	2133
No 3	746	2035	1539
Average	784	2055	2157
Standard deviation (Absolute)	90	133	630
Standard deviation (%)	11.4%	6.5%	29.2%

Table 3.2-3. Calculation of uncertainty in extraction. THC is given as mg THC/kg dry sediment

Parallel	THC in sample 1)	THC in sample 2)	THC in sample 3)
No 1	1682	2637	4993
No 2	2070	2996	3801
No 3	1743	2775	2746
Average	1832	2802	3847
Standard deviation (Absolute)	209	181	1125
Standard deviation (%)	11.4%	6.5%	29.2%

For THC, both based on wet and dry sediment, a variation up to 30% was observed due to uncertainty in extraction. This means it is impossible to say that a change in THC is significant unless it is larger than 30%.
In tables 3.2-4 to 3.2-7 the calculated THC in the samples treated in the thesis are presented.

Table 3.2-4. Concentration of THC / wet sediment in **test 1**, aerobic conditions. Beryl A, test 1, incubation temperature 20°C and incubation time 28 days is given as the average of three parallels.

Sample description	**Day 1** mg THC/kg wet sediment	**Day 28** mg THC/kg wet sediment	**Day 56** mg THC/kg wet sediment	**Standard deviation (%)**
Beryl A, 10°C	962	688	962	18
Beryl A, 20°C	1139	784	1286	24
Beryl A, 20°C, N+P	1279	533	890	**41**
Beryl A, 5°C	1124	1077	1203	6

Table 3.2-5. Concentration of THC / dry sediment in **test 1**, aerobic conditions. Beryl A, test 1, incubation temperature 20°C and incubation time 28 days is given as the average of three parallels.

Sample description	**Day 1** mg THC/kg dry sediment	**Day 28** mg THC/kg dry sediment	**Day 56** mg THC/kg dry sediment	**Standard deviation (%)**
Beryl A, 10°C	1867	1513	2445	24
Beryl A, 20°C	1861	1832	2879	27
Beryl A, 20°C, N+P	2294	1287	2176	29
Beryl A, 5°C	1921	2444	2506	14

Table 3.2-6. Concentration of THC / wet sediment in **test 2**, anaerobic conditions. Beryl A, test 2, incubation temperature 20°C and nutrients added and incubation time 1 day is given as the average of three parallels. The same for Beryl A, test 2, incubation temperature 5°C and incubation time 56 days.

Sample description	**Day 1** mg THC/kg wet sediment	**Day 28** mg THC/kg wet sediment	Day 56 mg THC/kg wet sediment	**Day 100** mg THC/kg wet sediment	**Standard deviation (%)**
Beryl A, 10°C	1692	1818	1768	2871	27
Beryl A, 20°C	2718	1328	2344	1933	28
Beryl A, 20°C, N+P	2157	2310	2606		10
Beryl A, 5°C	2601	2062	2055		14

Table 3.2-7. Concentration of THC / dry sediment in **test 2**, anaerobic conditions. Beryl A, test 2, incubation temperature 20°C and nutrients added and incubation time 1 day is given as the average of three parallels. The same for Beryl A, test 2, incubation temperature 5°C and incubation time 56 days.

Sample description	**Day 1** mg THC/kg dry sediment	**Day 28** mg THC/kg dry sediment	**Day 56** mg THC/kg dry sediment	**Day 100** mg THC/kg dry sediment	**Standard deviation (%)**
Beryl A, 10°C	2970	3422	2378	3972	21
Beryl A, 20°C	4477	1836	3128	2643	**37**
Beryl A, 20°C, N+P	3847	3402	3500		7
Beryl A, 5°C	3981	2924	2802		20

With the exception of two samples, the standard deviation (%) is less then 30%. In figure 3.2-1 the time series of Beryl A, test 1 and incubation temperature 10°C is illustrated. The error bars indicate that the change is not significant.

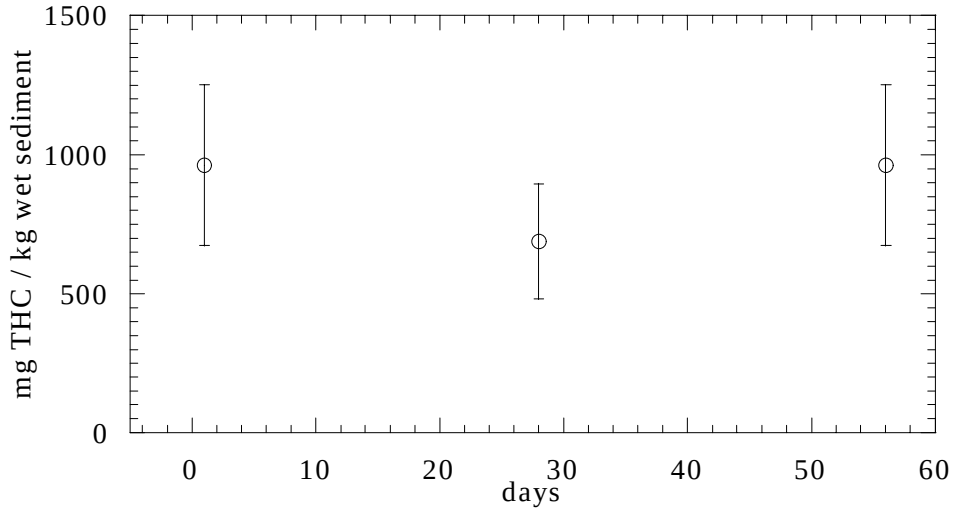

Figure 3.2-1. Time series of Beryl A, test 1 and incubation temperature 10°C Error bars indicating 30% uncertainty.

For the two samples where the standard deviation is more than 30%, no clear pattern of degradation is observed (figures 3.2-2 and 3.2-3).

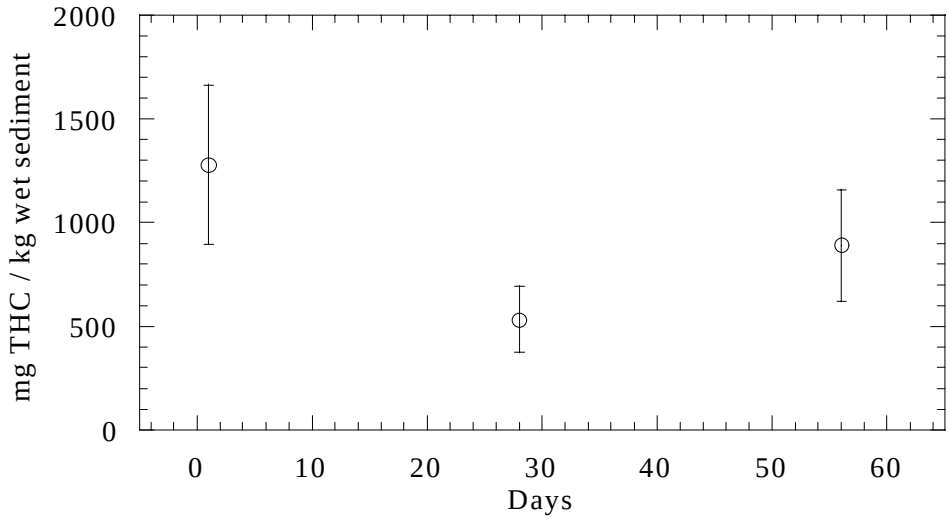

Figure 3.2-2. Beryl A, test 1, incubation temperature 20°C and nutrients added. Error bars indicating 30% uncertainty.

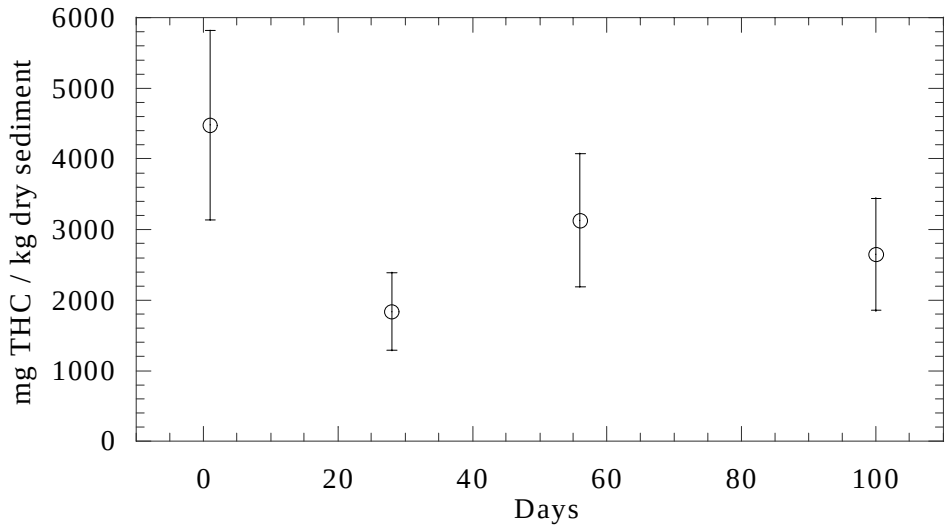

Figure 3.2-3. Beryl A, test 2, incubation temperature 20°C. Error bars indicating 30% uncertainty.

All together this means that no significant change in THC is observed, and increasing temperature and addition of nutrients do not speed up the degradation. These same variations in THC appearing without a pattern were also observed in the UKOOA project. Thorough investigations showed that the main reason for this variation was inhomogeneous test material from the concrete mixer. It was not the mixing procedure that failed, but the nature of the sediment (clayish) made it difficult to collect representative samples.

3.3 Aromatic content from fluorescence analysis

It was impractical to make the initial solutions for fluorescence analyses based on weight. Investigations of the pipette indicated that the volume is stabilizing after the pipette tip has been wetted two to three times. The accuracy of volumetric sample amounts was found to be satisfactory for the purpose of this work.

Table 3.3-1. Investigation of uncertainty in pipette.

Parallel	Pipette not wetted	Pipette wetted one time	Pipette wetted two times	Pipette wetted three times	Pipette wetted four times
No1	0.7415	0.8489	0.9362	0.9274	0.8503
No 2	0.7571	0.8226	1.0637	0.8998	1.0040
No 3	0.7590	0.8264	0.8758	0.9097	0.8435
No 4	0.7382	0.8575	0.8754	0.8955	0.8666
No 5	0.7129	0.8885	0.9161	0.8853	0.8744
No 6	0.6653	0.7768	0.8540	0.9014	0.8738
No 7	0.7073	0.8385	0.8111	0.8643	0.8846
No 8	0.7129	0.8431	0.8678	0.8919	0.9055
No 9	0.6506	0.7666	0.8303	0.7947	0.8139
No 10	0.6939	0.7937	0.8963	0.8530	0.8949
Average	0.7139	0.8263	0.8927	0.8823	0.8812

The stabilizing effect is better seen in figure 3.3-1.

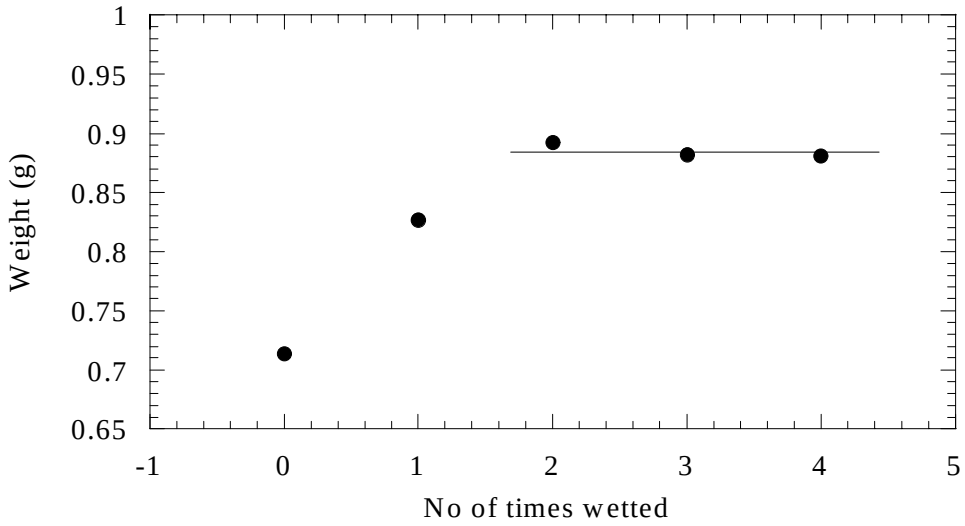

Figure 3.3-1. Weight of 885µL solvent. Pipette tip wetted none, one, two, three and four times before weight was recorded.

The pipette was to give a volume of 885 µL, and with a density of 0.99 g/cm^3 that corresponds to 0.8415g. From table 3.3-1 it should be noted that the volumes pipetted are too high, but satisfyingly reproducible so the error will be the reproducible for all samples.

Daily measurements of the standard solution of pyrene (20ppm) for instrument check up, showed a standard deviation (%) of 7%. This is quite large variation due to the instrument. The solution measured was the same each day, and a total of ten measurements were made. No dilutions of this solution were made, so all uncertainty must be attributed to the instrument.

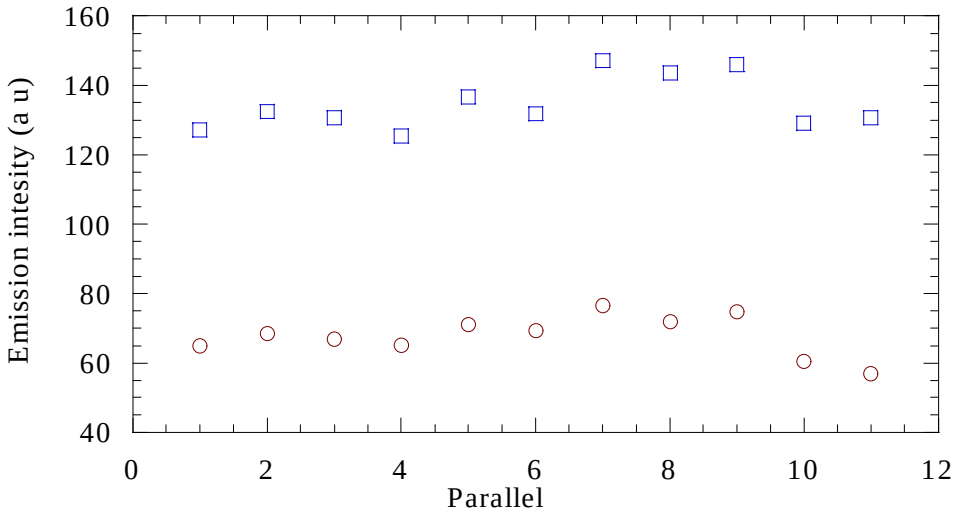

Figure 3.3-2. Variations in emission intensity of pyrene standard solution, 20 ppm. Blue rectangles show emission intensity recorded at excitation wavelength 340.47 and red circles at 328.42 in SFS 43.

All extracted sediment samples were analyzed by fluorescence. The three samples that were extracted in three parallels gave a lower standard deviation (%) than in GC-FID. The three samples were:

1) Beryl A, test 1, incubation temperature 20°C and incubation time 28 days
2) Beryl A, test 2, incubation temperature 5°C and incubation time 56 days
3) Beryl A, test 2, incubation temperature 20°C, nutrients added and incubation time 1 day

Table 3.3-2. **Sample 1**. Emission intensity recorded 43nm higher than the excitation wavelength.

Excitation wavelength	**Emission intensity 1st parallel**	**Emission intensity 2nd parallel**	**Emission intensity 3rd parallel**	**Standard deviation (%)**
281	105	105	103	1.11
288	159	156	153	1.92
330	398	414	427	3.52
339	406	416	428	2.64
362	282	288	307	4.46
386	283	290	308	4.39

Table 3.3-3. **Sample 2**. Emission intensity recorded 43nm higher than the excitation wavelength.

Excitation wavelength	Emission intensity 1st parallel	Emission intensity 2nd parallel	Emission intensity 3rd parallel	Standard deviation (%)
281	121	131	129	4.17
288	177	186	185	2.70
330	439	419	433	2.38
339	434	419	433	1.96
362	299	281	299	3.55
386	296	277	298	3.99

Table 3.3-4. **Sample 3**. Emission intensity recorded 43nm higher than the excitation wavelength.

Excitation wavelength	Emission intensity 1st parallel	Emission intensity 2nd parallel	Emission intensity 3rd parallel	Standard deviation (%)
281	120	109	112	5.00
288	166	160	162	1.88
330	403	433	419	3.59
339	405	441	416	4.39
362	274	302	285	4.92
386	267	301	283	6.00

The highest standard deviations (%) that were observed for each wavelength are presented in table 3.3-5.

Table 3.3-5. The highest standard deviations (%) observed for each excitation wavelength.

Excitation wavelength	Highest standard deviations (%) observed
281	5.00
288	2.70
330	3.59
339	4.39
362	4.92
386	6.00

The fact that the standard deviations (%) observed for fluorescence measurements are smaller than those for GC-FID, and that in chapter 3.2 a deviation of nearly 30% was attributed to the extraction procedure, this means that fluorescence is a less sensitive method than GC-FID. Taking the instrument uncertainty of approximately 7% to consideration, the uncertainty at the different wavelengths is as presented in table 3.3-6.

Table 3.3-6. Uncertainty at different wavelengths of excitation due to work up and instrument.

Excitation wavelength	Standard deviations (%)
281	12.00
288	9.70
330	10.59
339	11.39
362	11.92
386	13.00

The shapes of the calibration curves for Beryl A, 20°C, day 1, test 1, are strongly affected by inner filter effect at the shortest wavelengths (figures 3.3-3 and 3.3-4), less at longer wavelengths (figures 3.3-5 and 3.3-6), and almost linear at the longest wavelengths (figures 3.3-7 and 3.3-8). In figure 3.3-5 to 3.3-8, relative concentration=1 refers to the initial solution (15 times dilution) described in chapter 2.4.4.2.

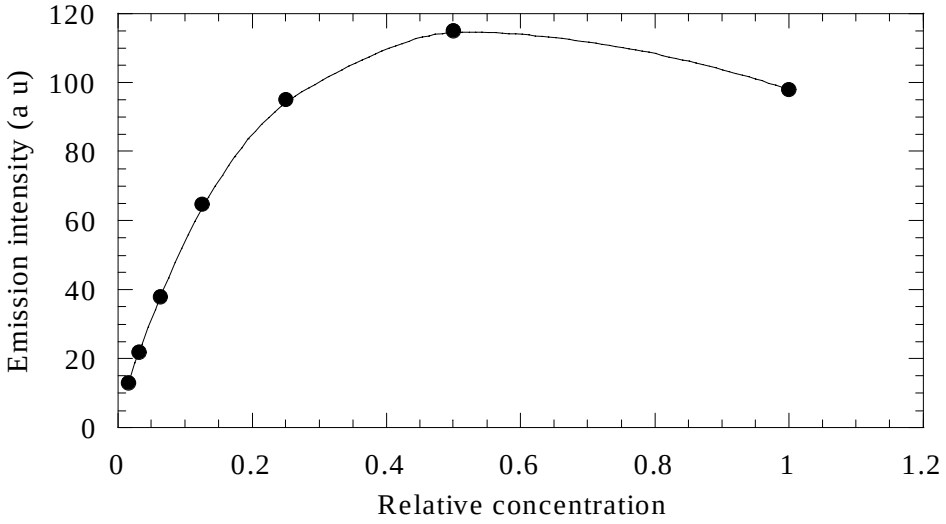

Figure 3.3-3. Calibration curve for Beryl A, 20°C, day 1, test 1. Excitation wavelength **281nm**. Emission intensity recorded 43nm higher than excitation wavelength.

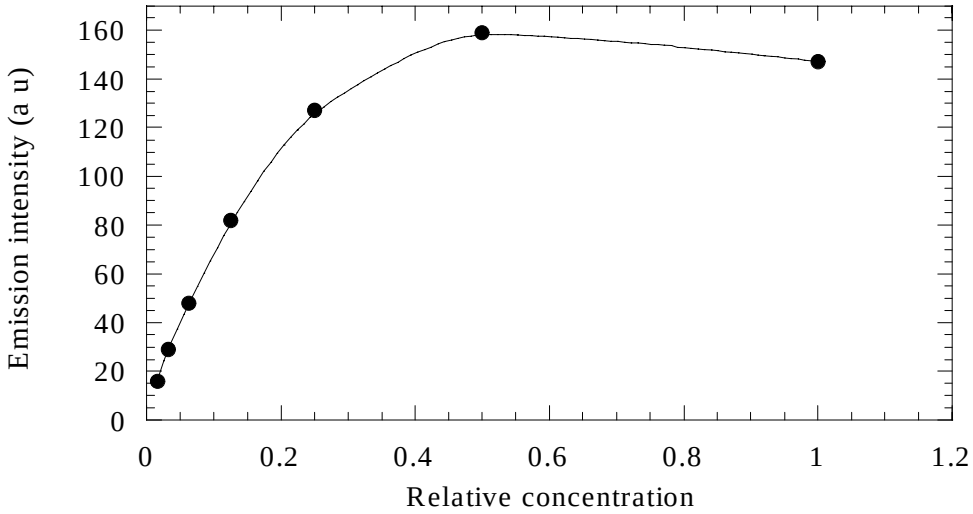

Figure 3.3-4. Calibration curve for Beryl A, 20°C, day 1, test 1. Excitation wavelength **288**nm. Emission intensity recorded 43nm higher than excitation wavelength.

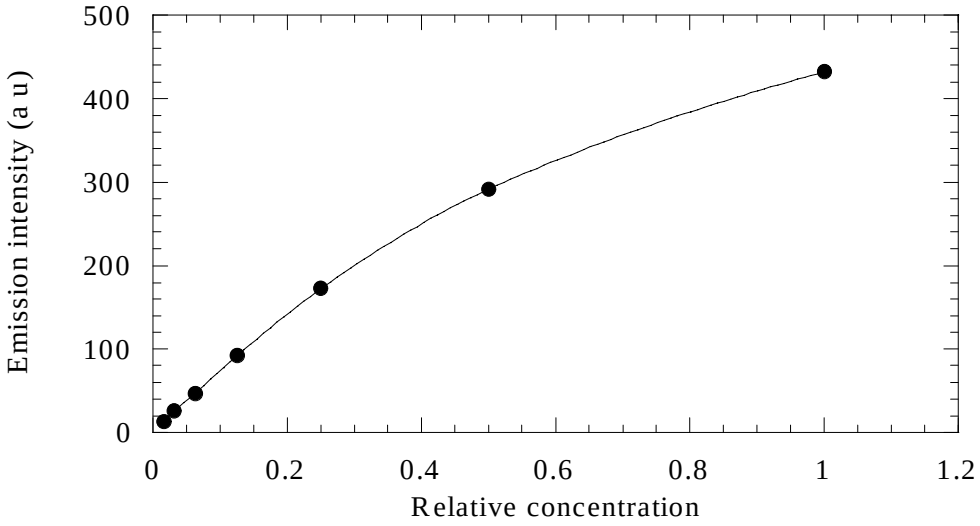

Figure 3.3-5. Calibration curve for Beryl A, 20°C, day 1, test 1. Excitation wavelength **330nm**. Emission intensity recorded 43nm higher than excitation wavelength.

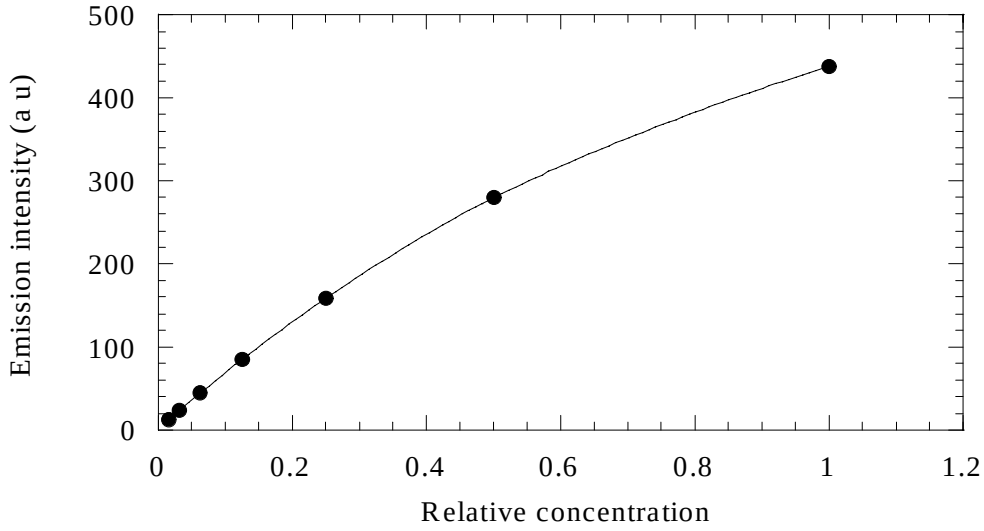

Figure 3.3-6. Calibration curve for Beryl A, 20°C, day 1, test 1. Excitation wavelength **339nm**. Emission intensity recorded 43nm higher than excitation wavelength.

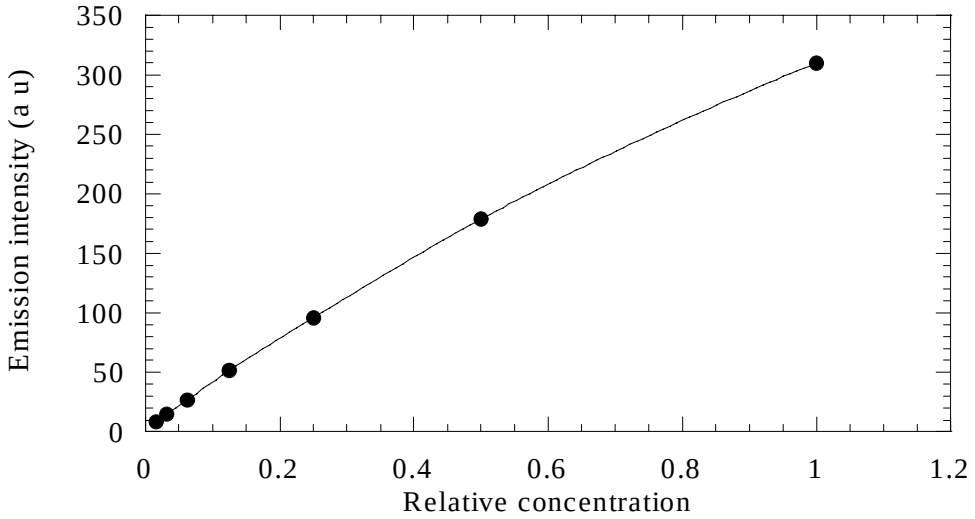

Figure 3.3-7. Calibration curve for Beryl A, 20°C, day 1, test 1. Excitation wavelength **362nm**. Emission intensity recorded 43nm higher than excitation wavelength.

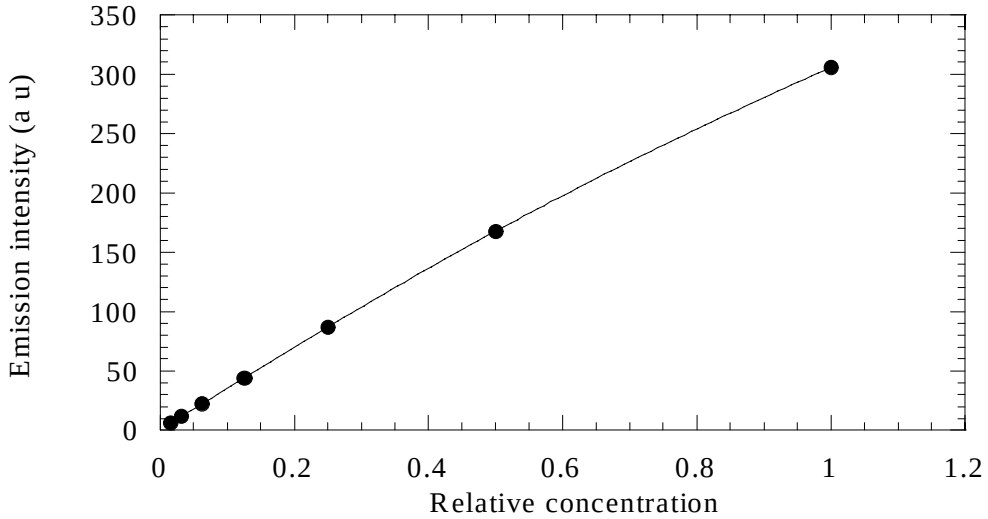

Figure 3.3-8. Calibration curve for Beryl A, 20°C, day 1, test 1. Excitation wavelength **386nm**. Emission intensity recorded 43nm higher than excitation wavelength.

Assuming that the concentration is highest at day 1, a decrease in emission intensity means a decrease in concentration for compounds being excited at 330, 339, 362 and 386nm. Due to the inner filter effect also an increase in emission intensity can mean a decrease in concentration for compounds being excited at 281 and 288nm.

Emission intensities for the samples in test 1, aerobic conditions, are presented in tables 3.3-7 to 3.3-10.

Table 3.3-7. Beryl A, incubation temperature 10°C, test 1. Emission intensities recorded 43 nm higher than excitation wavelength.

Excitation wavelength	Day 1	Day 28	Day 56	Standard deviation (%)
281nm	97	102	118	10.38
288nm	147	158	180	10.39
330nm	395	429	397	4.69
339nm	403	438	393	5.74
362nm	279	303	262	7.32
386nm	275	302	254	8.69

Comparing with the uncertainties in table 3.3-6, the only significant change is observed at 288nm. A small increase in intensity at short wavelengths indicates a slight decrease in aromatic content with few rings. For the other wavelengths the intensity is increasing from day 1 to day 28, and then decreasing from day 28 to day 56. According to the calibration curves at these wavelengths, this makes no sense with respect to degradation.

Table 3.3-8. Beryl A, incubation temperature 20°C, test 1. Emission intensities recorded 43 nm higher than excitation wavelength. Day 28 is the average of three parallels.

Excitation wavelength	Day 1	Day 28	Day 56	Standard deviation (%)
281nm	98	104	102	3.01
288nm	147	156	162	4.87
330nm	432	413	422	2.25
339nm	438	417	431	2.49
362nm	310	292	298	3.06
386nm	306	294	302	2.03

None of the deviations for the sample incubated at 20° are significant. A small tendency of increasing emission intensity at 288nm is however observed, maybe indicating a very small decrease in concentration.

Table 3.3-9. Beryl A, incubation temperature 20°C and nutrients added, test 1. Emission intensities recorded 43 nm higher than excitation wavelength.

Excitation wavelength	Day 1	Day 28	Day 56	Standard deviation (%)
281nm	82	118	119	19.82
288nm	129	176	177	17.07
330nm	392	442	457	7.91
339nm	403	445	467	7.42
362nm	280	304	345	10.61
386nm	279	300	358	13.10

For the sample added nutrients and incubated at 20°C, an increase in emission intensity at 281 and 288nm from day 1 to day 28 is seen, indicating a decrease in concentration of aromatics consisting of few rings. At the other wavelengths the change is not significant. The tendency seen is an increase in emission intensity that should indicate an increase in concentration over time, also not making any sense with respect to degradation.

Table 3.3-10. Beryl A, incubation temperature 5°, test 1. Emission intensities recorded 43 nm higher than excitation wavelength.

Excitation wavelength	Day 1	Day 28	Day 56	Standard deviation (%)
281nm	83	87	93	5.74
288nm	126	136	137	4.57
330nm	409	439	404	5.54
339nm	418	447	404	5.18
362nm	300	325	282	7.14
386nm	310	331	285	7.46

For the sample incubated at 5°C no changes were significant, indicating no degradation.

Emission intensities for the samples in test 2, anaerobic conditions, are presented in tables 3.3-11 to 3.3-14.

Table 3.3-11. Beryl A, incubation temperature 10°, test 2. Emission intensities recorded 43 nm higher than excitation wavelength.

Excitation wavelength	Day 1	Day 28	Day 56	Standard deviation (%)
281nm	130	158	131	11.37
288nm	186	216	196	7.66
330nm	394	362	486	15.55
339nm	391	346	484	17.29
362nm	270	229	343	20.57
386nm	262	217	348	24.15

For the sample incubated at 10°C, anaerobic conditions, the change in emission intensity for excitation wavelengths 330, 339, 362 and 386nm is significant. The intensity is however decreasing from day 1 to day 28, and increasing from day 28 to day 56. According to the calibration curves this should mean a decrease in concentration from day 1 to day 28 and an increase from day 28 to day 56. This is an indication that the experiment was not performed and set up ideally.

For none of the other samples in test 2 significant changes were observed (tables 3.3-12 to 3.3-14).

Table 3.3-12. Beryl A, incubation temperature 20°, test 2. Emission intensities recorded 43 nm higher than excitation wavelength.

Excitation wavelength	Day 1	Day 28	Day 56	Day 100	Standard deviation (%)
281nm	122	130	142	146	8.39
288nm	176	188	200	203	6.56
330nm	380	410	387	412	4.12
339nm	376	402	379	406	4.00
362nm	252	269	254	271	3.83
386nm	248	263	245	261	3.60

Table 3.3-13. Beryl A, incubation temperature 20°and nutrients added, test 2. Emission intensities recorded 43 nm higher than excitation wavelength. Day 1 is the average of three parallels.

Excitation wavelength	Day 1	Day 28	Day 56	Standard deviation (%)
281nm	114	114	119	2.50
288nm	163	167	177	4.27
330nm	418	453	547	4.85
339nm	421	462	467	5.61
362nm	287	341	345	9.99
386nm	284	354	358	12.54

Table 3.3-14. Beryl A, incubation temperature 5°, test 2. Emission intensities recorded 43 nm higher than excitation wavelength. Day 56 is the average of three parallels.

Excitation wavelength	Day 1	Day 28	Day 56	Standard deviation (%)
281nm	118	136	127	7.09
288nm	176	189	183	3.56
330nm	428	401	430	3.86
339nm	426	395	429	4.52
362nm	297	269	293	5.29
386nm	294	263	290	5.97

3.4 Correlation between THC and aromatics

Due to large uncertainty in measurements of both THC and aromatics it is difficult to predict any correlation between THC and aromatics. Figures 3.4-1 and 3.4-2 visualize this.

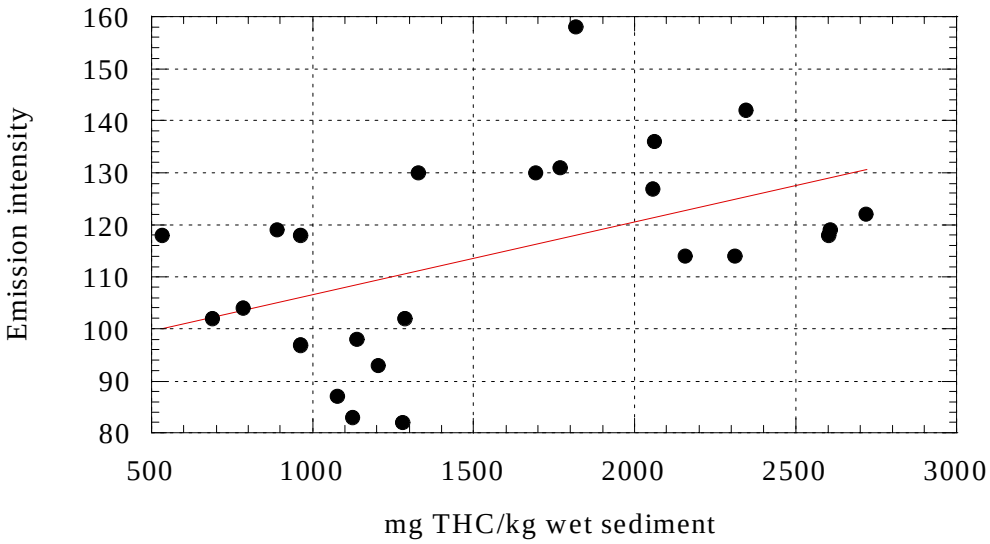

Figure 3.4-1. Correlation between mg THC/kg wet sediment and emission intensities of 24 samples from both the aerobic and anaerobic test. Excitation wavelength 281nm. Correlation coefficient 0.48808.

The best correlation of mg THC/kg wet sediment and aromatics observed was 0.48808 at excitation wavelength 281nm, indicating a slight positive correlation.

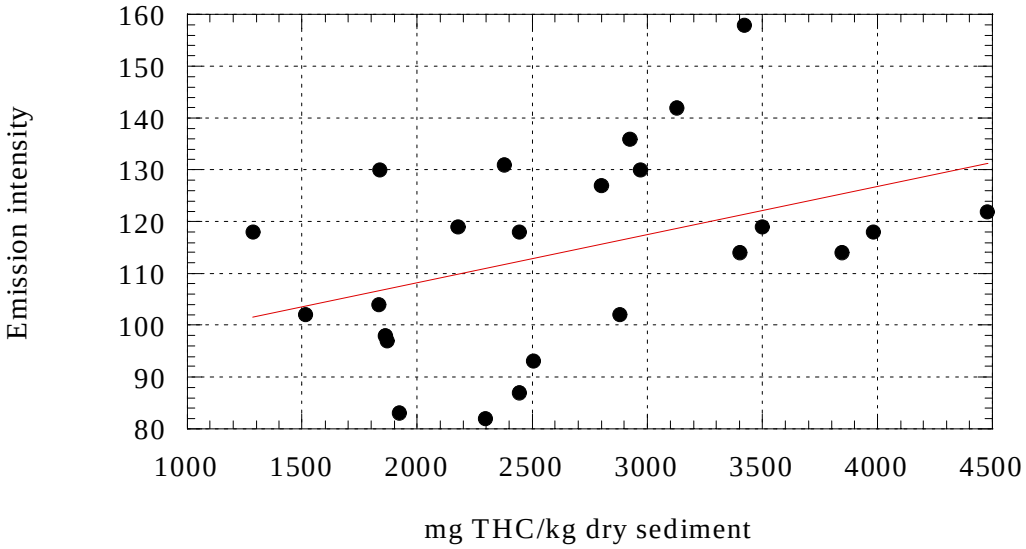

Figure 3.4-1. Correlation between mg THC/kg dry sediment and emission intensities of 24 samples from both the aerobic and anaerobic test. Excitation wavelength 281nm. Correlation coefficient 0.4015.

The best correlation of mg THC/kg dry sediment and aromatics observed was 0.4015 for excitation wavelength 281nm, also indicating a slight positive correlation.

Correlations for the other wavelengths are presented in appendix 7.2. The correlation coefficient seems to be decreasing as the wavelength of excitation increases. At the highest wavelengths no correlation is observed.

One factor making it difficult to predict the correlation is that the data points are very close to each other, covering a narrow range of concentrations. If samples covering a broader concentration range were plotted in the same diagram as the 24 plotted in figure 3.4-1, the 24 data points would probably appear as one point.

4 Discussion

Degradation of hydrocarbons in sediment or on the sea floor is traditionally measured by a set of parameters [15] including THC and microbial activity.

THC is measured by gas chromatography with flame ionisation detector (GC-FID). This is a time consuming and expensive method. The work on this thesis was done to investigate if fluorescence could be used as a screening method for THC in sediment samples of the UKOOA project, and also for similar tests in the future. A fluorescence measurement takes a few minutes to perform.

The preliminary work showed that the fluorescence response was low, and that the relation between concentration and emission intensity was not necessarily linear. Diluting a sample often resulted in an increase in emission intensity. These observations lead to fundamental investigations on inner filter effect, resonance energy transfer and self-absorption. These are all aspects appearing to make fluorescence quite difficult for quantitative and qualitative analysis. It is for instance not possible to make standard calibration curves for quantitative measurements. The first sample in a time series has to be diluted to make a calibration curve for each time series (figures 3.3-3 to 3.3-8). This curve cannot be used for other types of material sample (i.e. other piles).

The main problem of inner filter effect in practical use of fluorescence is the non-linear relation between concentration and response (figure 3.1.1-1). The linear part of the calibration curve is often very small, and is also dependent on the wavelength of excitation (figure 3.1.1-4 contra 3.1.1-5). The shorter the excitation wavelength is, the smaller is the linear part of the calibration curve. It is often tempting to think that calibration curves are linear, and hence conclude that an increase in response means an increase in concentration. Due to the shape of the calibration curves affected by the inner filter effect, this might not be the correct conclusion.

The practical problem with RET is that the response of a certain concentration of a fluorescent compound may vary greatly, depending on which other compounds that are present. In the experimental investigations the response of a constant concentration of naphthalene was varying from 400-1200 (a u) depending on the amount of antracene present (figure3.1.2-3). With increasing concentration of antracene the response of naphthalene was decreasing non-linearly (figures 3.1.2-4 and 3.1.2-5). The response at a certain wavelength and constant concentration of a fluorescent species will depend on the combination and concentration of other both fluorescent and non-fluorescent species present.

With self-absorption the spectrum of a fluorescent species will depend on the concentration of this species. At one concentration a characteristic spectrum with emission maximums at certain wavelengths is observed (figure 2.3.5.1-2). At another concentration some of the emission maximums might disappear (figure 2.3.5.1-3), and others may appear. Comparing responses at a certain wavelength in the spectrum might result in different observations than if response was recorded at another wavelength. Another complicating fact is that self-absorption also depends on the presence of other compounds. In the case of increasing concentration of antracene in the presence of naphthalene (figure 3.1.3-9), no self-absorption was observed.

It is very important to be aware of these aspects, otherwise the use of fluorescence data might lead to wrong conclusions.

Investigations of THC showed that the uncertainty in injection and integration was 1.72%. In this connection an uncertainty of up to 30% was assigned sampling and extraction. Fluorescence measurements on the same samples as those analysed on THC only showed an uncertainty up to 13%. This means that fluorescence is a less sensitive method than GC-FID, not reflecting the actual uncertainty.

The UKOOA project was designed as a degradation study where the traditional parameters for degradation were used. These parameters were also used in other parts of the UKOOA project (table 1-1). The samples used to investigate the correlation between THC and aromatics were those used in the traditional UKOOA degradation project. These appeared to not be ideal for the correlation study. The main reason for this was the unexpected low degradation. Due to low degradation the concentration in the samples for the correlation study were covering a too narrow range. This means that if samples covering a broader concentration range were used for the correlation study, the data points presented in figure 3.4-1 and 3.4-2 would probably appear as one point. Another reason that this material was not ideal was the nature of the material. The cutting was very clayish, making it difficult to collect representative samples.

The ideal start would have been a model study. Standards covering a broad region of THC should have been made from non-contaminated reference sediment. These standards should have been extracted and analysed on both GC-FID and fluorescence. If a correlation had been observed, real samples could have been analysed on fluorescence, and a prediction of THC could have been made quickly and at low expenses.

From the samples analysed it is difficult to say anything about the correlation between THC and aromatics. There is, however, no basis to conclude that no such correlation exists.

5 Conclusions and recommendations for further work

From the results obtained no conclusion about the correlation between THC and aromatic content can be drawn.

This work has, however, shown how important it is to be aware of certain fundamental aspects before evaluating results from fluorescence measurements. Without this awareness wrong conclusions can easily be made.

This work has also shown that it is valuable to invest time in pre-studies. From thorough pre-studies time and costs can be saved in the main study, and reliable results are more probable.

Recommendations for further work would be a model study of samples covering a broad region of THC, and hence an experimental set-up of “real samples” assuring homogeneity at starting point.

6 References

1. Trisha O'Reilly. *Newsletter: UKOOA Drill Cuttings Initiative*, Issue No 4, Autumn 2000. UK Offshore Operators Association Limited.

2. Gunvor Elingsen. Master's Thesis. *Application of absorption and fluorescence spectroscopy to the study of crude oil*. Stavanger College (1996): p. 42

3. Douglas A. Skoog, Donald M. West, F. James Holler. *Fundamentals of analytical chemistry*. 7th edition. Saunders college publishing (1996): chapter 25

4. Tyge Greibrokk, Elsa Lundanes, Knut E Rasmussen. *Kromatografi – Separasjon og deteksjon*. 3rd edition. Universitetsforlaget AS (1998): chapters 1,8,16

5. Douglas A. Skoog, F. James Holler, Timothy A. Nieman. *Principles of instrumental analysis.* 5th edition. Saunders College Publishing (1997): Pp 355-367

6. Douglas A. Skoog, Donald M. West, F. James Holler. *Fundamentals of analytical chemistry*. 7th edition. Saunders college publishing (1996): Pp 601-607

7. Gunvor Elingsen. Master's Thesis. *Application of absorption and fluorescence spectroscopy to the study of crude oil*. Stavanger College (1996): Pp 8-15

8. Gunvor Elingsen. Master's Thesis. *Application of absorption and fluorescence spectroscopy to the study of crude oil*. Stavanger College (1996): p. 45

9. Gunn Marit Solli, Peter Ruoff. *Inner filter effect: Phase relationship between oscillatory fluorescence and oscillatory Ru(II) concentrations in the Belousov_Zhabotinsky reaction*. J. Chem. Phys. Vol. 103. No. 4, 22 July 1995: Pp 1440-1447

10. Joseph R. Lakowicz. *Principles of Fluorescence Spectroscopy*. 2nd edition. Kluwer Academic/Plenum Publishers (1998): Pp. 13-14

11. Joseph R. Lakowicz. *Topics in Fluorescence Spectroscopy-Volume 2 Principles.* Plenum Press (1991): Pp. 127-128

12. Joseph R. Lakowicz. *Principles of Fluorescence Spectroscopy*. 2nd edition. Kluwer Academic/Plenum Publishers (1998): p. 55

13. Grethe Kjeilen, Troels Jacobsen, RF-Rogaland Research: *New advances in cost-effectively decommissioning drill-cuttings piles without disturbing the marine environment*. IIR's 5th Annual Offshore Decommissioning conference: Driving Down Costs and Exploiting new technical innovations for decommissioning offshore installations.

14. Statens forurensnings tilsyn (SFT). *"guidelines 99:01; Environmental monitoring of petroleum activities on the Norwegian shelf"*.

15. Robert E. Hinchee, Bruce C. Alleman, Ron E. Hoeppel, Ross N.Miller. *Hydrcarbon Bioremediation.* Lewis Publishers (1994): Pp 107-124, 219-236

7 Appendix

7.1 Integrated gas chromatogram

7.2 Figures illustrating correlation between THC and aromatics

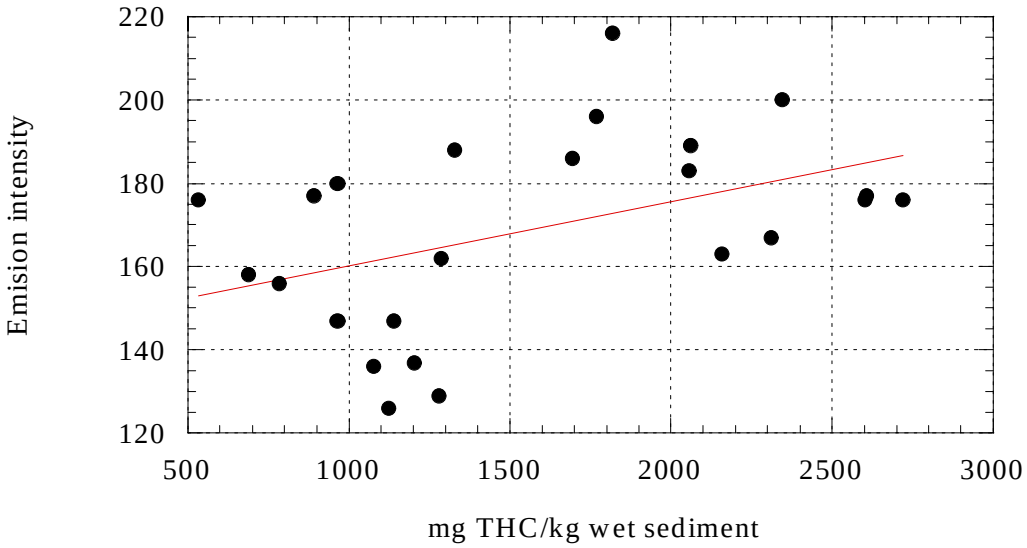

Figure 7.2-1. Correlation between mg THC/kg wet sediment and emission intensities of 24 samples from both the aerobic and anaerobic test. Excitation wavelength 288nm. Correlation coefficient 0.44286.

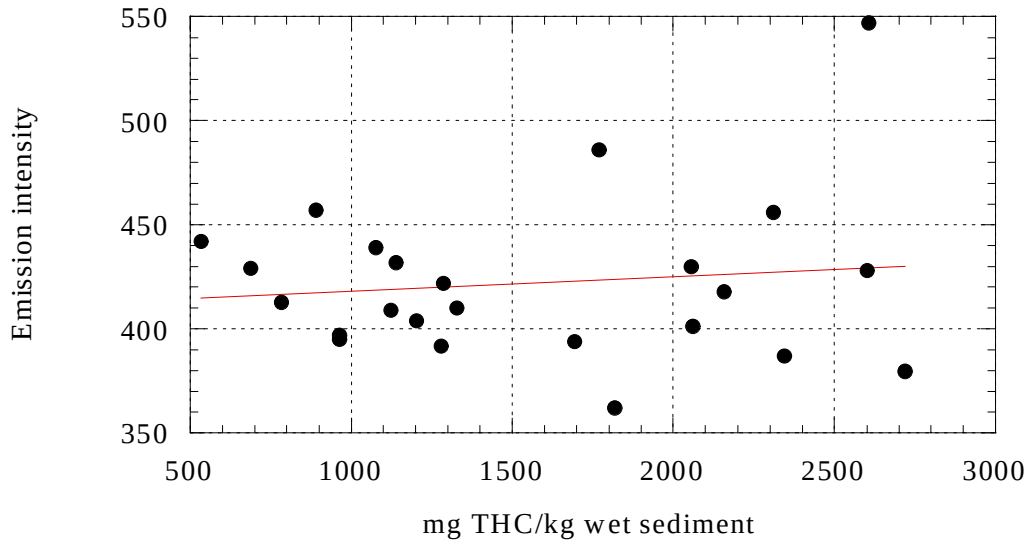

Figure 7.2-2. Correlation between mg THC/kg wet sediment and emission intensities of 24 samples from both the aerobic and anaerobic test. Excitation wavelength 330nm. Correlation coefficient 0.11997.

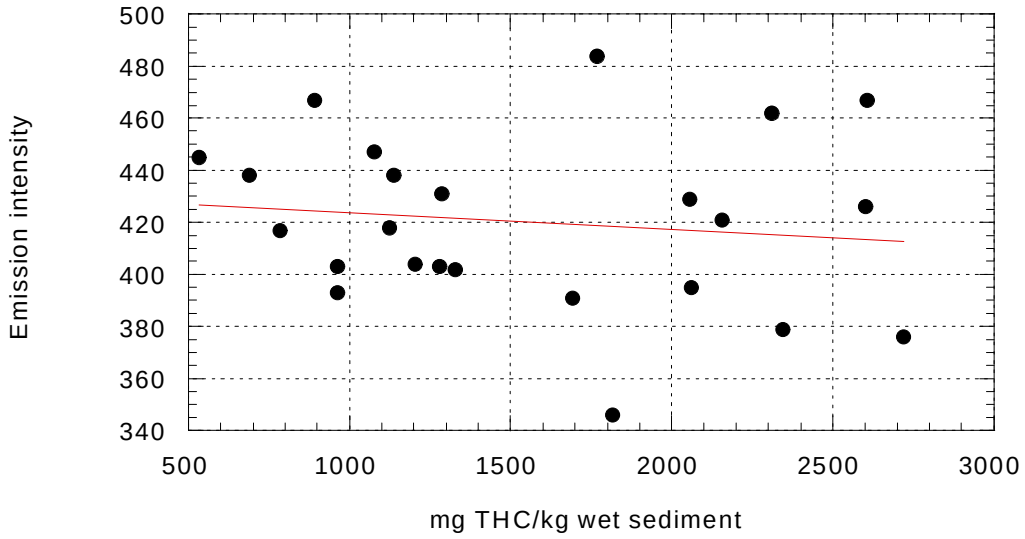

Figure 7.2-3. Correlation between mg THC/kg wet sediment and emission intensities of 24 samples from both the aerobic and anaerobic test. Excitation wavelength 339nm. Correlation coefficient 0.13002.

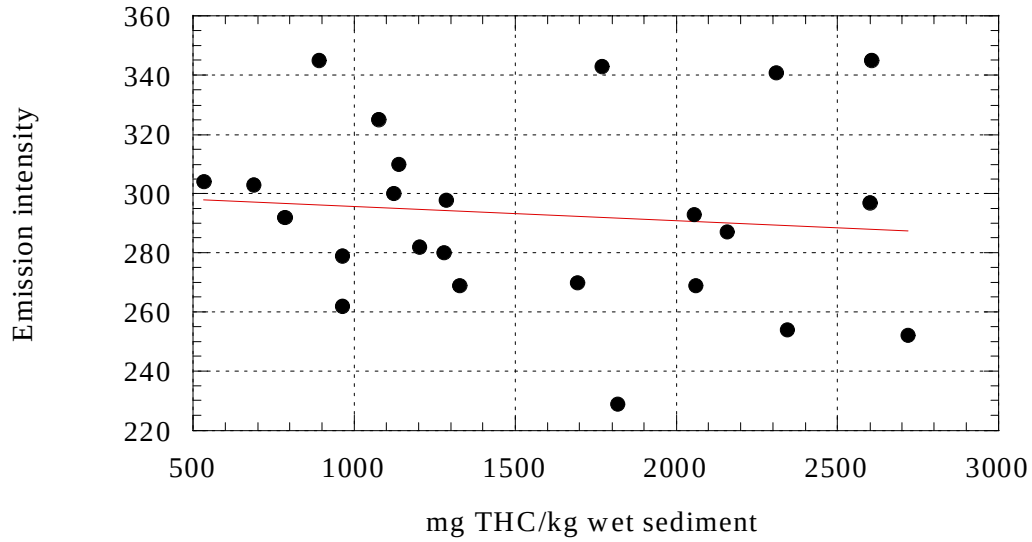

Figure 7.2-4. Correlation between mg THC/kg wet sediment and emission intensities of 24 samples from both the aerobic and anaerobic test. Excitation wavelength 362nm. Correlation coefficient 0.0.10349.

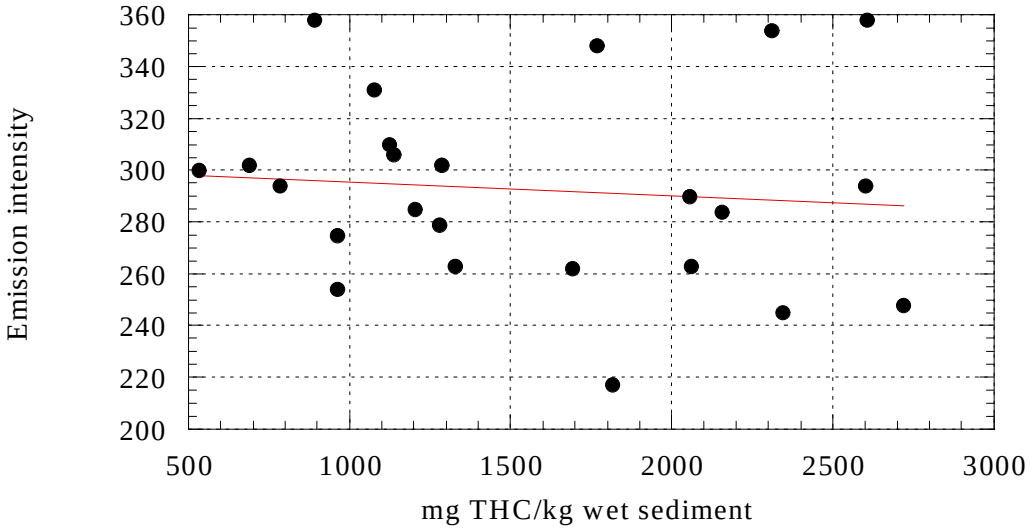

Figure 7.2-5. Correlation between mg THC/kg wet sediment and emission intensities of 24 samples from both the aerobic and anaerobic test. Excitation wavelength 362nm. Correlation coefficient 0.094694.

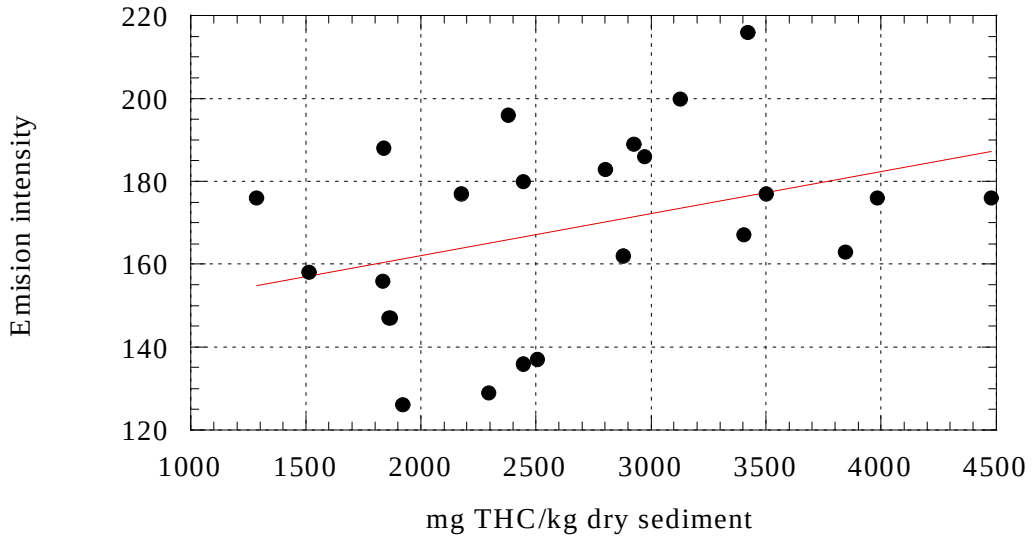

Figure 7.2-6. Correlation between mg THC/kg dry sediment and emission intensities of 24 samples from both the aerobic and anaerobic test. Excitation wavelength 288nm. Correlation coefficient 0.36009.

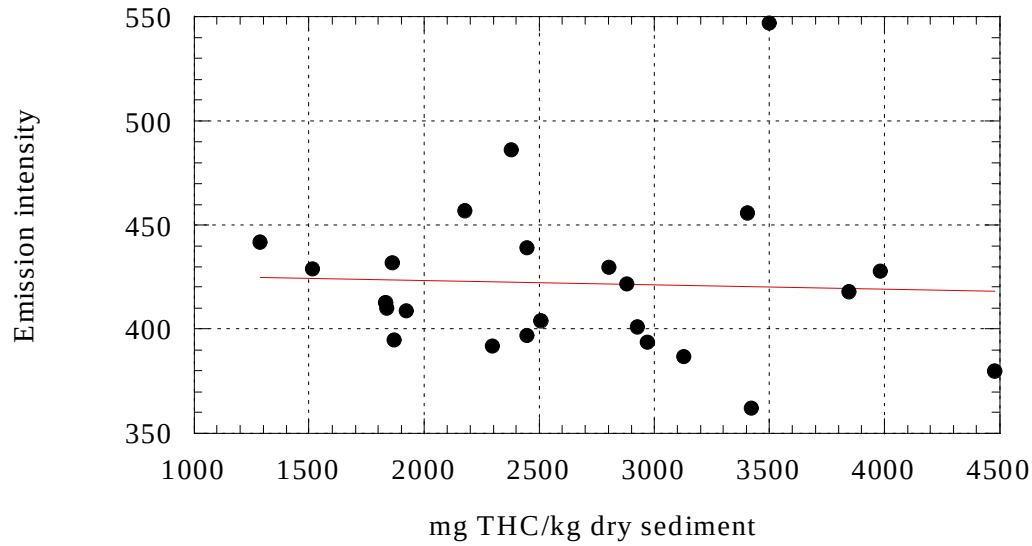

Figure 7.2-7. Correlation between mg THC/kg dry sediment and emission intensities of 24 samples from both the aerobic and anaerobic test. Excitation wavelength 330nm. Correlation coefficient 0.04493.

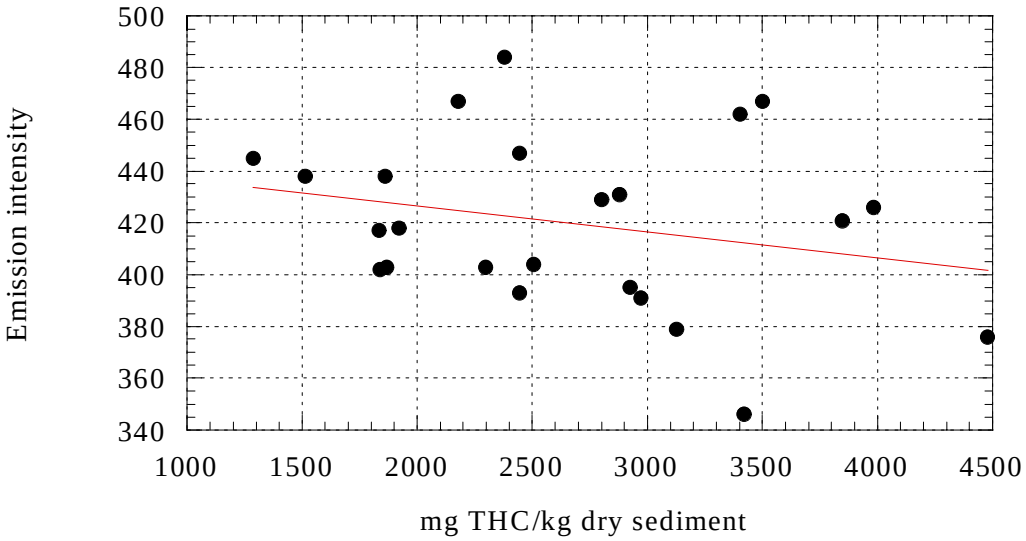

Figure 7.2-8. Correlation between mg THC/kg dry sediment and emission intensities of 24 samples from both the aerobic and anaerobic test. Excitation wavelength 339nm. Correlation coefficient 0.25061.

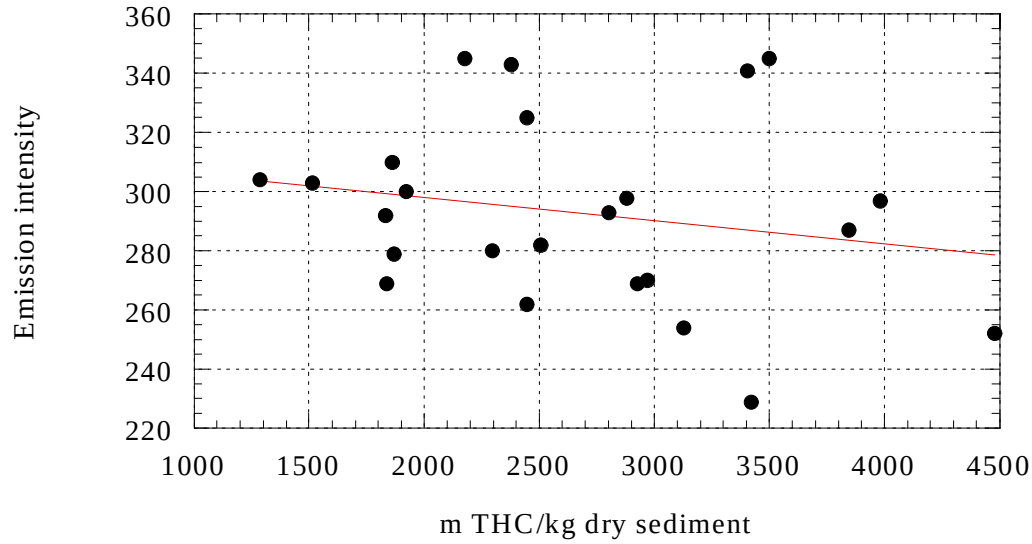

Figure 7.2-9. Correlation between mg THC/kg dry sediment and emission intensities of 24 samples from both the aerobic and anaerobic test. Excitation wavelength 362nm. Correlation coefficient 0.20819.

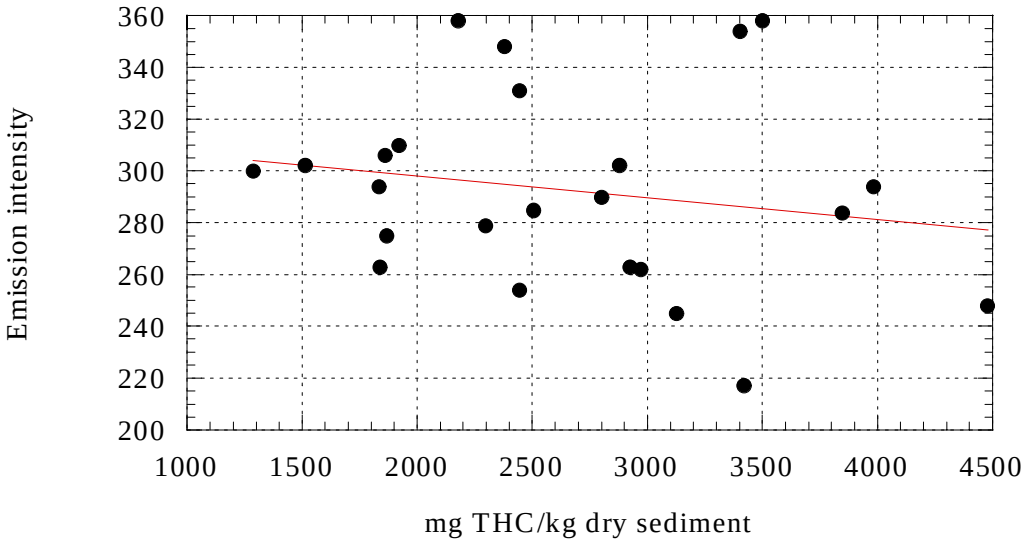

Figure 7.2-10. Correlation between mg THC/kg dry sediment and emission intensities of 24 samples from both the aerobic and anaerobic test. Excitation wavelength 386nm. Correlation coefficient 0.18643.